Dimensional synthesis of wide-band waveguide filters without global optimization

Zhang, Qingfeng

2010

Zhang, Q. (2010). Dimensional synthesis of wide-band waveguide filters without global optimization. Doctoral thesis, Nanyang Technological University, Singapore.

https://hdl.handle.net/10356/46259

https://doi.org/10.32657/10356/46259

Dimensional Synthesis of Wide-band Waveguide Filters without Global Optimization

ZHANG Qingfeng

School of Electrical & Electronic Engineering

A thesis submitted to the Nanyang Technological University
in fulfillment of the requirements for the degree of
Doctor of Philosophy

2010

STATEMENT OF ORIGINALITY

I hereby certify that the work embodied in this thesis is the result of original research and has not been submitted for a higher degree to any other University or Institution.

Date	ZHANG Qingfeng

DEDICATION

To

My supervisor

And

My parents and my wife.

ACKNOWLEDGEMENTS

I am sincerely grateful to all the individuals who have contributed to the successful completion of my graduate studies and this research thesis.

First and foremost, I wish to express gratitude to my supervisor, Professor LU Yilong, for his careful guidance, stimulating suggestion, exact insight and profound knowledge in supervising my research project. Without his encouragement and enlightenment that carried me on through difficulties, I could not come this far so smoothly for my graduate study.

I would like to thank Dr. Amir Khurrum RASHID who shared his knowledge and experience unselfishly. I also want to thank Mr. LIM Cheng Chye for his technical assistance.

Especially, I am very grateful for the love and support of my parents and my dear wife LI Bing.

Finally, I want to give my thanks to Nanyang Technological University for the full scholarship support.

SUMMARY

This Ph.D. dissertation presents a dimensional synthesis method for the design of wide-band filters without resorting to global full-wave optimization. The wide-band filters include direct-coupled waveguide filters, in-line pseudo-elliptic waveguide filters and cross-coupled waveguide filters. The type of the wide-band filters cover not only half-wavelength-resoantor filters, but also quarter-wavelength-resonator filters.

After literature survey is summarized, a new mapping method, edge frequency mapping method, is proposed for the synthesis of wide-band bandpass filters. Then we apply it to the design of direct-coupled waveguide filters and propose a dimensional synthesis method without global full-wave optimization, in which an improved full-wave model for the waveguide iris and an iteration design procedure are employed.

Since the pseudo-elliptic waveguide filters has more practical applications than direct-coupled waveguide filters, we propose three approaches to extend the dimensional synthesis method to include pseudo-elliptic waveguide filters. The first approach is to employ the cavity-backed K-inverters, which can produce transmission zeros in the out-of-band response, however, whose frequency response in the passband is similar to that of normal iris K-inverters. The second approach is to employ the customized resonators, which can produce transmission zeros in the out-of-band response, however, whose frequency response in the passband is similar to that of normal half-wavelength-transmission-line resonators. The two approaches can be applied to the synthesis of in-line pseudo-elliptic waveguide filters. The third approach is applied to the synthesis of cross-coupled waveguide filters. In order to apply the edge frequency mapping method, a direct-

coupled filter network equivalent to the cross-coupled filter network is proposed based on the even-mode and odd-mode analysis.

In addition to the pseudo-elliptic waveguide filters, we also extend the dimensional synthesis method to include quarter-wavelength-resonator bandpass filters. Compared with the half-wavelength-resonator bandpass filter, the quarter-wavelength-resonator bandpass filter has many advantages. To apply the edge frequency mapping method to the quarter-wavelength-resonator bandpass filters, a new lowpass prototype filter with alternative K-inverters and J-inverters is proposed. The decomposition approach for frequency-dispersive inverters and the synthesis procedure are also modified to be suitable for the dimensional synthesis of quarter-wavelength-resonator bandpass filters.

TABLE OF CONTENTS

LIST OF FIGURES

LIST OF TABLES

CHAPTER 1
INTRODUCTION

1.1 Background

The term *microwaves* may be used to describe electromagnetic (EM) waves with frequencies ranging from 300 MHz to 300 GHz, which correspond to wavelengths (in free space) from 1 m to 1 mm. Over the past one hundred years, microwave technology has become a ubiquitous technology which finds applications in communications, radar, navigation, radio astronomy, sensing, medical instrumentation and many more [1]-[2].

Filters play important roles in many microwave applications. They are used to separate or combine different frequencies. The electromagnetic spectrum is limited and has to be shared; filters are used to select or confine the microwave signals within assigned spectral limits. The design of microwave filters was started prior to the war, a particularly significant early paper in 1937 by W. P. Mason and R. A. Sykes [3]. Over the past seven decades, significant developments have taken place in the design of microwave filters [3]-[4]. Microwave filters have found massive applications in military, satellite communications, cellular radio and so on.

The first real driver for microwave filters was the invention of radar in World War II. The military applications led to significant developments in filters at various laboratories [5]. Military applications required wide-band and tunable devices for electronic support measures receivers, which led to the development of highly selective wide-band waveguide filters, coaxial resonator and suspended-substrate multiplexers and electronically tunable filters. Initially, rectangular waveguide filter was an important candidate in military applications. Methods of accurately designing this kind of filter for wide-band operation occupied several workers for a considerable period [6]-[8]. The advantages of waveguide filters are its high Q and high power handling ability [9]. The disadvantage of using waveguide filters is the relatively large size required for low-frequency operation. Therefore, much smaller

filters may be constructed using TEM transmission lines. The most significant developments were the parallel coupled-line filter [10], which has numerous applications in the interdigital filter [11] and the combline filter [12]-[13]. Yttrium-iron-garnet (YIG) filters [14] are commonly employed as electronically tunable filters which are used in scanning receivers as they give relatively fine frequency resolution.

The applications in satellite communications began with the Intelsat I-III series of satellites, which established the viability of voice communications in the late 1960s. This created the need for high-performance filters and multiplexers [15]. Initially rectangular waveguide filters were employed and the problem was that the multiplexers were very large and heavy. To solve this problem, the first major innovations was the use of dual-mode filters, where size reduction is obtained by exciting two orthogonal degenerate modes in the same physical cavity [16]-[19]. Since then dual-mode filters became the satellite industry standard. Indeed, new types of dual-mode filter are still being reported, e.g., [20]. Triple mode designs [21] and quadruple mode designs [22] offer further size reduction. However, these designs are very sensitive and suffer from poor temperature stability. The use of dielectric resonators constructed from low-loss high-permittivity temperature stable ceramics enables high-Q filters to be realized in a fraction of the volume and weight of air-filled waveguide devices [23]-[24]. High-temperature superconductivity also shows considerable promise, because superconductivity enables resonators with much higher unloaded Q to be constructed in a very small size, provided that the filters are cooled to 77K [25]-[27]. Besides, surface acoustic wave (SAW) filters also have applications in the satellite industry due to their extremely sharp selectivity [28]. Satellite communications also stimulated work on filter transfer functions and network synthesis. A new method of computing symmetrical transfer functions with arbitrary passband ripple and transmission zero locations was reported in [29]. A comprehensive theory of symmetrical dual-mode filters [30] and asymmetrical dual-mode filters [31]-[32] were also established.

In addition to the military and satellite communications, cellular radio also provided a significant driver for filter technology. The base-station requires filters

with good temperature stability, high Q, and small volume and considerable research has been carried out [33]. Dual-mode dielectric-resonator filters have been shown to achieve a high Q realized in approximately one-half the physical volume of coaxial filters [34]. The single-mode dielectric-loaded waveguide filters also gave significant volume reduction compared to coaxial filters [35]. The triple-mode dielectric resonator filters [36]-[37], and a reflection mode approach to triple-mode dielectric-resonator filters [38], were also proposed as smaller alternatives. Superconducting base-station filters are also of interest because of their high Q realizable in a very small physical size [39]-[40]. Recently, one of the main drivers for base-station filters has been the desire to reduce costs, which is focused on the computer-aided and automatic filter alignment [41]-[43]. Compared to base-station filters, the filters used in cellular radio handsets have completely different requirements. For the second-generation TDMA systems, the handset filters have very demanding specifications on the size, price and stopband attenuation [44]. Although the advances in SAW filters design have enabled them to compete in this market [45], their power handling and temperature stability is poor. The developments in film bulk acoustic resonator (FBAR) filters [46]-[47] and micromachined electromechanical systems (MEMS) filters [48] show impressive performance. Also the use of tunable filters [49]-[51] may be useful in handsets for future systems operating at many different frequencies. In addition to the passive resonators used in handset filter technologies, several workers investigated the active filters using the negative resistance [52]-[53] and active matching techniques [54]-[55]. It is also possible to construct active microwave filters based on recursive and transversal principles, which was demonstrated in [56]-[57]. The use of analog varactor tuned phase shifters also enables the realization of tunable active filters [58]. The problem of the active filters is the noise performance and nonlinearity.

Over the past seven decades, significant developments have taken place in the design of microwave filters. Its applications in military, satellite communications and cellular radio provide a significant driver for the development of microwave filter technologies. Although the synthesis of microwave filter is already a mature technology, there is still much that can be done.

1.2 Motivation

1.2.1 Analysis and Design of Waveguide Filters

Waveguide filters are still a preferred option when power handling, losses and selectivity are the main concerns in the application, for example, space systems [59]. For the accurate and efficient electromagnetics analysis of waveguide filters, the traditional method is to divide the complete structure into simpler key building blocks [60]. Most convenient waveguide filters are implemented in a direct-coupled cavity configuration [3] and can be seen as a simple cascade connection of waveguides with different cross sections. To perform the electromagnetics analysis of planar waveguide junctions, the classic modal methods formulated in terms of generalized scattering matrics (GSMs), generalized admittance matrics (GAMs), or generalized impedance matrics (GIMs) are widely employed [61]-[63] when the junctions involve waveguides with a standard cross section (i.e., rectangular, circular and even elliptical shapes) or the waveguide mode functions are known analytically or numerically. For dealing with more complicated or general shapes, less efficient space segmentation techniques, such as finite element method (FE) [64] or finite-difference time-domain (FDTD) [65] methods are employed. A third option is the hybrid method which suitably combine efficient modal techniques with flexible segmentation schemes, i.e., the mode-matching FE (MM/FE) method [66], boundary contour mode-matching (BCMM) method [67], and the hybrid technique combining MM, FE, method of moments, and finite differences (MM/FE/MoM/FD) [68]. An alternative hybrid technique for the fast and rigorous computation of modal chart of arbitrarily shaped waveguides is the boundary integral-resonant mode expansion (BI-RME) method, which was originally proposed in [69]-[70], and later was revisited to cope with more complex waveguide profiles [71].

Since extremely fast and precise electromagnetic analysis methods are already available, recent efforts are being devoted to their integration within modern CAD tools, which are typically driven by optimization algorighms. A wide survey of technical contributions on this research area can be found in [72]-[73]. Even though optimization methods are extremely use useful, their direct application to the filter design problem may not result in good solutions. They should be wisely combined

with synthesis techniques, such as those based on network theory [8] and coupling matrics [74], which provide good initial points that help to find the optimal solution with reduced computational efforts. This combined strategy has been applied to the fast and automated design of waveguide filters and diplexers for direct use in space systems [75]-[76]. However, the synthesis of waveguide filters with optimization still cost much computational effort. Therefore, the design techniques without excessive global optimization are highly demanded in the filter design. They can significantly improve the accuracy, time, and complexity of the design procedure.

1.2.2 Synthesis of Wide-Band Direct-Coupled Waveguide Filters without Optimization

Recently, the design techniques for wide-band bandpass filters without excessive global optimization have become more and more important. With the improvement of these techniques, the accuracy, time, and complexity of the design procedure can be improved significantly. The excessive use of optimization can be avoided especially in complicated structures where there are numerous dimensions to be optimized.

In the classic method [77]-[78], we employ network theory with immittance inverters to design bandpass filters. By using impedance or admittance inverters, microwave bandpass filters can be designed conveniently. However, the inverters have to be frequency-independent theoritically, which is not true for practical cases. One of the most serious degradations in frequency response of a bandpass filter from the ideal one is due to the frequency sensitivity of the inverters. Because of the frequency dependence of the inverters, bandpass filters designed with the classic method, in which the inverter values are taken only at the center frequency, give good results only for very narrow bandwidth and excessive optimizations have to be employed.

The general procedure for the design of direct-coupled filters was first devised by Cohn [6], and then Matthaei, Young and Jones [77] introduced a bandwidth contraction factor and a deviation of center frequency for direct-coupled cavity filters to predict the change caused by the frequency-dependent inverters using design

graphs. Levy, [8], suggested “ideal transformers with frequency-dependent turns ratio” on both sides of the inverters. However, these techniques still cannot give good in-band equal ripple performance for wide-band filters, moreover, they do not give the desired dimensional information directly.

A dimensional synthesis procedure for H-plane waveguide iris filters was proposed in [79], in which each waveguide iris is modeled as a frequency-dependent inverter having series reactance on each side. This enables reactance slope parameter corrections to be introduced in the dimensional synthesis procedure. However, the iris model in [79] is still not good enough because the extracted K-inverter is still frequency-dependent though some of its frequency dependence information is included in derivation of slope parameters. Besides, the parameters are corrected only once in the synthesis procedure and the results could be better if an iteration procedure can be employed. Therefore, it is an urgent work to explore a new dimensional synthesis method for the design of wide-band waveguide direct-coupled filters without resorting to global full-wave optimizaiton.

1.2.3 Synthesis of Wide-Band In-Line Pseudo-Elliptic Waveguide Filters

Although the filter in waveguide technology is a classical subject, the development of elliptic and pseudo-elliptic waveguide filters deserves further attention. Waveguide filters with transmission zeros can obtain sharp cutoff skirts which can increase the selectivity of filters.

Generally, filters with transmission zeros are designed according to three slightly different approaches. Cross-coupled resonator filters [17] are well known as the first approach, in which the destructive interference is introduced by multiple paths to produce transmission zeros. The generation of real transmission zeros in this approach often requires coupling coefficients of mixed signs. The second approach known as extracted pole technique [80] was a breakthrough which allows the individual control of transmission zeros. Compared with the cross-coupled techniques, the extracted pole technique has its advantage in that it can generate transmission zeros individually and requires the coupling coefficients of only one type. Despite these advantages, the extracted pole technique has its drawbacks in that

the assumed constant phase shifts in the main line are not readily realized or even adequately approximated except for narrowband applications. Some flexibility was added with the concept of nonresonating nodes in [81]-[82]. The phase shifts in the main line of the filter are eliminated and replaced by constant reactance to reduce the effect of dispersion. This technique allows the design process to be modular [83] or to have some interesting topologies [84] avoiding the use of phase shifts inherent in the extracted pole technique. Two applications of nonresonating nodes technique are reported in [85]-[86].

Although the three approaches mentioned above are widely employed to design pseudo-elliptic waveguide filters, they are only applicable to narrowband cases. Due to the frequency dispersion of coupling coefficients, excessive global full-wave optimizations have to be employed in the design of wide-band pseudo-elliptic waveguide filters. So far no synthesis method has been reported for the design of pseudo-elliptic waveguide filters without global full-wave optimization. Therefore, it is a challenging work and may find wide applications in the future.

1.2.4 Synthesis of Wide-Band Cross-Coupled Waveguide Filters

Pseudo-elliptic microwave filters, which find ever-increasing applications in a wide range of modern communication systems, are often designed as a set of cross-coupled resonators [17], [87]-[88]. Cross coupling between non-adjacent resonators in the pseudo-elliptic filters is used to bring the transmission zeros from infinity to finite positions in the complex plane. These filters can provide a skirt selectivity, or a flat group delay, or even both simultaneously.

Both positive and negative couplings are needed to generate transmission zeros at finite frequencies for achieving a high selectivity in a cross-coupled filter [89]. The actual implementation of cross coupling is either physical or modal. In the case of physical cross coupling, a physical element is employed, such as a metal rod in waveguide combline resonator filter [90], electrical probe in the combline filter [91], a square aperture at the center of the broad walls in the canonical folded waveguide filter [92]-[93]. An alternative approach is the use of other modes, propagating or evanescent, as separate paths for energy flow. Some designs based on this technique

used higher order modes in waveguide cavities to generate the transmission zeros for a pseudo-elliptic response [94].

Although these techniques mentioned above are widely employed to design cross-coupled waveguide filters, they are only applicable to narrowband cases. Due to the limitation of the circuit model and frequency dispersion problem, excessive global full-wave optimizations have to be employed in the design of wide-band cross-coupled waveguide filters. Therefore, it is necessary to explore a synthesis method for the design of wide-band cross-coupled waveguide filters without resorting to global full-wave optimization.

1.2.5 Synthesis of Wide-Band Bandpass Filters with Quarter-Wavelength Resonators

Usually, bandpass filters are designed with half-wavelength transmission lines, which will resonate at the center frequency. Quarter-wavelength-resonator bandpass filters belong to a different type of bandpass filters, which are composed of quarter-wavelength transmission lines with alternative K-inverters and J-inverters, as well as alternative high and low impedance levels. Their advantages over filters with half-wavelength resonators include [95]: shorter length, second passband is centered at $3f_0$ instead of $2f_0$ (f_0 is center frequency), mid-stop-band attenuation is higher, precision design for a prescribed insertion loss characteristic is tractable to greater bandwidths, can be made in “bar transmission line” form without dielectric supports.

So far, however, the design techniques for quarter-wavelength-resonator bandpass filters are still designed by the classic method in [95] and no improved synthesis method has been reported. Therefore, it is necessary to explore a synthesis method for the design of wide-band quarter-wavelength-resonator filters without resorting to global full-wave optimization.

1.3 Objectives

The goal of this dissertation is to develop a dimensional synthesis method for the design of wide-band filters without resorting to global full-wave optimization. The wide-band filters include direct-coupled waveguide filters, in-line pseudo-elliptic

waveguide filters and cross-coupled waveguide filters. The type of the wide-filters cover not only half-wavelength-resoantor filters, but also quarter-wavelength-resoantor filters. The research work is expeted to provide the design guideline for the exploration of synthesis method for wide-band bandpass filters in the future. The objectives of our research can be divided into the following five parts:

1.3.1 Analysis and Design of Waveguide Filters

- To develop an edge frequency mapping method suitable for the synthesis of wide-band bandpass filters.
- To develop an improved model to deal with frequency-dependent K-inverters.
- To apply the edge frequency mapping method to the synthesis of bandpass filters with frequency-dependent K-inverters.

1.3.2 Synthesis of Wide-Band Direct-Coupled Waveguide Filters without Optimization

- To build up an improved full-wave model for the waveguide iris.
- To apply the edge frequency mapping method to the waveguide direct-coupled filter and obtain the synthesis formula.
- To employ a iteration procedure to solve the synthesis formula and obtain the converged K-parameters.
- To find a easy and fast method to extract the iris element parameters from the scattering parameters.

1.3.3 Synthesis of Wide-Band In-Line Pseudo-Elliptic Waveguide Filters

- To develop an approach that can extend the synthesis method for direct-coupled waveguide filters to include the in-line pseudo-elliptic waveguide filters: using some special K-inverters or special resonators.

- To realize the special K-inverters that can be employed for the synthesis of in-line pseudo-elliptic waveguide filters.
- To realize the special resonators that can be employed for the synthesis of in-line pseudo-elliptic waveguide filters.
- To derive the dimensional synthesis method for in-line pseudo-elliptic wavguide filters without optimization.

1.3.4 Synthesis of Wide-Band Cross-Coupled Waveguide Filters

- To develop an approach that can extend the synthesis method for direct-coupled waveguide filters to include the cross-coupled waveguide filters.
- To derive the dimensional synthesis method for cross-coupled wavguide filters without optimization.

1.3.5 Synthesis of Wide-Band Bandpass Filters with Quarter-Wavelength Resonators

- To derive the equivalent network for the quarter-wavelength-resonator bandpass filter.
- To derive an alternative lowpass prototype filter that has the similar form to the equivalent network of the quarter-wavelength-resonator filter.
- To apply the edge frequency mapping to the quarter-wavelength-resonator bandpass filter and derive the synthesis formula.
- To apply the synthesis method to practical filters and derive the dimensional synthesis method.

1.4 Major Contributions

The research work achieved in this Ph.D. dissertation will contributes to the development of the synthesis method for the design of wide-band bandpass filters

without optimization. The major contributions of this dissertation are listed as follows:

1) Propose an edge frequency mapping method that can be applied to the synthesis of wide-band filters. A general model for frequency-dependent K-inverter has been presented, in which the frequency-dependent K-inverter was decomposed into frequency-invariant K-inverter with two exponent-weighted frequency-dependent transformers added on both sides.

2) Propose an improved full-wave model for the waveguide iris, which composed of a frequency-dependent K-inverter with two extra transmission lines on both sides. By applying the edge frequency mapping method, as well as the improved iris model, we derive the synthsis formula and then employ an iteration procedure to synthesize the Chebyshev response without global full-wave optimization. (See Pub. [5])

3) Extend the dimensional sythesis method for direct-coupled waveguide filters to include in-line pseudo-elliptic waveguide filters using the cavity-backed K-inverters, which can produce transmission zeros in the out-of-band response, however, whose frequency response in the passband is similar to that of normal iris inverters. Two novel realizations of the cavity-backed K-inverters are also presented. (See Pub. [6], [8])

4) Extend the dimensional sythesis method for direct-coupled waveguide filters to include in-line pseudo-elliptic waveguide filters using the customized resonators, which can produce transmission zeros in the out-of-band response, however, whose frequency response in the passband is similar to that of normal half-wavelength-transmission-line resonators.

5) Extend the dimensional sythesis method for direct-coupled waveguide filters to include cross-coupled waveguide filters. Two cross-coupled filter network suitable for the synthesis of wide-band Chebyshev passband response were proposed. An direct-coupled network equivalent to the cross-coupled network was derived using the even-mode and odd-mode analysis. The dimensional synthesis procedure was presented for the

design of wide-band cross-coupled waveguide filters without global full-wave optimization. (See Pub. [7])

6) Propose a synthsis method for the design of quarter-wavelength-resonator bandpass filters without global full-wave optimization. An alternative lowpass prototype filter was derived in order to apply the edge frequency mapping method to the equivalent network of the quarter-wavelength-resonator bandpass filter. By applying the synthesis method to rectangular coaxial filters, a dimensional synthesis method was presented for the design of quarter-wavelength-resoantor rectangular coaxial filters without global opimizaion. (See Pub. [3])

1.5 Organization of the Thesis

The Ph.D. dissertation is organized as follows:

In CHAPTER 2, we review some basic theory and techniques for the synthesis of bandpass filters. The traditional synthesis method is first introduced based on the circuit model. We then review some techniques for dealing with the frequency-dispersive inverters in the synthesis of direct-coupled waveguide filters. Finally, we briefly introduce the design techniques for bandpass filters with quarter-wavelength resonators.

In CHAPTER 3, we present a new transformation method, the edge frequency mapping method, for the design of wide-band bandpass filters. In the new mapping method, the distributed-element bandpass filter is directly transformed from the lowpass prototype filter and the reactance values at the center frequency and band edge frequency are employed in the transformation. Besides, a more general approach to deal with the frequency-dispersive inverters is also introduced.

CHAPTER 4 presents a dimensional synthesis method, based on the edge frequency mapping method, for the design of wide-band direct-coupled waveguide bandpass filters without resort to global full-wave optimization. An improved full-wave waveguide iris model is introduced and an iteration procedure is also presented. Some further improvements to the synthesis techniques are introduced finally.

CHAPTER 5 introduces an extended dimensional synthesis method for the design of in-line pseudo-elliptic waveguide filters without resort to global full-wave optimization. In the approach, we employ two novel cavity-backed inverters, which produce transmission zero in the out-of-band response, however, whose frequency response in the passband is similar to that of normal iris inverters. Based on the cavity-backed inverters, a dimensional synthesis method is presented for the design of in-line pseudo-elliptic waveguide filters without global full-wave optimization.

CHAPTER 6 introduces another extension technique for in-line pseudo-elliptic waveguide filters. Alternatively, we employ the customized resonators, which can produce transmission zero in the out-of-band response, however, whose frequency response in the passband is similar to that of normal half-wavelength-transmission-line resonators. Based on the customized resonators, a dimensional synthesis method is presented for the design of in-line pseudo-elliptic waveguide filters without global full-wave optimization.

CHAPTER 7 introduces an extended dimensional synthesis method for the design of symmetric wide-band waveguide cross-coupled filters without resorting to global full-wave optimization. In this method, we introduce two filter circuit models suitable for the synthesis of wide-band cross-coupled filters. Besides, a novel physical realization of the cross-coupled K-inverter is introduced.

CHAPTER 8 introduces a dimensional synthesis method for the design of wide-band quarter-wavelength-resonator bandpass filters. An alternative lowpass prototype filter is proposed to enable the edge frequency mapping method to be applied. By applying the synthesis method to rectangular coaxial filters, a dimensional synthesis method was presented for the design of quarter-wavelength-resoantor rectangular coaxial filters without global opimizaion.

Finally, conclusions and recommendations are made in CHAPTER 9.

CHAPTER 2
LITERATURE REVIEW OF WIDE-BAND BANDPASS FILTERS DESIGN

2.1 Introduction

Since the microwave filters was first designed in 1937 [3], significant developments have taken place over the past seven decades. Here we put our emphasis on some techniques for wide-band filters, especially for waveguide filters. In the second section of this chapter, we will introduce some basic circuit models for the design of bandpass filters. In the third section, we will review some synthesis techniques for waveguide direct-coupled filters in [8] and [79]. In the last section of this chapter, we will review the bandpass filters with quarter-wavelength resonators [95].

2.2 Design of Bandpass Filters Based on Circuit Models

2.2.1 Ladder Network for Lowpass Prototype Filters

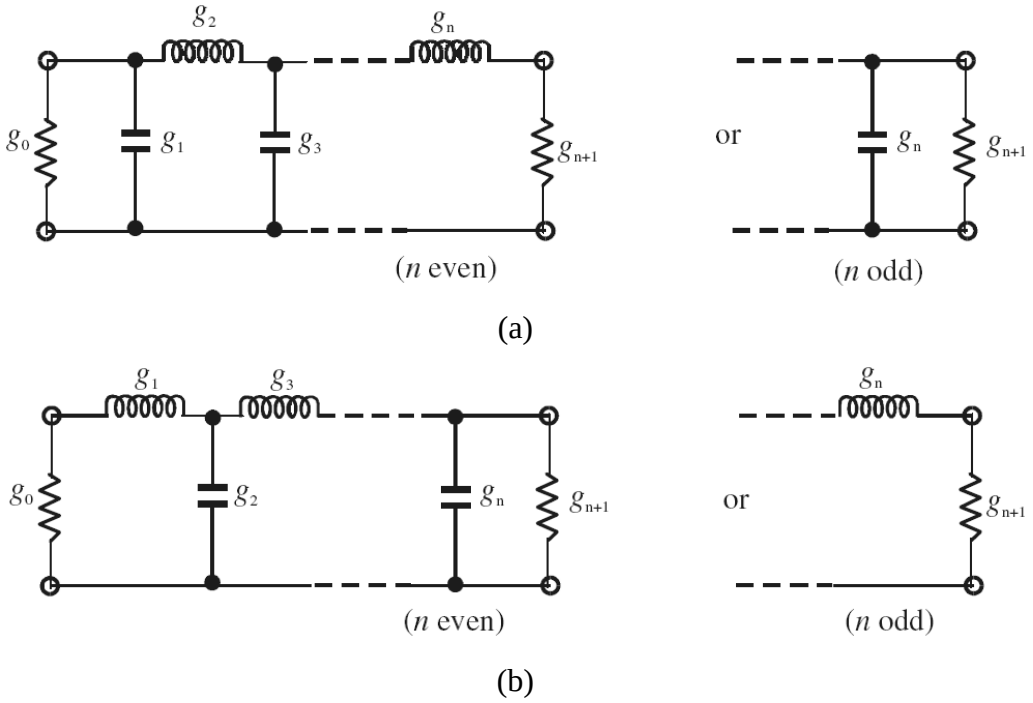

Fig. 2.1 Lowpass prototype filters with (a) a ladder network and (b) its dual.

Two basic ladder networks [78] for *n*-pole lowpass prototype filters are shown in Fig. 2.1, where g_i, for i=1 to n, represent either the inductance of a series inductor or the capacitance of a shunt capacitor; g_0 and g_{n+1} are the resistance or conductance of the source and load, respectively. A lowpass prototype filter is in general defined as the lowpass filter whose element values are normalized to make the source resistance or conductance equal to one, denoted by g_0=1, and cutoff angular frequency to be unity, denoted by Ω_1=1(rad/s).

The two ladder network in Fig. 2.1 can be employed to produce Butterworth or Chebyshev response. For the Chebyshev lowpass prototype filters with a required passband ripple L_{Ar} dB, all the elements in Fig. 2.1 can be calculated as [78]

$$\begin{cases} g_0 = 1 \\ g_1 = \dfrac{2}{\gamma}\sin\left(\dfrac{\pi}{2n}\right) \\ g_i = \dfrac{1}{g_{i-1}} \dfrac{4\sin\left[\dfrac{(2i-1)\pi}{2n}\right]\cdot\sin\left[\dfrac{(2i-3)\pi}{2n}\right]}{\gamma^2+\sin^2\left[\dfrac{(i-1)\pi}{n}\right]} \\ g_{n+1} = \begin{cases} 1 & \text{for } n \text{ odd} \\ \coth^2(\beta/4) & \text{for } n \text{ even} \end{cases} \end{cases}, \tag{2-1}$$

where

$$\begin{cases} \beta = \ln\left[\coth\left(\dfrac{L_{Ar}}{17.37}\right)\right] \\ \gamma = \sinh\left(\dfrac{\beta}{2n}\right) \end{cases}. \tag{2-2}$$

2.2.2 Lowpass Prototype Filters with Immittance Inverters

Immittance inverters are either impedance or admittance inverters, which have the ability to shift impedance or admittance levels depending on the choice of K or J parameters. The impedance inverter, known as K-inverter, has the ABCD matrix expressed as

$$\begin{bmatrix} A & B \\ C & D \end{bmatrix} = \begin{bmatrix} 0 & \mp jK \\ \pm\dfrac{1}{jK} & 0 \end{bmatrix} \quad . \tag{2-3}$$

By using the K-inverters, the ladder network in Fig. 2.1 can be converted to an equivalent circuit as shown in Fig. 2.2, which would be more convient for implementation with microwave structures. The values of K-inverters in Fig. 2.2 can be expressed as

$$\begin{cases} K_{0,1} = \sqrt{\dfrac{Z_0 L_{a1}}{g_0 g_1}} \\ K_{i,i+1} = \sqrt{\dfrac{L_{ai} L_{a(i+1)}}{g_i g_{i+1}}}\Bigg|_{i=1,2.....n-1} \\ K_{n,n+1} = \sqrt{\dfrac{L_{an} Z_{n+1}}{g_n g_{n+1}}} \end{cases} \quad . \tag{2-4}$$

where g_i are the element values of the prototype filters in Fig. 2.1. The element values Z_0, Z_{n+1} and L_{ai} in Fig. 2.2 may be chosen arbitrarily and the filter response will be identical to that of the original prototype, provided that the values of K-inverters are specified as indicated in (2-4).

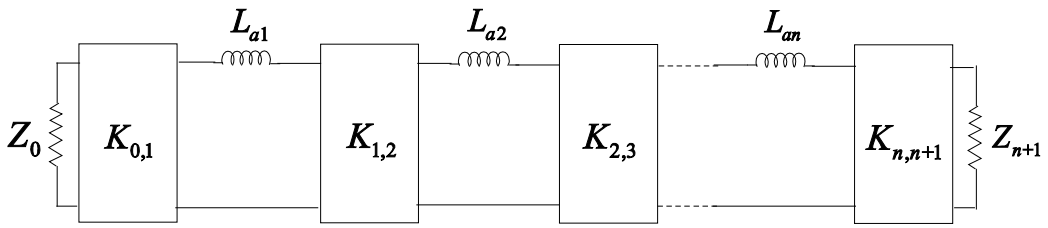

Fig. 2.2 Lowpass prototype filters with immittance inverters.

2.2.3 Bandpass Filters with Lumped-Element Resonators

The bandpass filters can be transformed from the lowpass prototype filter in Fig. 2.2. The required frequency transformation can be expressed as

$$\Omega = \frac{\Omega_1}{FBW}\left(\frac{\omega}{\omega_0} - \frac{\omega_0}{\omega}\right) \tag{2-5}$$

with

$$\begin{cases} FBW = \dfrac{\omega_2 - \omega_1}{\omega_0} \\ \omega_0 = \sqrt{\omega_1 \omega_2} \end{cases}, \tag{2-6}$$

where ω_0 denote the center angular frequency, ω_1 and ω_2 indicate the passband edge angular frequency, and *FBW* is defined as the fractional bandwidth.

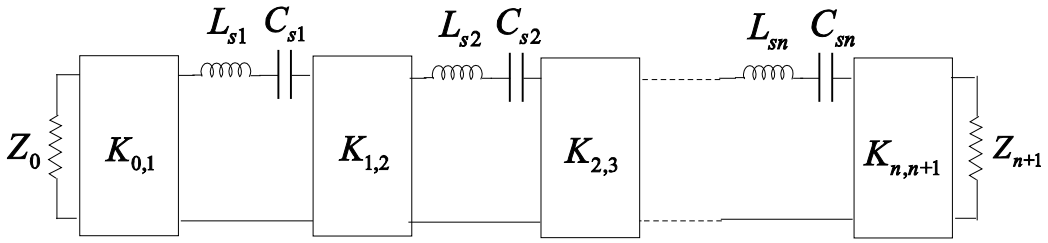

Fig. 2.3 Bandpass filters with lumped-element resonators.

If we apply the frequency transformation to the reactive elements in the lowpass prototype filter in Fig. 2.2, we can get the bandpass filter with lumped-element resonators as shown in Fig. 2.3. The lumped-element resonators can be calculated as

$$\begin{cases} L_{si} = \left(\dfrac{\Omega_1}{FBW\,\omega_0} \right) L_{ai} \\ C_{si} = \dfrac{1}{\omega_0^2 L_{si}} \end{cases}. \tag{2-7}$$

By substituting (2-4) with (2-7), we can get

$$\begin{cases} K_{0,1} = \sqrt{\dfrac{Z_0 FBW\,\omega_0 L_{s1}}{\Omega_1 g_0 g_1}} \\ K_{i,i+1} = \dfrac{FBW\,\omega_0}{\Omega_1} \sqrt{\dfrac{L_{si} L_{s(i+1)}}{g_i g_{i+1}}} \Bigg|_{i=1,2.....n-1} \\ K_{n,n+1} = \sqrt{\dfrac{L_{sn} FBW\,\omega_0 Z_{n+1}}{\Omega_1 g_n g_{n+1}}} \end{cases}. \tag{2-8}$$

2.2.4 Bandpass Filters with Distributed-Element Resonators

Although the bandpass filter in Fig. 2.3 are very useful in ideal circuit applications, it cannot be applied to the practical microwave bandpass filters, because the practical resonators are all distributed elements. So we should deal with the bandpass filter as shown in Fig. 2.4.

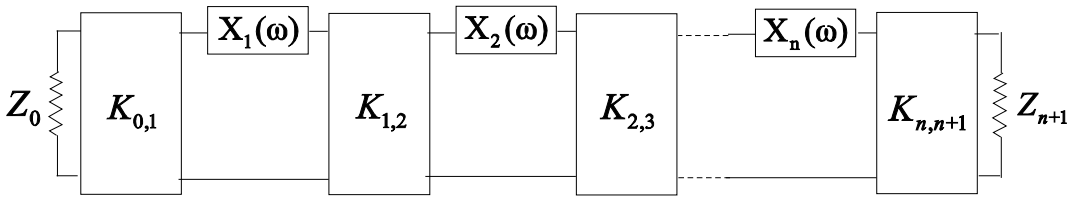

Fig. 2.4 Bandpass filters with distributed-element resonators.

To draw an equivalence between the bandpass filter in Fig. 2.4 and in Fig. 2.3, we should derive a transformation between the distributed-element resonators and the lumped-element resonators. In the traditional method [77]-[78], the distributed-element resonator reactance and reactance slope are made equal to their corresponding lumped-element resonator values at the center frequency. So we can get

$$L_{si} + \frac{1}{\omega_0^2 C_{si}} = \frac{dX_i(\omega)}{d\omega}\bigg|_{\omega=\omega_0} \quad . \tag{2-9}$$

By substituting (2-9) with (2-7), we can get

$$\omega_0 L_{si} = \frac{\omega_0}{2} \cdot \frac{dX_i(\omega)}{d\omega}\bigg|_{\omega=\omega_0} \quad . \tag{2-10}$$

If we define the reactance slope parameter as

$$x_i = \frac{\omega_0}{2} \cdot \frac{dX_i(\omega)}{d\omega}\bigg|_{\omega=\omega_0} \quad , \tag{2-11}$$

we can get $x_i = \omega_0 L_{si}$. By substituting it into (2-8), we can calculate the K-parameter in Fig. 2.4 as

$$\begin{cases} K_{0,1} = \sqrt{\dfrac{Z_0 FBW x_1}{g_0 g_1}} \\ K_{i,i+1} = FBW \sqrt{\dfrac{x_i x_{i+1}}{g_i g_{i+1}}}\Bigg|_{i=1,2.....n-1} \\ K_{n,n+1} = \sqrt{\dfrac{x_n FBW Z_{n+1}}{g_n g_{n+1}}} \end{cases} . \tag{2-12}$$

2.3 Techniques for Direct-Coupled Waveguide Filters

2.3.1 Decomposition of the Frequency-Dependent K-Inverters

In practical applications, all the K-inverters are frequency-dependent, which is different from the ideal K-inverters in Fig. 2.4. In the classic method [8], the K-inverter was approximated to be proportional to frequency. So the frequency-dependent K-inverter is represented by the matrix

$$\begin{bmatrix} 0 & jmK \\ j/mK & 0 \end{bmatrix} , \tag{2-13}$$

where $m = \dfrac{\omega}{\omega_0}$. (2-14)

In order to obtain a K-inverter which is truly frequency-invariant, it is necessary to split matrix (2-13) into three parts:

$$\begin{bmatrix} 0 & jmK \\ j/mK & 0 \end{bmatrix} = \begin{bmatrix} \sqrt{m} & 0 \\ 0 & 1/\sqrt{m} \end{bmatrix} \begin{bmatrix} 0 & jK \\ j/K & 0 \end{bmatrix} \begin{bmatrix} 1/\sqrt{m} & 0 \\ 0 & \sqrt{m} \end{bmatrix} . \tag{2-15}$$

So the frequency-dependent K-inverter has been decomposed into a frequency-invariant K-inverter bounded by two ideal transformers with frequency-dependent turns ratio. The transformers can be absorbed by the adjacent transmission line resonator and the new resonator can be calculated as

$$\begin{bmatrix} 1/\sqrt{m} & 0 \\ 0 & \sqrt{m} \end{bmatrix} \begin{bmatrix} \cos\theta & jZ_0 \sin\theta \\ j\sin\theta/Z_0 & \cos\theta \end{bmatrix} \begin{bmatrix} \sqrt{m} & 0 \\ 0 & 1/\sqrt{m} \end{bmatrix}$$

$$= \begin{bmatrix} \cos\theta & jZ_0 \sin\theta / m \\ jm \sin\theta / Z_0 & \cos\theta \end{bmatrix} \quad . \tag{2-16}$$

The new resonator still can be approximated by a transmission line

$$\begin{bmatrix} \cos\theta^* & jZ_0 \sin\theta^* \\ j \sin\theta^* / Z_0 & \cos\theta^* \end{bmatrix} \quad . \tag{2-17}$$

Near the center frequency, an equivalence between (2-16) and (2-17) can be approximated by

$$\sin\theta^* = \sin\theta / m \quad . \tag{2-18}$$

It is noted from (2-18) that the transmission line has been corrected due to the frequency dependence of K-inverters.

2.3.2 Iris Model with Frequency-Dependent Inverter

In the last section we have introduced the frequency-dependent K-inverters, which were decomposed into frequency-invariant K-inverter bounded by two frequency-dependent transformers. The frequency-dependent transformers can be absorbed by the adjacent resonators to modify the final parameters for K-inverters and resonators. In practical microwave structures for K-inverters, e.g., a waveguide iris, they should be modeled as more than frequency-dependent inverters. An effective full-wave iris model was introduced in [79], as shown in Fig. 2.5, in which the iris is modeled as a frequency-dependent K-inverter with two series reactances added to each side.

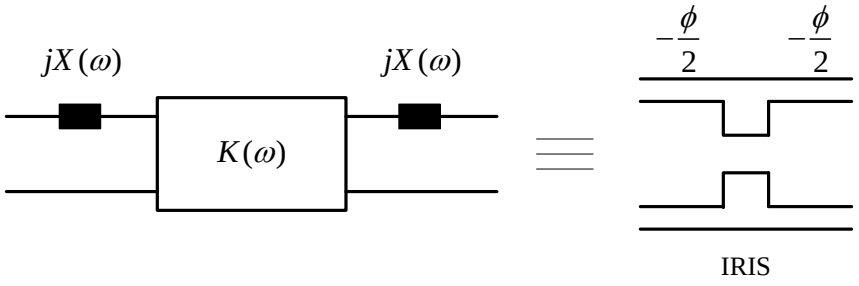

Fig. 2.5 Iris model with frequency-dependent inverter.

The waveguide iris with two negative transmission lines can be analyzed using a full-wave program. The ABCD matrix of the model on the left side of Fig. 2.5 can be calculated as

$$\begin{bmatrix} 1 & jX(\omega) \\ 0 & 1 \end{bmatrix} \begin{bmatrix} 0 & jK(\omega) \\ \dfrac{j}{K(\omega)} & 0 \end{bmatrix} \begin{bmatrix} 1 & jX(\omega) \\ 0 & 1 \end{bmatrix}$$
$$= \begin{bmatrix} -\dfrac{X(\omega)}{K(\omega)} & jK(\omega)\left(1-\dfrac{X^2(\omega)}{K^2(\omega)}\right) \\ \dfrac{j}{K(\omega)} & -\dfrac{X(\omega)}{K(\omega)} \end{bmatrix} \quad . \tag{2-19}$$

If the ABCD matrix derived from the full-wave analysis of the right side of Fig. 2.5 is expressed in the form

$$ABCD = \begin{bmatrix} D_{11}(\omega) & D_{12}(\omega) \\ D_{21}(\omega) & D_{22}(\omega) \end{bmatrix} \quad . \tag{2-20}$$

Then the parameters in (2-19) can be obtained as

$$\begin{cases} K(\omega) = \dfrac{j}{D_{21}(\omega)} \\ X(\omega) = -K(\omega) \cdot D_{11}(\omega) \end{cases} \quad . \tag{2-21}$$

By using the expression above, it is possible to calculate the reactance slope parameters for the series reactance, which can be added to reactance slope parameters of the resonators. This enables a correction factor to be applied to calculate improved inverters. The advantage of the iris model in Fig. 2.5 lies in that two series reactances are included in the model due to the frequency dispersion of the negative transmission lines added on both sides of the iris.

2.4 Bandpass Filters with Quarter-Wavelength Resonators

Usually, bandpass filters are designed with half-wavelength transmission lines, which will resonate at the center frequency. Quarter-wavelength-resonator bandpass filters, as shown in Fig. 2.6, belong to a different type of bandpass filters, which are

composed of quarter-wavelength transmission lines with alternative K-inverters and J-inverters, as well as alternative high and low impedance levels. Advantages over filters with half-wavelength resonators include [95]: shorter length, second passband is centered at $3f_0$ instead of $2f_0$ (f_0 is center frequency), mid-stop-band attenuation is higher, precision design for a prescribed insertion loss characteristic is tractable to greater bandwidths, can be made in "bar transmission line" form without dielectric supports.

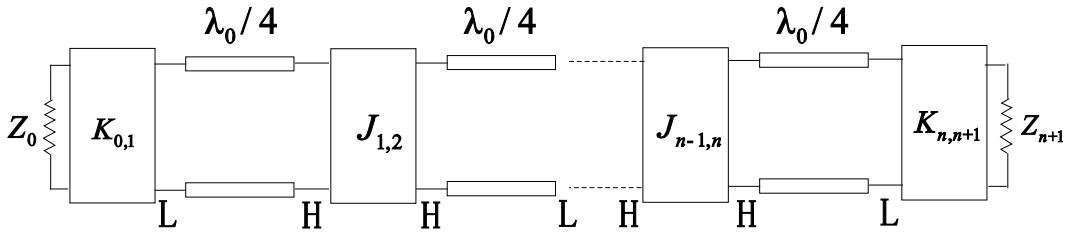

Fig. 2.6 Bandpass filters with quarter-wavelength resonators.

In order to analyze the bandpass filter in Fig. 2.6, we first should derive the equivalent network of the quarter-wavelength transmission lines as shown in Fig. 2.7. The input impedance can be expressed as

$$Z_{in} = Z_0 \cdot \frac{Z_L + jZ_0 \tan\dfrac{\pi\omega}{2\omega_0}}{Z_0 + jZ_L \tan\dfrac{\pi\omega}{2\omega_0}} \quad . \tag{2-22}$$

where Z_0 is the characteristic impedance of the transmission line and ω_0 is the center frequency when the transmission line is quarter wavelength. If $|Z_L| >> Z_0$, (2-22) can be approximated by

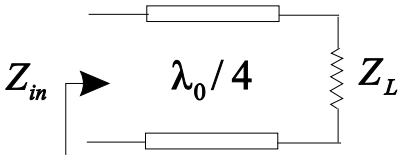

Fig. 2.7 Quarter-wavelength transmission line with a load.

$$Z_{in} \approx Z_0 \cdot \frac{Z_L + jZ_0 \tan\dfrac{\pi\omega}{2\omega_0}}{jZ_L \tan\dfrac{\pi\omega}{2\omega_0}} = jX(\omega) + \frac{Z_0^2}{Z_L} \quad , \tag{2-23}$$

where

$$X(\omega) = -Z_0 \cot\frac{\pi\omega}{2\omega_0} \approx \frac{\pi Z_0}{2}\left(\frac{\omega - \omega_0}{\omega_0}\right) \quad . \tag{2-24}$$

If $|Z_L| << Z_0$, (2-22) can be approximated by

$$Z_{in} \approx Z_0 \cdot \frac{jZ_0 \tan\dfrac{\pi\omega}{2\omega_0}}{Z_0 + jZ_L \tan\dfrac{\pi\omega}{2\omega_0}} = \frac{1}{jB(\omega) + \dfrac{Z_L}{Z_0^2}} \quad , \tag{2-25}$$

where

$$B(\omega) = -Y_0 \cot\frac{\pi\omega}{2\omega_0} \approx \frac{\pi Y_0}{2}\left(\frac{\omega - \omega_0}{\omega_0}\right) \quad . \tag{2-26}$$

It is noted from (2-23) and (2-25) that the quarter-wavelength transmission line with a high level load can be equivalent to a unit K-inverter with a series resonator and the quarter-wavelength transmission line with a low level load can be equivalent to a unit J-inverter with a shunt resonator. The alternative K-inverter and J-inverter can be calculated as [95]

$$\begin{cases} \dfrac{K_{0,1}}{Z_0} = \sqrt{\dfrac{\pi}{2\delta g_0 g_1}} \\ \dfrac{K_{i,i+1}}{Z_0} = \dfrac{\pi}{2\delta}\sqrt{\dfrac{1}{g_i g_{i+1}}}\Bigg|_{i=2,4,6.....}, \quad \dfrac{J_{i,i+1}}{Y_0} = \dfrac{\pi}{2\delta}\sqrt{\dfrac{1}{g_i g_{i+1}}}\Bigg|_{i=1,3,5.....} \\ \dfrac{K_{n,n+1}}{Z_0} = \sqrt{\dfrac{\pi}{2\delta g_n g_{n+1}}}\ \Bigg| n \text{ is even}, \quad \dfrac{J_{n,n+1}}{Y_0} = \sqrt{\dfrac{\pi}{2\delta g_n g_{n+1}}}\ \Bigg| n \text{ is odd} \end{cases} \tag{2-27}$$

and

$$\begin{cases} \delta = \dfrac{\omega_2 + \omega_1}{\omega_2 - \omega_1} \\ \omega_0 = \dfrac{2\omega_1\omega_2}{\omega_1 + \omega_2} \end{cases}, \tag{2-28}$$

where ω_1 and ω_2 are the lower and higher edge angular frequencies, respectively.

2.5 Summary

In this chapter, we have reviewed some basic theory and techniques for the synthesis of bandpass filters. The traditional synthesis method was first introduced based on the circuit model. We then reviewed some techniques to deal with the frequency-dispersive inverters in the synthesis of direct-coupled waveguide filters. Finally, we briefly introduced the design techniques for bandpass filters with quarter-wavelength resonators.

CHAPTER 3
EDGE FREQUENCY MAPPING METHOD FOR THE SYTHESIS OF BANDPASS FILTERS

3.1 Introduction

In the first section of last chapter, we have reviewed the classic synthesis method for the design of bandpass filters. In the method, the distributed-element bandpass filter in Fig. 2.4 is transformed from the lumped-element bandpass filter in Fig. 2.3. Then the reactance slope parameters, defined in (2-11), are introduced to make the distributed resonator reactance and reactance slope equal to their corresponding lumped-resonator values at the center frequency. However, this method has some limitations. The employment of reactance slope parameters assumes that the distributed reactance is linearly dependent of frequency, which is not accurate for waveguide resonators in a wide frequency band.

In the next section of this chapter, we will introduce a new transformation method, the edge frequency mapping method, for the design of wide-band bandpass filters. In the new mapping method, the distributed-element bandpass filter is directly transformed from the lowpass prototype filter and the reactance values at the center frequency and band edge frequency are employed in the transformation. In the following sections, the edge frequency mapping method is then applied to the design of different kinds of bandpass filters, including the distributed-element bandpass filters with frequency-dependent inverters. In the last section, we will discuss the advantage of the edge frequency mapping method over the classic transformation method.

3.2 The Edge Frequency Mapping Method

In the edge frequency mapping method, the distributed-element bandpass filter in Fig. 2.4 is directly transformed from the lowpass prototype filter in Fig. 2.2. The generalized mapping function can be presented as

$$f:\ \Omega L_{ai} \rightarrow X(\omega)\ \ , \tag{3-1}$$

where Ω and ω are employed to represent the angular frequency of the lowpass prototype filter and the bandpass filter, respectively. The transformation should satisfy the following conditions:

$$\begin{cases} X(\omega_0) = 0 \\ \left|X(\omega_1)\right| = \Omega_1 L_{ai} \\ \left|X(\omega_2)\right| = \Omega_1 L_{ai} \end{cases}, \tag{3-2}$$

where ω_0, ω_1 and ω_2 indicate the center angular frequency, lower and upper edge angular frequency of the bandpass filter, respectively, and Ω_1 is the cutoff angular frequency of the lowpass prototype filter. By solving (3-1) and (3-2), we can get

$$\begin{cases} X(\omega_0) = 0 \\ \left|X(\omega_1)\right| = \left|X(\omega_2)\right| \end{cases} \tag{3-3}$$

and

$$\begin{cases} L_{ai} = \left|X(\omega_1)\right| / \Omega_1 \\ f:\ \dfrac{\Omega}{\Omega_1} = \dfrac{X(\omega)}{\left|X(\omega_1)\right|} \end{cases}. \tag{3-4}$$

Equation (3-3) indicates the condition imposed for the bandpass filter and (3-4) presents the mapping function for the transformation from the lowpass prototype filter to the bandpass filter. The K-parameters can be calculated by

$$\begin{cases} K_{0,1} = \sqrt{\dfrac{Z_0 L_{a1}}{g_0 g_1}} \\ K_{i,i+1} = \sqrt{\dfrac{L_{ai} L_{a(i+1)}}{g_i g_{i+1}}}\Bigg|_{i=1,2.....n-1} \\ K_{n,n+1} = \sqrt{\dfrac{L_{an} Z_{n+1}}{g_n g_{n+1}}} \end{cases}, \tag{3-5}$$

where L_{ai} is expressed in (3-4).

It is noted from (3-3) and (3-4) that the reactance values at the center frequency and band edge frequency are employed in the transformation. The edge frequency mapping method is a more general mapping method than the classic transformation method, which will be verified in the following sections. In the following sections, the edge frequency mapping method will be applied to the design of lumped-element bandpass filter and distributed-element bandpass filter, respectively. It will be also applied to the design of distributed-element bandpass filter with frequency-dependent K-inverters.

3.3 Application of the Edge Frequency Mapping Method

3.3.1 Lumpled-Element Bandpass Filters

To verify the edge frequency mapping method, we first apply it to the design of lumped-element bandpass filters in Fig. 2.3. The lumped series resonator can be expressed as

$$X(\omega) = \omega L_{si} - 1/\omega C_{si} \quad . \tag{3-6}$$

So the mapping function can be described as

$$f:\ \Omega L_{ai} \rightarrow \omega L_{si} - 1/\omega C_{si} \quad . \tag{3-7}$$

By applying (3-2), we can get

$$\begin{cases} \omega_0 L_{si} - 1/\omega_0 C_{si} = 0 \\ \omega_1 L_{si} - 1/\omega_1 C_{si} = -\Omega_1 L_{ai} \\ \omega_2 L_{si} - 1/\omega_2 C_{si} = \Omega_1 L_{ai} \end{cases} . \tag{3-8}$$

By solving (3-8), we can obtain

$$\begin{cases} \omega_0 = \sqrt{\omega_1 \omega_2} \\ L_{si} = \Omega_1 L_{ai} / FBW \cdot \omega_0 \\ C_{si} = 1/\omega_0^2 L_{si},\ FBW = (\omega_2 - \omega_1)/\omega_0 \end{cases} \tag{3-9}$$

and

$$f:\ \frac{\Omega}{\Omega_1}=\frac{1}{FBW}\left(\frac{\omega}{\omega_0}-\frac{\omega_0}{\omega}\right) \quad . \tag{3-10}$$

It is noted that (3-9) and (3-10) are the same as (2-5), (2-6) and (2-7) which is introduced in the last chapter.

3.3.2 Distributed-Element Bandpass Filters

Since most practical microwave resonators are distributed elements, the edge frequency mapping method is now applied to the design of distributed-element bandpass filters in Fig. 2.4. Usually, the half-wavelength transmission lines are employed as the distributed-element resonators. In previous theories, e.g., [8], it has been shown that the transmission line near half wavelength can be represented as a series reactance and calculated as

$$X(\omega)=Z_0\sin\theta=Z_0\sin\left(2\pi\cdot\frac{l}{\lambda_g(\omega)}\right) \quad , \tag{3-11}$$

where Z_0, l and $\lambda_g(\omega)$ are the characteristics impedance, length and guided wavelength of the transmission line, respectively. So the mapping function can be presented as

$$f:\ \Omega L_{ai}\rightarrow Z_0\sin\left(2\pi\cdot\frac{l_i}{\lambda_g(\omega)}\right) \quad . \tag{3-12}$$

By applying (3-3) and (3-4), we can get

$$\begin{cases} l_i=\lambda_g(\omega_0)/2 \\ 1/\lambda_g(\omega_1)+1/\lambda_g(\omega_2)=2/\lambda_g(\omega_0) \end{cases} \tag{3-13}$$

and

$$\begin{cases} L_{ai}=(Z_0/\Omega_1)\sin\left[\pi\cdot\lambda_g(\omega_0)/\lambda_g(\omega_1)\right] \\ f:\ \dfrac{\Omega}{\Omega_1}=\dfrac{\sin\left[\pi\cdot\lambda_g(\omega_0)/\lambda_g(\omega)\right]}{\sin\left[\pi\cdot\lambda_g(\omega_0)/\lambda_g(\omega_1)\right]} \end{cases} \quad . \tag{3-14}$$

It is noted from (3-13) that the equivalent inductance L_{ai} is a constant for all the elements. By taking the following notation

$$L_{ai} / Z_0 = \Omega_1 \sin(\pi \cdot \lambda_g(\omega_0) / \lambda_g(\omega_1)) = L \tag{3-15}$$

and substituting (3-15) into (3-5), the K-parameter can be calculated as

$$\begin{cases} K_{0,1} / Z_0 = \sqrt{\dfrac{L}{g_0 g_1}} \\ K_{i,i+1} / Z_0 = \dfrac{L}{\sqrt{g_i g_{i+1}}} \Big| i = 1, 2.....n-1 \\ K_{n,n+1} / Z_0 = \sqrt{\dfrac{L}{g_n g_{n+1}}} \end{cases} . \tag{3-16}$$

3.4 Synthesis of Distributed-Element Bandpass Filters with Frequency-Dependent K-Inverters

3.4.1 Improved Frequency-Dependent Inverters Model

In the above section we have applied the edge frequency mapping method to the design of distributed-element bandpass filters with ideal K-inverters. However, the practical K-inverters are all frequency dependent. To deal with the frequency dispersion problem of K-inverters, we employ an improved inverter model based on [8] which has been reviewed in the last chapter. In the improved model, we employ the weighted exponent in the decomposition of the frequency-dependent K-inverters. Also the transformer turns ratio has a more general definition as

$$m_{i,i+1}(\omega) = K_{i,i+1}(\omega) / K_{i,i+1}(\omega_0) \quad . \tag{3-17}$$

The ABCD matrix of the frequency-dependent K inverters is decomposed as

$$\begin{bmatrix} 0 & jK_{i,i+1}(\omega_0) m_{i,i+1}(\omega) \\ \dfrac{j}{K_{i,i+1}(\omega_0) m_{i,i+1}(\omega)} & 0 \end{bmatrix}$$

$$= \begin{bmatrix} m_{i,i+1}^{i/n}(\omega) & 0 \\ 0 & m_{i,i+1}^{-i/n}(\omega) \end{bmatrix} \begin{bmatrix} 0 & jK_{i,i+1}(\omega_0) \\ \dfrac{j}{K_{i,i+1}(\omega_0)} & 0 \end{bmatrix} \begin{bmatrix} m_{i,i+1}^{i/n-1}(\omega) & 0 \\ 0 & m_{i,i+1}^{1-i/n}(\omega) \end{bmatrix} \quad . \quad (3\text{-}18)$$

According to (3-18), the decomposition of every inverter is shown in Fig. 3.1. It can be seen that the transformer is added only on one side for the first and last inverter by using the weight exponent. So the frequency dependence of the two end inverters can be distributed equally to all the others.

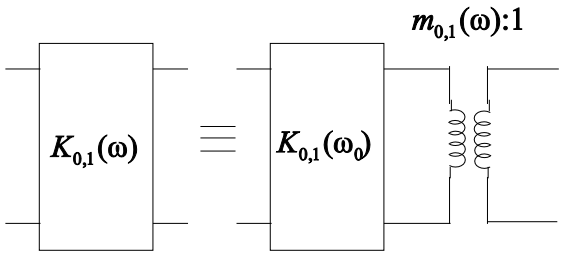

(a)

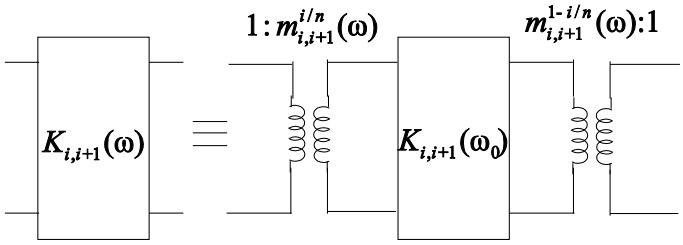

(b)

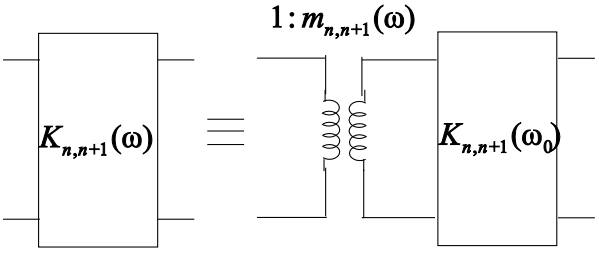

(c)

Fig. 3.1 Decomposition of frequency-dependent K inverters. (a) The first inverter (b) The (i+1)th inverter (c) The last inverter.

3.4.2 Synthesis Using the Edege Frequency Mapping Method

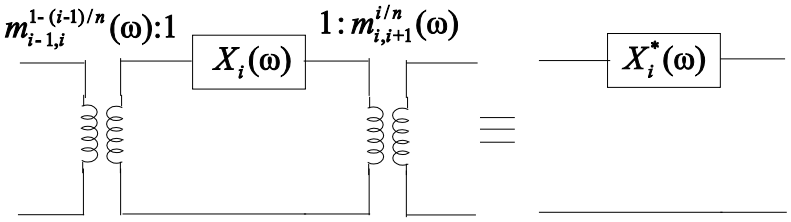

Fig. 3.2 Transformers absorbed by the adjacent resonator elements.

The transformers can be absorbed by the adjacent series resonator elements as shown in Fig. 3.2. The transfer matrix of the new resonator elements is given by

$$\begin{bmatrix} m_{i-1,i}^{(i-1)/n-1}(\omega) & 0 \\ 0 & m_{i-1,i}^{1-(i-1)/n}(\omega) \end{bmatrix} \begin{bmatrix} 1 & jX_i(\omega) \\ 0 & 1 \end{bmatrix} \begin{bmatrix} m_{i,i+1}^{i/n}(\omega) & 0 \\ 0 & m_{i,i+1}^{-i/n}(\omega) \end{bmatrix}$$
$$= \begin{bmatrix} m_{i-1,i}^{(i-1)/n-1}(\omega) \cdot m_{i,i+1}^{i/n}(\omega) & j \cdot m_{i-1,i}^{(i-1)/n-1}(\omega) \cdot m_{i,i+1}^{-i/n}(\omega) \cdot X_i(\omega) \\ 0 & m_{i-1,i}^{1-(i-1)/n}(\omega) \cdot m_{i,i+1}^{-i/n}(\omega) \end{bmatrix} . \quad (3\text{-}19)$$

Since the transformer turns ratio *m* is very close to 1, the following approximation can be made:

$$m_{i-1,i}^{(i-1)/n-1}(\omega) \cdot m_{i,i+1}^{i/n}(\omega) \approx 1 \quad . \quad (3\text{-}20)$$

So the new distributed resonator elements can be also regarded as a series reactance and it is calculated as

$$X_i^*(\omega) = m_{i-1,i}^{(i-1)/n-1}(\omega) \cdot m_{i,i+1}^{-i/n}(\omega) \cdot X_i(\omega) \quad . \quad (3\text{-}21)$$

If the half-wavelength transmission line is employed as the distributed-element resonators, we can substitute (3-21) with (3-11) and get the new reactance as

$$X_i^*(\omega) = m_{i-1,i}^{(i-1)/n-1}(\omega) \cdot m_{i,i+1}^{-i/n}(\omega) \cdot Z_0 \sin\left(\frac{2\pi l_i}{\lambda_g(\omega)}\right) \quad . \quad (3\text{-}22)$$

By applying the edge frequency mapping method to the new resonator, the mapping function can be expressed as

$$f:\ \Omega L_{ai} \rightarrow m_{i-1,i}^{(i-1)/n-1}(\omega)\cdot m_{i,i+1}^{-i/n}(\omega)\cdot Z_0 \sin\left(\frac{2\pi l_i}{\lambda_g(\omega)}\right) \quad . \tag{3-23}$$

By applying (3-3) and (3-4), we can get

$$\begin{aligned} &m_{i-1,i}^{(i-1)/n-1}(\omega_1)\cdot m_{i,i+1}^{-i/n}(\omega_1)\cdot \sin\left(\frac{\pi\cdot\lambda_g(\omega_0)}{\lambda_g(\omega_1)}\right)+ \\ &m_{i-1,i}^{(i-1)/n-1}(\omega_2)\cdot m_{i,i+1}^{-i/n}(\omega_2)\cdot \sin\left(\frac{\pi\cdot\lambda_g(\omega_0)}{\lambda_g(\omega_2)}\right)=0 \end{aligned} \tag{3-24}$$

and

$$\begin{cases} l_i = \dfrac{\lambda_g(\omega_0)}{2} \\ L_{ai} = \dfrac{Z_0}{\Omega_1} m_{i-1,i}^{(i-1)/n-1}(\omega_1)\cdot m_{i,i+1}^{-i/n}(\omega_1)\cdot \sin\left(\dfrac{\pi\cdot\lambda_g(\omega_0)}{\lambda_g(\omega_1)}\right) \end{cases} . \tag{3-25}$$

Equation (3-24) presents the equations that the edge angular frequency should satisfy. It can be noted that the edge angular frequencies ω_1 and ω_2 satisfy different equations for different resonators. However, if all the K-inverters have similar frequency dispersion performance, (3-24) still can be nearly satisfied. The K-parameters can be calculated by substituting (3-5) with (3-25) and the detailed calculation procedure will be introduced in the next chapter. It is also noted from (3-25) that the frequency dependence information of the K-inverters is fully considered and used to correct the K-parameters.

3.5 Discussion

The edge frequency mapping method has been introduced and applied to three kinds of bandpass filters in this chapter. The advantage of the edge frequency mapping method over the traditional mapping method can be summarized as two catagories: 1) more accuracy can be obtained in the band edge frequency so that the method can be applied to the design of bandpass filters with wider bandwidth; 2) the frequency dependence information is fully included in the synthesis so that the method can be

easily applied to the design of bandpass filters with frequency-dependent inverters. The two advantage will be discussed more detailedly as follows.

3.5.1 More Accuracy In The Band Edge Frequency

In the classic transformation method, the distributed-element bandpass filter is transformed from the lumped-element bandpass filter. In the ideal case, the reactance of the distributed-element resonators should equal to that of the lumped-element resonators at all frequencies. In practice, however, they approximate the reactances of the lumped-element resonators only near resonance because only the reactance and reactance slope are made equal to their corresponding lumped-element resonator values at the center frequency. For this, the quantity called the reactance slope parameter is introduced as defined in (2-11).

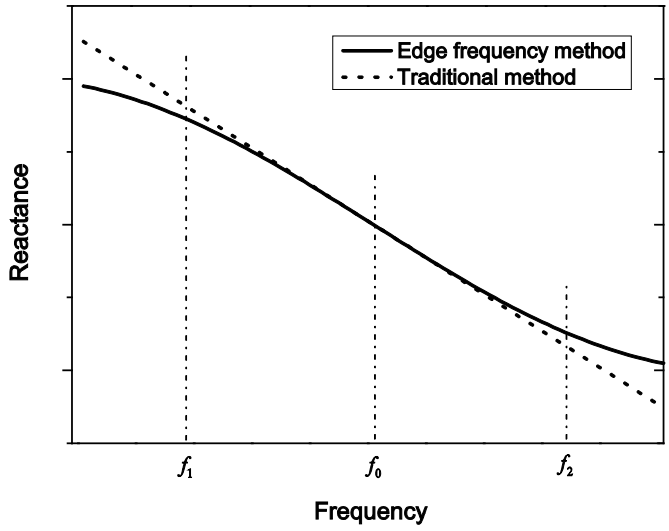

Fig. 3.3 The resonator models employed by the edge frequency method and the traditional transformation method

Fig. 3.3 shows two resonator models employed by the edge frequency mapping method and the traditional transformation method. The solid curve presents the frequency dependence of the resonator reactance, which is directly employed in the edge frequency method. The traditional transformation method employs the tangent line, plotted as the dotted line in Fig. 3.3, to approximate the real reactance curve. It is noted that the tangent line can approximate the curve only near the center frequency. Therefore, for the wide-band filters designed using the traditional

transformation method, the equal-ripple performance will be degraded especially near the edge frequency.

3.5.2 Frequency Dependence Fully Included In the Sythesis

As expressed in (3-25), the frequency dependence information of the K-inverter is fully included and can be used to correct the K-parameters at the center frequency. However, we will prove that, if the traditional mapping method is employed, the frequency dependence information cannot be included in the synthesis. The detailed derivation is given as follows.

Equation (3-21) presents the new series reactance which absorbs the transformer turns ratio decomposed from the frequency-dependent K-inverter and the equation can be written as

$$X_i^*(\omega) = m_{i-1,i}^{(i-1)/n-1}(\omega) \cdot m_{i,i+1}^{-i/n}(\omega) \cdot X_i(\omega) \quad . \tag{3-26}$$

From the definition of the general transformer turns ratio in (3-17), it is noted that the turns ratio should satisfy

$$\begin{cases} m_{i-1,i}(\omega_0) = 1 \\ m_{i,i+1}(\omega_0) = 1 \end{cases} \quad . \tag{3-27}$$

According to the traditional transformation method, the reactance should satisfy

$$X_i^*(\omega_0) = 0 \quad . \tag{3-28}$$

Substituting (3-26) with (3-27) and (3-28), we can get

$$X_i(\omega_0) = 0 \quad . \tag{3-29}$$

According to the definition expressed in (2-11), the reactance slope parameter of the new resonator can be calculated as

$$x = \frac{\omega_0}{2} \cdot \frac{dX_i^*(\omega)}{d\omega}\bigg|_{\omega=\omega_0}$$

$$= \frac{\omega_0}{2} \cdot X_i(\omega_0) \cdot \left. \frac{d(m_{i-1,i}^{1-(i-1)/n}(\omega) \cdot m_{i,i+1}^{-i/n}(\omega))}{d\omega} \right|_{\omega=\omega_0} + \frac{\omega_0}{2} \cdot m_{i-1,i}^{1-(i-1)/n}(\omega_0) \cdot m_{i,i+1}^{-i/n}(\omega_0) \cdot \left. \frac{dX_i(\omega)}{d\omega} \right|_{\omega=\omega_0} \quad . \tag{3-30}$$

Substituting (3-30) with (3-27) and (3-29), we can get

$$x = \frac{\omega_0}{2} \cdot \left. \frac{dX_i(\omega)}{d\omega} \right|_{\omega=\omega_0} \quad . \tag{3-31}$$

It is noted from (3-31) that the frequency dependence information of the K-inverter is not included in the reactance slope parameter of the new resonator. In other words, the frequency dependence of the K-inverters has no contribution to the correction of the K-parameters if we employ the traditional transformation method in the synthesis.

3.6 Summary

In this chapter, we have introduced the edge frequency mapping method for the design of wide-band bandpass filters. In the new mapping method, the distributed-element bandpass filter was directly transformed from the lowpass prototype filter and the reactance values at the center frequency and band edge frequency were employed in the transformation. A more general approach to deal with the frequency-dispersive inverters was also introduced and then the edge frequency mapping method was applied. The advantage of the edge frequency mapping method over the classic method has also been discussed in the chapter.

CHAPTER 4
DIMENSIONAL SYNTHESIS OF WIDE-BAND DIRECT-COUPLED WAVEGUIDE FILTERS

4.1 Introduction

The general procedure for the design of direct-coupled filters was first revised by Cohn [6]. Then Matthaei, Young and Jones [77] introduced a bandwidth contraction factor and a deviation of center frequency for direct-coupled cavity filters to predict the change caused by the frequency-dependent inverters using design graphs. Levy, [8], suggested “ideal transformers with frequency-dependent turns ratio” on both sides of the inverters. However, these techniques still cannot give good in-band equal ripple performance for wide-band waveguide filters, moreover, they do not give the desired dimensional information directly.

A dimensional synthesis procedure for H-plane waveguide iris filters was proposed in [79], in which each waveguide iris is modeled as a frequency-dependent inverter having series reactance on each side. This enables reactance slope parameter corrections to be introduced in the dimensional synthesis procedure. However, the iris model in [79] is still not good enough. The extracted K-inverter is still frequency-dependent though some of its frequency-dependent information is included in the slope parameters of the series reactances in the model. Besides, the parameters are corrected only once in the synthesis procedure and the results could be better if an iteration procedure can be employed.

In the last chapter we have introduced the edge frequency mapping method and applied it to the design of bandpass filters with frequency-dependent inverters. In this chapter we will propose a dimensional synthesis method, based on the edge frequency mapping method, for the design of wide-band direct-coupled waveguide bandpass filters without resort to global full-wave optimization. The theory of the synthsis method will be presented in the second section and two design examples

will be given in the third section. In the last section of this chapter, we will introduced some further improvements to the synthesis techniques.

4.2 Theory

4.2.1 Improved Waveguide Iris Model

In order to apply the edge frequency mapping method to the design of waveguide iris filters, it is necessary to derive an accurate iris model as the K-inverter. The earlier model in [6] gives good results for rather narrow bandwidths and an improved one was proposed in [8], where the frequency dependence of the irises is modeled as ideal inverter with frequency-dependent transformers on each side that can be absorbed by the adjacent resonators. The latest iris model was presented in [79], where the waveguide iris was modeled as a frequency-dependent K-inverter and the series reactances added to each side.

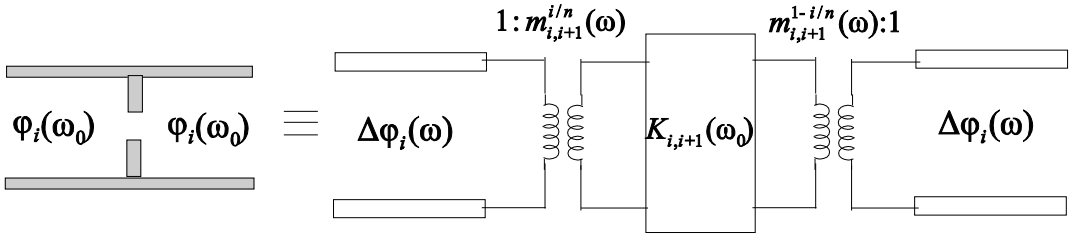

Fig. 4.1 Improved iris model.

In this section, we propose an improved iris model, as shown in Fig. 4.1, which consists of an ideal K-inverter with the exponent-weighted turns ratio and extra transmission lines added on both sides. The extra transmission lines are added on both sides because the K-inverter consists of not only the iris, but also the negative-length compensated transmission lines, whose phases will change with the frequency as the waveguide wavelength changes with the frequency. Actually the series reactance in the iris model [79] also results from the frequency variance of the negative-length compensated transmission lines added on both sides of the waveguide iris. The extra transmission lines in the proposed model here can be presented as

$$\begin{aligned}\Delta\varphi_i(\omega) &= \left(\frac{\lambda_g(\omega_0)}{\lambda_g(\omega)} - 1\right)\varphi_i(\omega_0) \\ &= \left(\sqrt{\frac{\omega^2 - \omega_c^2}{\omega_0^2 - \omega_c^2}} - 1\right)\varphi_i(\omega_0)\end{aligned} \quad , \tag{4-1}$$

where ω_c is the cutoff angular frequency of the waveguide and $\varphi_i(\omega_0)$ is the phase of the negative-length compensated transmission line at the center frequency.

4.2.2 Filter Synthesis

In the improved iris model introduced above, the extra transmission lines and the transformers can be absorbed by the adjacent resonators. By applying (3-22) and (4-1), the new resonator can be expressed as

$$\begin{aligned}X_i(\omega) &= m_{i-1,i}^{(i-1)/n-1}(\omega)\cdot m_{i,i+1}^{-i/n}(\omega) \\ &\cdot Z_0 \sin\left[\frac{2\pi l_i}{\lambda_g(\omega)} + \left(\sqrt{\frac{\omega^2 - \omega_c^2}{\omega_0^2 - \omega_c^2}} - 1\right)\left(\varphi_{i-1}(\omega_0) + \varphi_i(\omega_0)\right)\right]\end{aligned} \quad . \tag{4-2}$$

The mapping function can be written as

$$\begin{aligned}f:\ \omega L_{ai} &\to m_{i-1,i}^{(i-1)/n-1}(\omega)\cdot m_{i,i+1}^{-i/n}(\omega) \\ &\cdot Z_0 \sin\left[\frac{2\pi l_i}{\lambda_g(\omega)} + \left(\sqrt{\frac{\omega^2 - \omega_c^2}{\omega_0^2 - \omega_c^2}} - 1\right)\left(\varphi_{i-1}(\omega_0) + \varphi_i(\omega_0)\right)\right]\end{aligned} \quad . \tag{4-3}$$

By applying (3-4), we can get

$$\begin{cases} l_i = \lambda_g(\omega_0)/2 \\ L_{ai} = (Z_0/\Omega_1)\cdot m_{i-1,i}^{(i-1)/n-1}(\omega_1)\cdot m_{i,i+1}^{-i/n}(\omega_1) \\ \qquad \cdot \sin\left[\pi\cdot\sqrt{\frac{\omega_1^2 - \omega_c^2}{\omega_0^2 - \omega_c^2}} + \left(\sqrt{\frac{\omega_1^2 - \omega_c^2}{\omega_0^2 - \omega_c^2}} - 1\right)\left(\varphi_{i-1}(\omega_0) + \varphi_i(\omega_0)\right)\right] \end{cases} \quad . \tag{4-4}$$

The K-parameters at the center frequency can be calculated using the equivalent inductance L_{ai} by substituting (3-5) with (4-4). However, the calculation of L_{ai} involves the turns ratio *m*, whose definition involves the K-parameters at the center

frequency. In order to calculate the required K-parameters at the center frequency, we employ an iteration procedure.

$K_{i,i+1}^{(j)}(\omega_0)$, $\varphi_i^{(j)}(\omega_0)$ and $L_{ai}^{(j)}$ are used to represent all the parameters after *j* iterations. The parameters after *j* iterations can be calculated by the parameters after (*j*-1) iterations using the formula

$$L_{ai}^{(j)} = \frac{Z_0}{\Omega_1} \cdot \left[\frac{K_{i-1,i}^{(j-1)}(\omega_1)}{K_{i-1,i}^{(j-1)}(\omega_0)} \right]^{(i-1)/n-1} \cdot \left[\frac{K_{i,i+1}^{(j-1)}(\omega_1)}{K_{i,i+1}^{(j-1)}(\omega_0)} \right]^{-i/n} \cdot \sin\left[\pi \cdot \sqrt{\frac{\omega_1^2 - \omega_c^2}{\omega_0^2 - \omega_c^2}} + \left(\sqrt{\frac{\omega_1^2 - \omega_c^2}{\omega_0^2 - \omega_c^2}} - 1 \right) \left(\varphi_{i-1}^{(j-1)}(\omega_0) + \varphi_i^{(j-1)}(\omega_0) \right) \right] , \quad (4\text{-}5)$$

$$\begin{cases} K_{0,1}^{(j)}(\omega_0) = \sqrt{\dfrac{Z_0 L_{a1}^{(j)}}{g_0 g_1}} \\ K_{i,i+1}^{(j)}(\omega_0) = \left. \sqrt{\dfrac{L_{ai}^{(j)} L_{a(i+1)}^{(j)}}{g_i g_{i+1}}} \right|_{i=1,2,\ldots,n-1} \\ K_{n,n+1}^{(j)}(\omega_0) = \sqrt{\dfrac{L_{an}^{(j)} Z_{n+1}}{g_n g_{n+1}}} \end{cases} . \quad (4\text{-}6)$$

It can be noted that (19) and (20) gives the calculation formulae for $L_{ai}^{(j)}$ and $K_{i,i+1}^{(j)}(\omega_0)$ but the formula for $K_{i,i+1}^{(j)}(\omega_1)$ and $\varphi_i^{(j)}(\omega_0)$ is not provided. Actually, these two parameters can be calculated from $K_{i,i+1}^{(j)}(\omega_0)$ using the cubic spline data interpolation functions, which will be introduced in the following section.

Since this is an iteration procedure, we should set initial parameters for the iteration. Actually, the initial parameters $K_{i,i+1}^{(0)}(\omega_0)$, $K_{i,i+1}^{(0)}(\omega_1)$, $\varphi_i^{(0)}(\omega_0)$ and $L_{ai}^{(0)}$ can be calculated using the ideal K-inverter model. For the ideal K-inverter, the exponent-weighted turns ratio and extra transmission lines are not considered. So the calculation of $L_{ai}^{(0)}$ is a compact form of (4-4) and it is written as

$$L_{ai}^{(0)} = \frac{Z_0}{\Omega_1} \cdot \sin\left(\pi \cdot \sqrt{\frac{\omega_1^2 - \omega_c^2}{\omega_0^2 - \omega_c^2}} \right) = L \quad . \quad (4\text{-}7)$$

Substituting (3-5) with (4-7), we can get

$$\begin{cases} K_{0,1}^{(0)}(\omega_0) = \sqrt{\dfrac{Z_0 L}{g_0 g_1}} \\ K_{i,i+1}^{(0)}(\omega_0) = \left.\dfrac{L}{\sqrt{g_i g_{i+1}}}\right|_{i=1,2,\ldots,n-1} \\ K_{n,n+1}^{(0)}(\omega_0) = \sqrt{\dfrac{L Z_{n+1}}{g_n g_{n+1}}} \end{cases} . \tag{4-8}$$

The other two initial parameters $K_{i,i+1}^{(0)}(\omega_1)$ and $\varphi_i^{(0)}(\omega_0)$ can be also calculated from $K_{i,i+1}^{(0)}(\omega_0)$ using the cubic spline data interpolation method introduced in the following section.

4.2.3 Iris Element Parameters Extraction

The bandpass filter realized in a rectangular waveguide is depicted in Fig. 4.2. In order to achieve the required Chebyshev response, the widths of the irises and the resonator lengths must be derived.

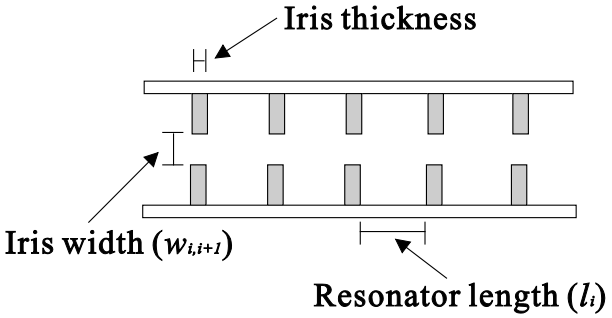

Fig. 4.2 H-plane waveguide bandpass filter.

For a given iris dimension, we can calculate the scattering parameters using a mode-matching program. The K-parameters and the phase of the compensated transmission line for the K-inverter can be calculated using the scattering parameters of the waveguide iris as [96]

$$K_{i,i+1}(\omega) = \sqrt{\frac{1-\left|S_{11}(\omega)_i\right|}{1+\left|S_{11}(\omega)_i\right|}} \tag{4-9}$$

and

$$\varphi_i(\omega) = \frac{1}{2}(\angle S_{11}(\omega)_i - \pi) \quad . \tag{4-10}$$

where $S_{11}(\omega)_i$ is the reflection coefficient of the iris element.

It is noted from (4-9) that it is very easy and fast to calculate the K-parameters for a given iris dimension by employing the mode-matching program. However, we usually need to calculate the iris dimension for the required K-parameters, which will cost much time if a search or matching program based on the mode-matching [79] is employed.

Here we use the cubic spline data interpolation to calculate the iris dimension and other parameters $K_{i,i+1}(\omega_1)$ and $\varphi_i(\omega_0)$. First we employ a mode-matching program to calculate the scattering parameters of the iris with a series of widths $[w]$. Then the sampling data of the K-parameters at the center frequency $[K(\omega_0)]$, the K-parameters at the lower edge frequency $[K(\omega_1)]$ and the phase of the compensated transmission line at the center frequency $[\varphi(\omega_0)]$ can be calculated using (4-9) and (4-10). With these sampling data, we can obtain the cubic spline functions. The relations among $w_{i,i+1}$, $K_{i,i+1}(\omega_0)$, $K_{i,i+1}(\omega_1)$ and $\varphi_i(\omega_0)$ can be expressed as

$$\begin{cases} w_{i,i+1} = S\left([K(\omega_0)],[w],K_{i,i+1}(\omega_0)\right) \\ \varphi_i(\omega_0) = S\left([K(\omega_0)],[\varphi(\omega_0)],K_{i,i+1}(\omega_0)\right) \\ K_{i,i+1}(\omega_1) = S\left([K(\omega_0)],[K(\omega_1)],K_{i,i+1}(\omega_0)\right) \end{cases} , \tag{4-11}$$

where the function $S([a],[b],x)$ denotes the cubic spline interpolation function based on the sampling data $[a]$ and $[b]$ and x is the interpolation variable. After the compensated transmission line phase $\varphi_i(\omega_0)$ is calculated, the lengths of the transmission-line resonator are given by

$$l_i = \frac{\lambda_g(\omega_0)}{2\pi}\left[\pi + \varphi_{i-1}(\omega_0) + \varphi_i(\omega_0)\right] \quad . \tag{4-12}$$

With this approach, the iris element parameters extracted using the mode-matching program is performed only one time and the sampling data can be calculated. The approach, therefore, presents a calculation procedure with the advantage that the solution is always possible and occurs rapidly, which is even faster than the matching approach in [79].

4.2.4 Design Procedure

The flow diagram of the design procedure is shown in Fig. 4.3, which comprises the following steps:

Step 1) First we should determine the center frequency and lower edge frequency according to the filter design requirement. Then different iris elements with a series of widths are chosen and the mode-matching program is employed to calculate the scattering parameters at the center frequency and lower edge frequency. By applying (4-9) and (4-10), the sampling data of the K-parameters at the center frequency and the lower edge frequency and the phase of the compensated transmission line are calculated.

Step 2) The ideal K-inverter model is employed to calculate the initial parameters $K_{i,i+1}^{(0)}(\omega_0)$ by applying (4-7) and (4-8). The other two initial parameters $K_{i,i+1}^{(0)}(\omega_1)$ and $\varphi_i^{(0)}(\omega_0)$ are obtained using the cubic spline data interpolation in (4-11) together with the sampling data in Step 1).

Step 3) Based on the initial parameters in Step 2), the improved iris model in Fig. 4.1 is then established. The corrected K-parameters at the center frequency $K_{i,i+1}^{(1)}(\omega_0)$ are calculated according to (4-5) and (4-6). Using the cubic spline data interpolation in (4-11) together with the sampling data in Step 1), the other two corrected parameters $K_{i,i+1}^{(1)}(\omega_1)$ and $\varphi_i^{(1)}(\omega_0)$ are obtained.

Step 4) A further improved iris model is then established based on the corrected parameters. By repeating Step 3), all the parameters $K_{i,i+1}^{(j)}(\omega_0)$, $K_{i,i+1}^{(j)}(\omega_1)$ and $\varphi_i^{(j)}(\omega_0)$ will be further corrected.

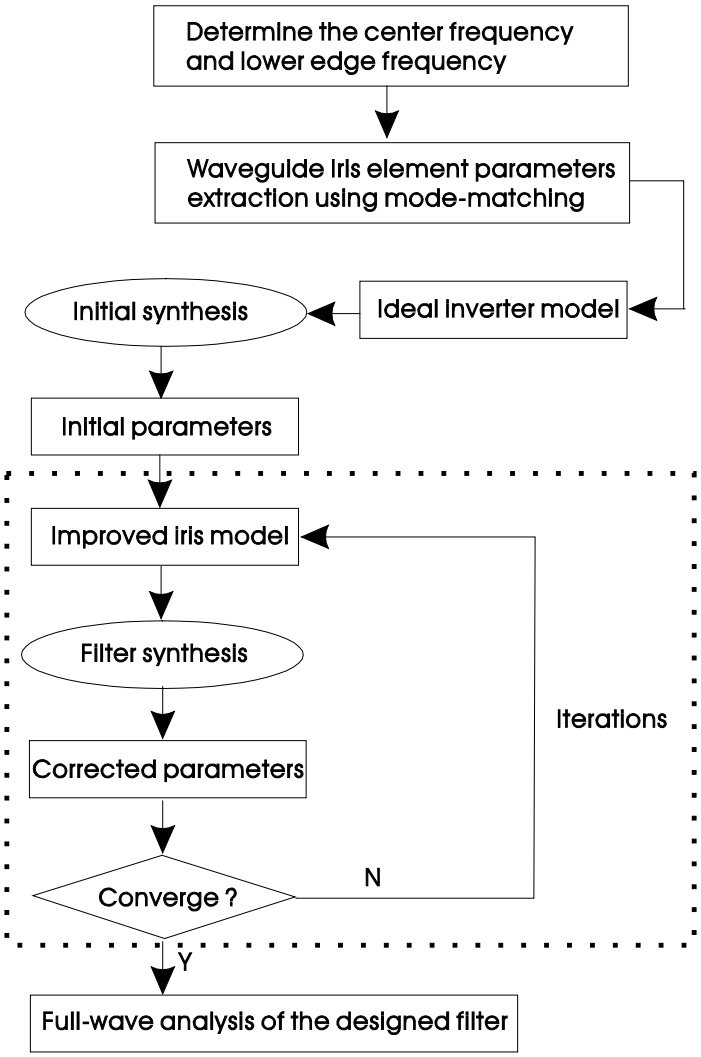

Fig. 4.3 Flow diagram of the design procedure.

Step 5) The Step 3) and Step 4) are repeated until the K-parameters $K_{i,i+1}^{(N)}(\omega_0)$ converge after N iterations. With the converged K-parameters, the iris widths and the resonator lengths are calculated using (4-11) and (4-12). Finally, a full-wave analysis of the computed filter is carried out before the designed filter is fabricated and measured.

4.2.5 Discussion

It is necessary to discuss the advantage of the proposed dimensional synthesis method over the latest method in [79]. Firstly, for the iris model in [79], which is composed of a frequency-dependent K-inverter with two series reactance on each

side, only the frequency dispersion of the series reactance is employed to correct the K-parameters. The K-inverter is still frequency-dependent and it is not decomposed into a frequency-invariant K-inverter with two frequency-dependent transformers on both sides. Therefore, the frequency dependence information of the K-inverter is not fully employed to correct the K-parameters. In the proposed iris model, the extra transmission lines are similar to the series reactance in [79]; however, the frequency-dependent K-inverter is further decomposed into frequency-invariant K-inverter with two frequency-dependent transformers on each side. Second, the proposed synthesis approach is based on the edge frequency mapping method while the synthesis approach in [79] is based on the traditional mapping method. The advantage of the edge frequency mapping method over the traditional method has been discussed in the last chapter. Finally, the design procedure in [79] corrects the K-parameters only once. The proposed synthesis method employs an iteration procedure to correct the K-parameters until they converge, which is supposed to obtain better performance.

4.3 Design Examples and Results

The previous theories of [8] do not give good results especially for a small number of cavities with a wide bandwidth requirement. This is thought to be due to the effect of the end irises and the frequency dependence of the K-inverters, which are taken into account here by using the improved iris model with the exponent-weighted transformers as well as extra transmission lines. The filters here are designed without global full-wave optimizations and are fabricated without tuning screws. Fig. 4.4 shows the convergence of the K-parameters after j iterations. It can be noted from the figure that the K-parameters converge very quickly after only about 5 iterations. So the whole design procedure takes only a few seconds in a modern personal computer after the iris element parameters are extracted using a mode-matching program. Two examples of four-pole filters with different bandwidths are presented here. WR90 waveguide (22.86mm$\times$10.16mm) is chosen as the house waveguide and the iris thickness is 1.5 mm. The other dimensions for the two filters are listed in Table I. The mode-matching program [105] and software CST Microwave Studio [97] are employed to calculate the theoretical scattering parameters before they are fabricated and measured using a vector network analyzer.

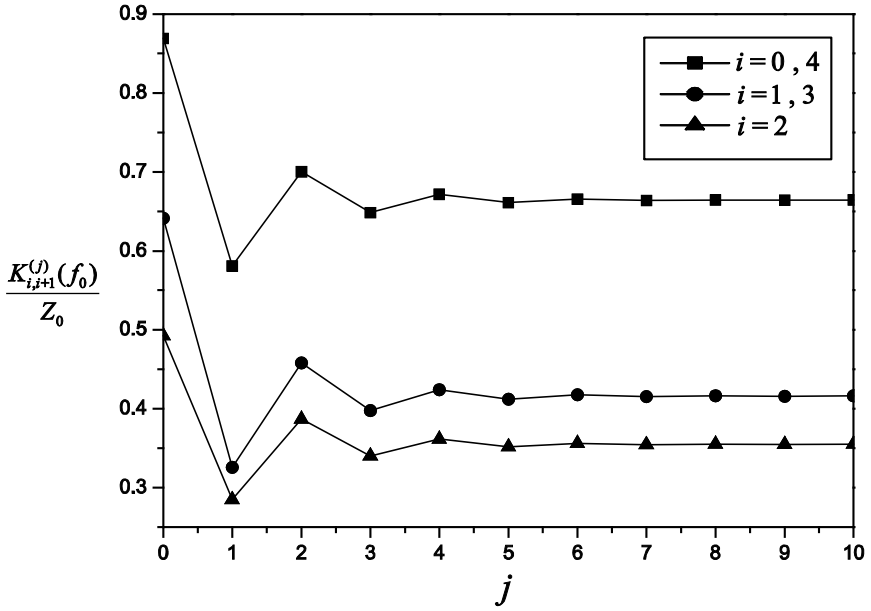

Fig. 4.4 The convergence of K-parameters after *j* iterations.

Table I: DIMENSIONS FOR THE FILTERS (UNITS: MILLIMETERS)

Bandwidth	$w_{0,1}$, $w_{4,5}$	$w_{1,2}$, $w_{3,4}$	$w_{2,3}$	l_1, l_4	l_2, l_3
17.6%	15.18	12.25	11.54	12.40	14.08
20.2%	15.85	13.03	12.25	11.78	13.32

Fig. 4.5 shows the fabricated photograph of the four-pole waveguide filter and Fig. 4.6 shows the measured and calculated scattering parameters for the four-pole waveguide iris filter with a 17.6% fractional bandwidth. It is noted from the figure that the scattering parameters of the measured results agree well with the calculated results. The equal ripple performance of the filter is also very good within the whole bandwidth (9.25-11.01 GHz). To show the advantage of the proposed method, comparisons between the full-wave curves using the classic method [8], the latest synthesis method [79] and the proposed method in this chapter are given in Fig. 4.7. The four-pole filter is designed for 20.2% fractional bandwidth (9.16-11.19 GHz). For such a wide bandwidth requirement, the equal ripple performance of the filter designed using the classic method in [8] is seriously degraded. It can be also seen

from the figure that the equal ripple performance of the filter designed using the proposed method is better than that using the latest synthesis method in [79].

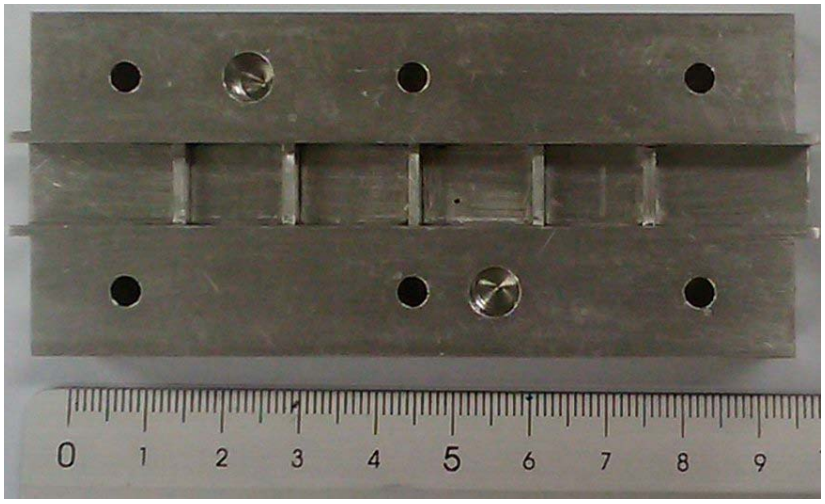

Fig. 4.5 Fabrication photograph of the four-pole waveguide filter.

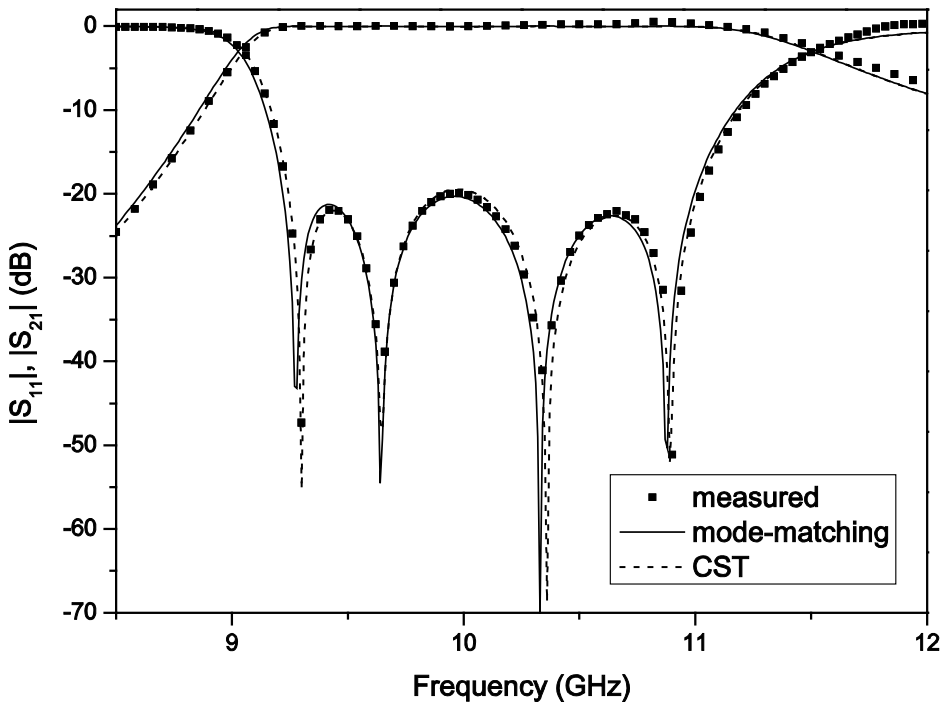

Fig. 4.6 Simulated and measured scattering parameters of the waveguide iris filters: Four-pole filter, 16.7% fractional bandwidth.

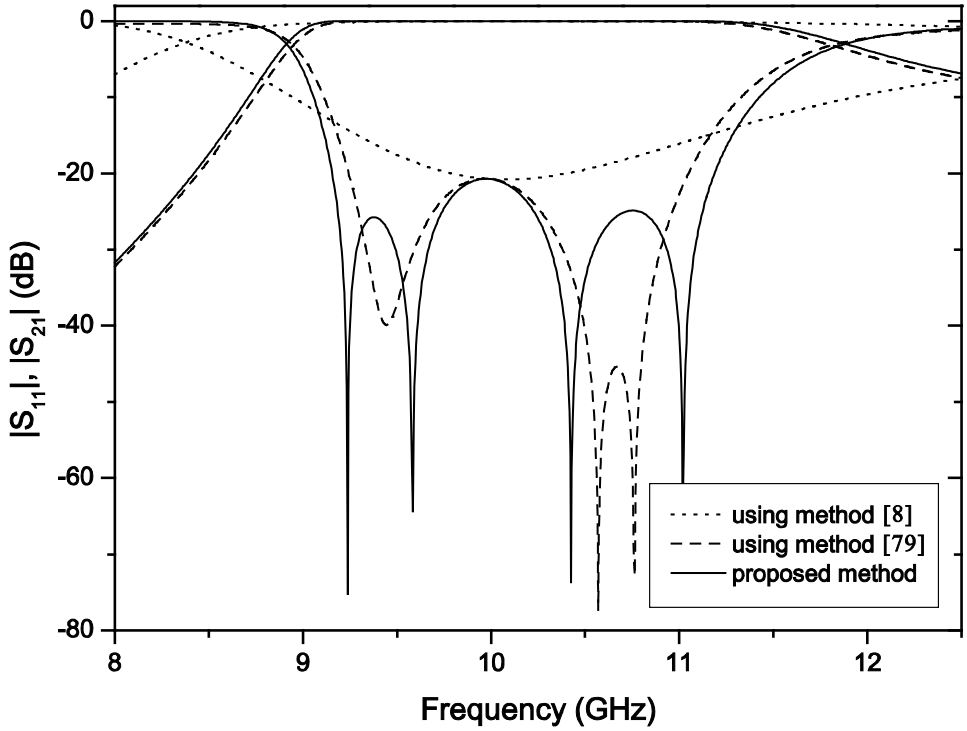

Fig. 4.7 Comparison between full-wave curves using the classic method [8], method [79] and with the proposed method: Four-pole filter, 20.2% fractional bandwidth.

4.4 Further Improvements

In the improved iris model in Fig. 4.1, two extra transmission lines are added on both sides of the frequency-dependent K-inverter and the phase of the extra transmission line is calculated using (4-1). However, we did not consider the frequency dispersion of the phase of the scattering parameters of the waveguide iris in the derivation of (4-1). If the phase of the scattering parameters of the waveguide iris is significantly frequency-dispersive, we need to consider it in the derivation. Therefore, it is necessary to derive a general formula for the extra transmission line in the improved waveguide iris model.

The network representation of the K-inverter using the scattering parameters of the waveguide iris is shown in Fig. 4.8, in which the left side is the scattering parameters of the waveguide iris with two compensate transmission lines and the right side is a frequency-dependent K-inverter with two extra transmission lines. On the left side, the phase of S_{11} can be expressed as

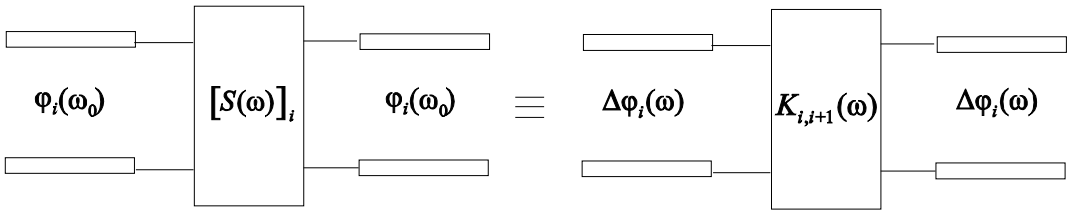

Fig. 4.8 Network representation of the K-inverter using the waveguide iris.

$$\angle S_{11}^{L} = \angle S_{11}(\omega)_i - 2\varphi_i(\omega_0)\cdot\sqrt{\frac{\omega^2-\omega_c^2}{\omega_0^2-\omega_c^2}} \quad . \tag{4-13}$$

By substituting (4-13) with (4-10), we can get

$$\angle S_{11}^{L} = \pi \quad 2\varphi_i(\omega) - 2\varphi_i(\omega_0)\cdot\sqrt{\frac{\omega^2-\omega_c^2}{\omega_0^2-\omega_c^2}} \quad . \tag{4-14}$$

The phase of S_{11} on the right side of Fig. 4.8 can be calculated as

$$\angle S_{11}^{R} = \pi 2 \quad \Delta\varphi_i(\omega) \quad . \tag{4-15}$$

Since the two phases in (4-14) and (4-15) should be the same, we can get

$$\Delta\varphi_i(\omega) = \varphi_i(\omega_0)\cdot\sqrt{\frac{\omega^2-\omega_c^2}{\omega_0^2-\omega_c^2}} - \varphi_i(\omega) \quad . \tag{4-16}$$

It is noted that (4-16) will be the same as (4-1) if the frequency dispersion is not considered for the phase of the scattering parameters of the waveguide iris. Since the calculation of the extra transmission line is corrected, the iteration formula (4-5) and (4-6) should also be corrected as

$$\begin{aligned} L_{ai}^{(j)} = \frac{Z_0}{\Omega_1}\cdot\left[\frac{K_{i-1,i}^{(j-1)}(\omega_1)}{K_{i-1,i}^{(j-1)}(\omega_0)}\right]^{(i-1)/n-1}\cdot\left[\frac{K_{i,i+1}^{(j-1)}(\omega_1)}{K_{i,i+1}^{(j-1)}(\omega_0)}\right]^{-i/n}\cdot\sin\left[\pi\cdot\sqrt{\frac{\omega_1^2-\omega_c^2}{\omega_0^2-\omega_c^2}}\right. \\ \left. +\sqrt{\frac{\omega_1^2-\omega_c^2}{\omega_0^2-\omega_c^2}}\left(\varphi_{i-1}^{(j-1)}(\omega_0)+\varphi_i^{(j-1)}(\omega_0)\right)-\left(\varphi_{i-1}^{(j-1)}(\omega_1)+\varphi_i^{(j-1)}(\omega_1)\right)\right] \end{aligned} \tag{4-17}$$

and

$$\begin{cases} K_{0,1}^{(j)}(\omega_0) = \sqrt{\dfrac{Z_0 L_{a1}^{(j)}}{g_0 g_1}} \\ K_{i,i+1}^{(j)}(\omega_0) = \sqrt{\left.\dfrac{L_{ai}^{(j)} L_{a(i+1)}^{(j)}}{g_i g_{i+1}}\right|_{i=1,2,\ldots,n-1}} \\ K_{n,n+1}^{(j)}(\omega_0) = \sqrt{\dfrac{L_{an}^{(j)} Z_{n+1}}{g_n g_{n+1}}} \end{cases} . \qquad (4\text{-}18)$$

The iteration formula (4-17) and (4-18) are more general than (4-5) and (4-6), especially for those K-inverters whose phase is significantly frequency-dispersive, e.g., the cavity-backed K-inverters which will be introduced in the next chapter.

4.5 Summary

In this chapter, we have presented a dimensional synthesis method, based on the edge frequency mapping method, for the design of wide-band direct-coupled waveguide bandpass filters without resort to global full-wave optimization. An improved iris model was introduced and an iteration procedure was also presented. As design examples, two filters with fractional bandwidth of 16.7% and 20.2% were designed, respectively. Finally, a more accurate phase is derived for the waveguide iris model and an improved synthesis formula is introduced.

CHAPTER 5
WIDE-BAND IN-LINE PSEUDO-ELLIPTIC WAVEGUIDE FILTERS WITH CAVITY-BACKED INVERTERS

5.1 Introduction

Generally, pseudo-elliptic filters are designed according to three slightly different approaches. Cross-coupled resonator filters [17] are well known as the first approach, in which the destructive interference is introduced by multiple paths to produce transmission zeros. The generation of real transmission zeros in this approach often requires coupling coefficients of mixed signs. The second approach known as extracted pole technique [80] was a breakthrough which allows the individual control of transmission zeros. Compared with the cross-coupled techniques, the extracted pole technique has its advantage in that it can generate transmission zeros individually and requires the coupling coefficients of only one type. Despite these advantages, the extracted pole technique has its drawbacks in that the assumed constant phase shifts in the main line are not readily realized or even adequately approximated except for narrowband applications. Some flexibility was added with the concept of nonresonating nodes in [81]-[82]. The phase shifts in the main line of the filter are eliminated and replaced by constant reactance to reduce the effect of dispersion. This technique allows the design process to be modular [83] or to have some interesting topologies [84] avoiding the use of phase shifts inherent in the extracted pole technique. Two applications of nonresonating nodes technique are reported in [85]-[86].

Although the three approaches mentioned above are widely employed to design pseudo-elliptic waveguide filters, they are only applicable to narrowband cases. Due to the frequency dispersion of coupling coefficients, excessive global full-wave optimizations has to be employed in the design of wide-band pseudo-elliptic

waveguide filters. So far no synthesis method has been reported for the design of wide-band pseudo-elliptic waveguide filters without global full-wave optimization.

In the last chapter a dimensional synthesis approach has been proposed for the design of wide-band direct-coupled waveguide filters without resorting to circuit or full-wave optimization. However, this technique is only applicable to the design of waveguide filters with Chebyshev responses. In this chapter, we will extend the synthesis technique to include in-line pseudo-elliptic waveguide filters. In the extended approach, we will employ two novel cavity-backed inverters, which produce transmission zero (TZ) in the out-of-band response, however, whose frequency response in the passband is similar to that of normal iris inverters. The realization of the cavity-backed inverters is left till Section 5.3.1. The design procedures for the passband and out-of-band filter responses are carried out separately. For the out-of-band response, the TZs are produced and individually controlled by cavity-backed inverters. For the passband response, since the cavity-backed inverters behave similar to normal iris inverters, an equal-ripple Chebyshev response is synthesized using the technique introduced in the previous chapter.

In the second section of this chapter, we will introduce the theory of the extended dimensional synthesis method. In the third and fourth section, three design examples and one experimental validation will be presented. In the last section, the advantage and limitation will be discussed.

5.2 Theory

5.2.1 Design Requirements for the Cavity-Backed Inverter

As one of the key parts in the synthesis, the design of cavity-backed inverters is very important. Fig. 5.1 shows the required K-parameter for the cavity-backed inverter and its comparison with that of the normal iris inverter. The normalized K-parameter is calculated by the equation

$$K = \sqrt{\frac{1-|S_{11}(\omega)|}{1+|S_{11}(\omega)|}} \quad , \tag{5-1}$$

where $S_{11}(\omega)$ is the reflection coefficient of the inverter at the angular frequency ω. As shown in Fig. 5.1, the cavity-backed inverter should produce a TZ at ω_z (when K is zero), and its frequency response should be similar to that of the normal iris inverter in the passband ($\omega_1 \leq \omega \leq \omega_2$). Besides, it is required that the position of the TZ can be individually controlled by some parameters of the cavity-backed inverter and the K-parameter in the passband can be adjusted by other independent parameters.

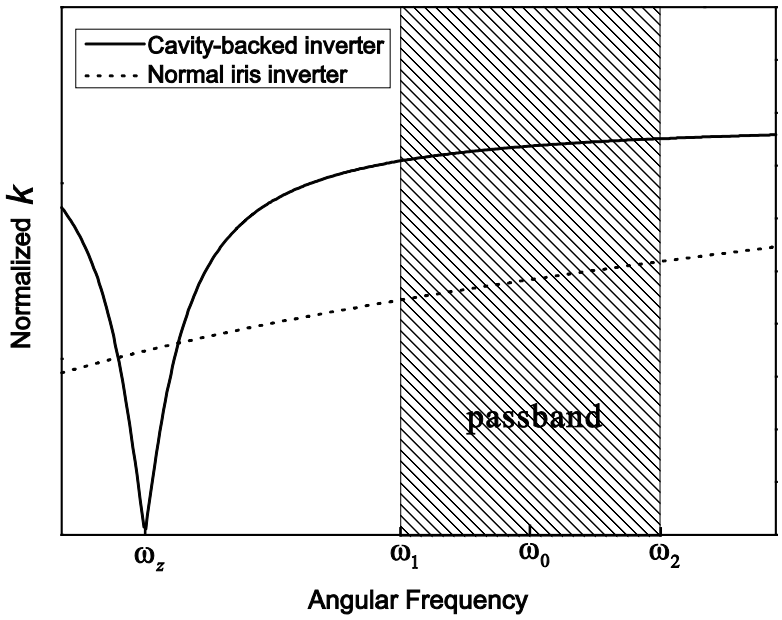

Fig. 5.1 The required frequency dependence of K-parameter for the cavity-backed inverter.

If the cavity-backed inverter satisfies the above requirements, we can substitute it for an iris inverter in the waveguide iris filter. Then we can obtain an equal-ripple chebyshev response in the passband ($\omega_1 \leq \omega \leq \omega_2$) by using the synthesis technique introduced in the last chapter. Also, the input impedance of the filter is purely imaginary at ω_z since the K-parameter of the cavity-backed inverter reaches zero. So the TZ of the cavity-backed inverter is also that of the whole filter. Therefore, a pseudo-elliptic response can be obtained because an equal-ripple reponse is obtained in the passband ($\omega_1 \leq \omega \leq \omega_2$) and one TZ is produced at ω_z. In the synthesis of the equal-ripple Chebyshev response in the passband, we employ the corrected iteration

formula (4-17) and (4-18) instead of (4-5) and (4-6), because the phase of the cavity-backed inverter is significantly frequency-dispersive.

5.2.2 Synthesis Procedure

The synthesis procedure comprises the following steps:

Step 1) Determine the center frequency, lower edge frequency and the positions of TZs for the waveguide filter.

Step 2) Design proper waveguide structures for the realization of the cavity-backed inverter according to the positions of TZs. Calculate the scattering parameter and K-parameter of the cavity-backed inverter and make sure it satisfies the requirements in Fig. 5.1.

Step 3) Decide which iris inverters to be substituted for. Extract element parameters for the cavity-backed inverters and iris inverters at the center frequency and lower edge frequency according to the method in the last chapter.

Step 4) Calculate the converged parameters using an iteration procedure according to the corrected formula (4-17) and (4-18) together with the procedure in the last chapter.

Step 5) Calculate the insertion loss and return loss of the designed filter before it is fabricated and measured.

5.3 Design Examples

5.3.1 Realization of the Cavity-Backed Inverter

As examples, we design X-band four-pole waveguide filters centered at 10 GHz with about 10% fractional bandwidth (9.5-10.5 GHz) and WR-90 is chosen as the house waveguide. As a key part in the design, the realization of the cavity-backed inverters should be designed first. Two novel realizations are displayed in Fig. 5.2 and Fig. 5.3, which consist of an E-plane iris with an aperture-coupled E-plane or H-plane cavity. The aperture-coupled E-plane or H-plane cavity is used to realize and control the TZs.

The E-plane iris is used to change the K-parameter in the passband. Fig. 5.4 and Fig. 5.5 show the frequency dependence of the normalized K-parameters for the two cavity-backed inverters, which are calculated using a mode-matching program. It is noted from Fig. 5.4 that the E-plane cavity-backed inverter can produce TZs in the lower frequency band and meanwhile behave less frequency-dispersive in the passband (9.5-10.5 GHz). The height of the E-plane iris has a main effect on the K-parameter in the passband and the positions of TZs are nearly fixed when the height of the E-plane iris is changing. It is also noted from Fig. 5.5 that the H-plane cavity-backed inverter can produce TZs in the upper frequency band. The E-plane iris height does not only affect the K-parameter, but also change a little the position of TZs. However, it still satisfies our requirements since the range of K-parameter in the passband for the inverter can be approximated.

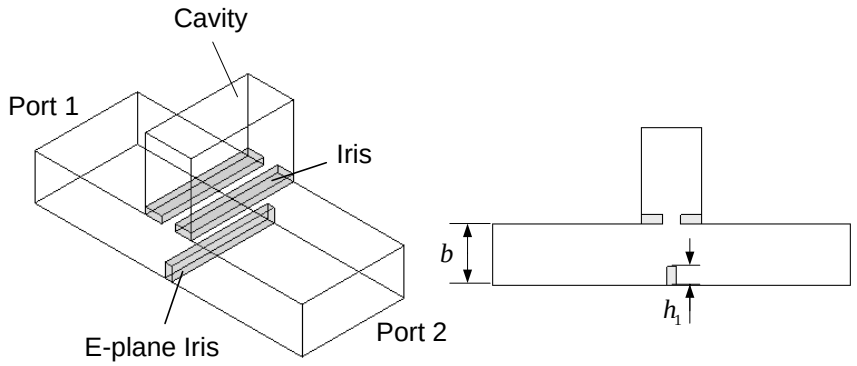

Fig. 5.2 Configuration of the E-plane cavity-backed inverter.

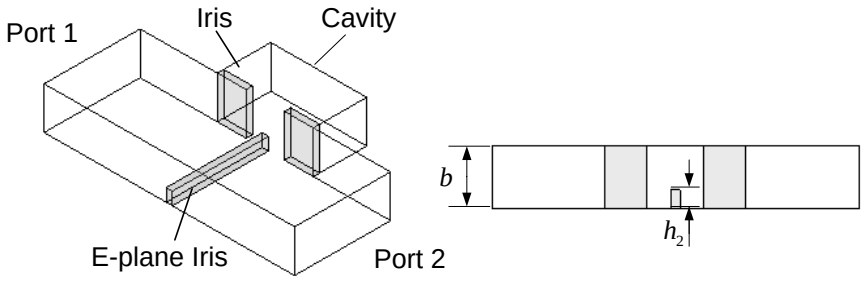

Fig. 5.3 Configuration of the H-plane cavity-backed inverter.

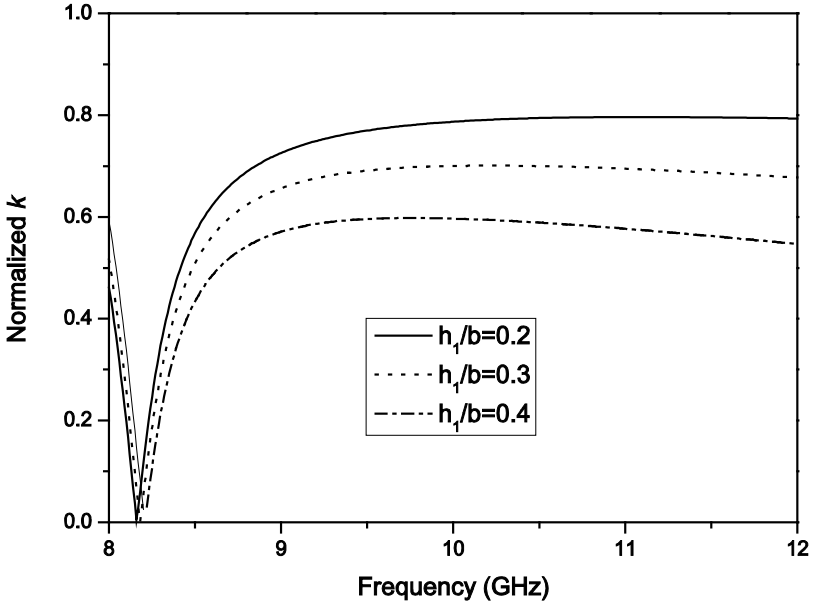

Fig. 5.4 The calculated frequency dependence of K-parameter for the E-plane cavity-backed inverter.

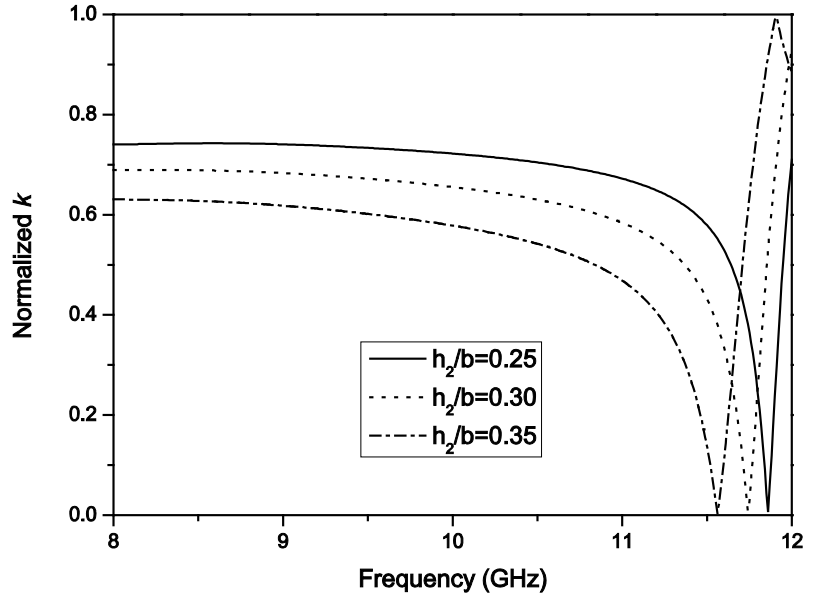

Fig. 5.5 The calculated frequency dependence of K-parameter for the H-plane cavity-backed inverter.

5.3.2 Pseudo-Elliptic Waveguide Filters with One or Two TZs

Since the cavity-backed inverters have been designed, they can be substituted for the iris inverters in the waveguide iris filter to produce TZs. An efficient mode-matching

program [105] is employed to calculate the scattering parameters of the cavity-backed inverter, iris inverter and the whole filter. The K-parameters converge after less than ten iterations and the whole synthesis procedure costs a modern personal computer only a few seconds.

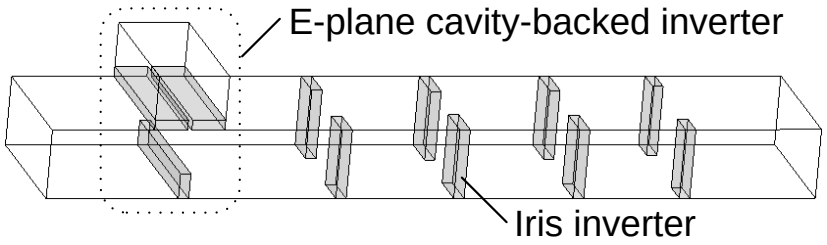

Fig. 5.6 Configuration of pseudo-elliptic waveguide filter with one TZ in the lower frequency band

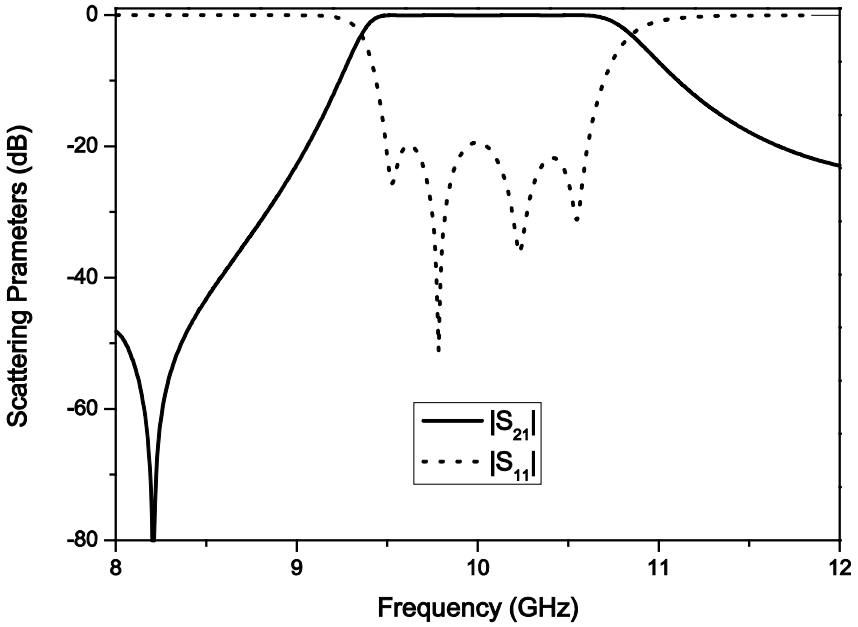

Fig. 5.7 Calculated scattering parameters of the filter in Fig. 5.6.

Fig. 5.6 depicts a four-pole wide-band pseudo-elliptic waveguide filter, with an E-plane cavity-backed structure as the first inverter, which can produce one TZ in the lower frequency band. The other four inverters are still iris structures and thereby the whole length of the filter is very close to that of the waveguide iris filter in the previous chapter. Fig. 5.7 displays the calculated scattering parameters of the filter. It can be seen that one TZ is produced at 8.20 GHz and a pseudo-elliptic response is

obtained within the whole frequency band. A good equal-ripple response is achieved for the reflection magnitude below −20 dB and the fractional bandwidth of the filter is about 11% (9.5-10.6 GHz).

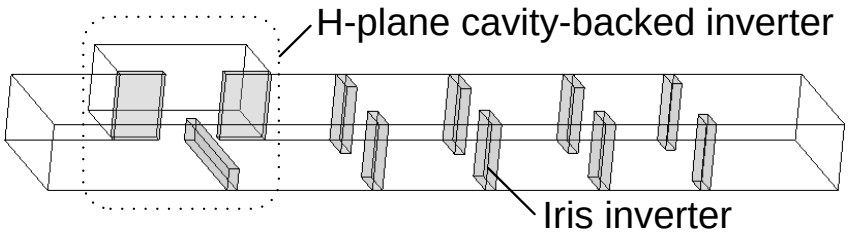

Fig. 5.8 Configuration of pseudo-elliptic waveguide filter with one TZ in the upper frequency band.

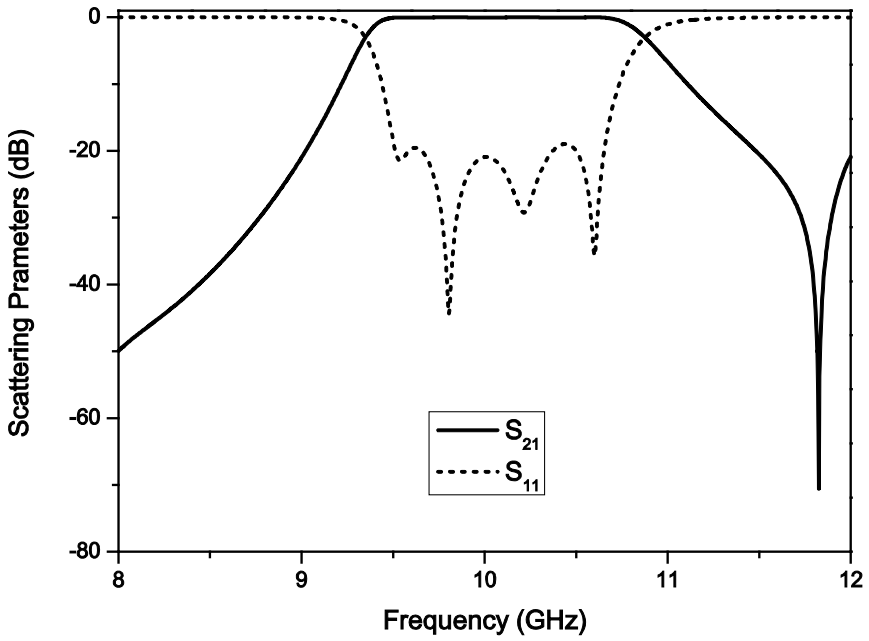

Fig. 5.9 Calculated scattering parameters of the filter in Fig. 5.8.

Fig. 5.8 depicts a four-pole wide-band pseudo-elliptic waveguide filter, with an H-plane cavity-backed structure as the first inverter, which can produce one TZ in the upper frequency band. Fig. 5.9 displays the calculated scattering parameters of the filter. It can be seen that one TZ is produced at 11.82 GHz and a pseudo-elliptic response is obtained within the whole frequency band. A good equal-ripple response is achieved for the reflection magnitude below −20 dB and the fractional bandwidth of the filter is about 11.4% (9.51-10.65 GHz).

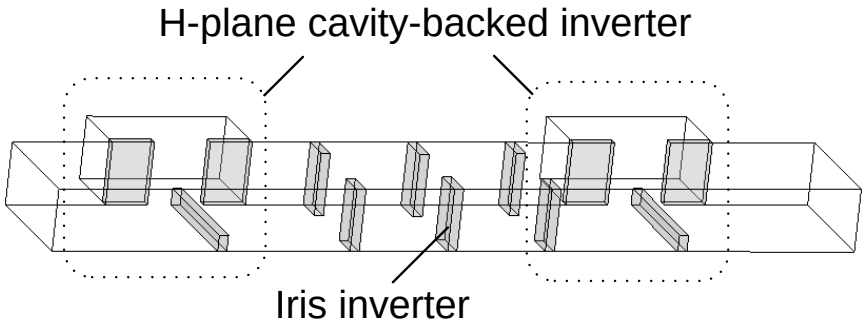

Fig. 5.10 Configuration of pseudo-elliptic waveguide filter with two TZs in the upper frequency band.

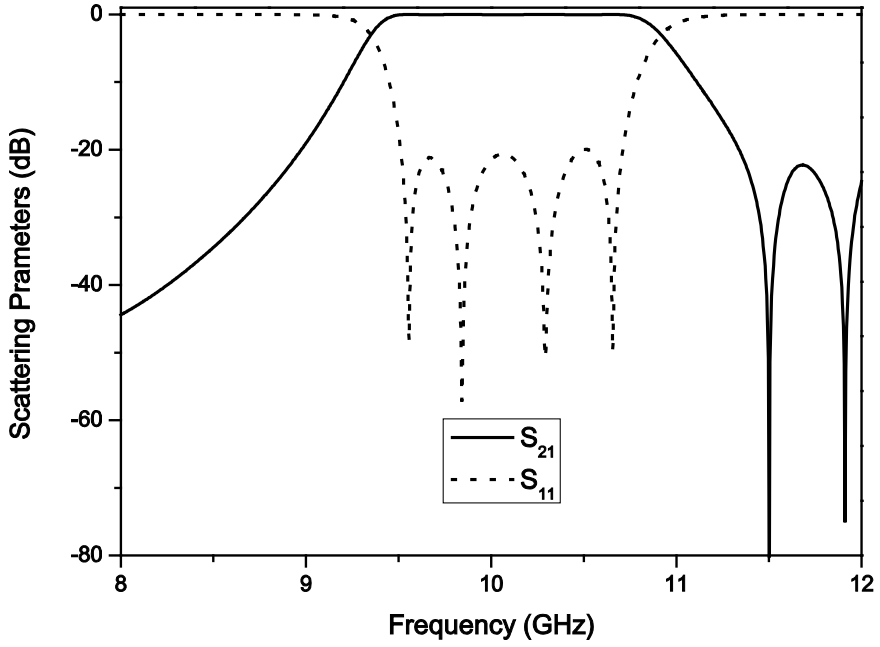

Fig. 5.11 Calculated scattering parameters of the filter in Fig. 5.10.

Fig. 5.10 also depicts a four-pole wide-band pseudo-elliptic waveguide filter, with two H-plane cavity-backed structures as both the first and last inverters, which can produce two TZs in the upper frequency band. Fig. 5.11 displays the calculated scattering parameters of the filter. It can be seen that two TZs are produced at 11.50 GHz and 11.91 GHz, respectively. A good equal-ripple response is achieved for the reflection magnitude below −20 dB and the fractional bandwidth of the filter is about 12% (9.51-10.71 GHz). The two TZs are arranged so that the out-of-band rejection in the upper frequency band is suppressed below −20 dB.

5.4 Experimental Validation

To provide a better verification on the dimensional synthesis method, we design and fabricate a wide-band pseudo-elliptic waveguide filter with two TZs, which are located in both lower and upper frequency bands. The E-plane cavity-backed structure is employed as the first inverter and the H-plane cavity-backed structure is employed as the last inverter. The dimension annotations for the pseudo-elliptic waveguide filter are shown in Fig. 5.12 and the calculated dimensions are listed in Table II. WR-90 (22.86 mm×10.16 mm) is chosen as the house waveguide and the thickness of the irises are all 1.5 mm.

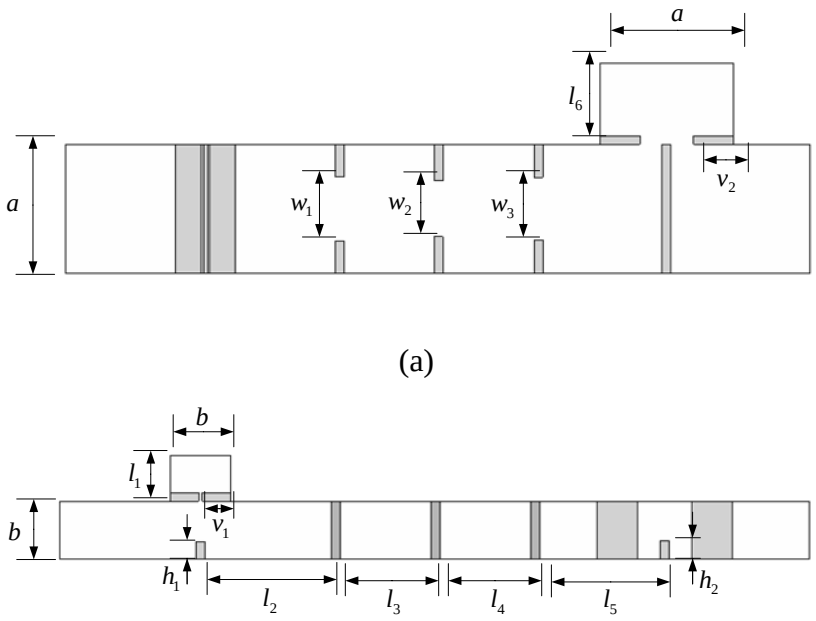

Fig. 5.12 Dimension annotation for the pseudo-elliptic waveguide filter: (a) Top view. (b) Side cross section view.

Table II: DIMENSIONS FOR THE PSEUDO-ELLIPTIC FILTERS (UNITS: MILLIMETERS)

v_1	v_2	h_1	h_2	w_1	w_2	w_3
4.78	6.86	3.10	3.28	11.37	9.93	11.04
l_1	l_2	l_3	l_4	l_5	l_6	
3.18	21.43	15.39	15.56	20.43	14.31	

The pseudo-elliptic waveguide filter is fabricated without tuning screws and Fig. 5.13 displays its fabrication photograph. The calculated and measured scattering parameters for the pseudo-elliptic waveguide filter are shown in Fig. 5.14. It can be seen that two TZs are produced at 8.52 GHz and 11.67 GHz, respectively. A good equal-ripple response is achieved for the reflection magnitude below −20 dB and the fractional bandwidth of the filter is about 11.3% (9.51-10.64 GHz). It is also noted from Fig. 5.12 that the measured TZs locations are in a good agreement with the calculated ones. The three ripples in the passband also agree well except the third one, with a deviation of about -2 dB, due to the fabrication tolerance.

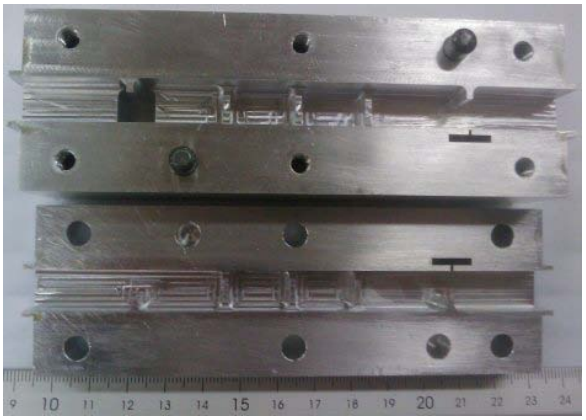

Fig. 5.13 Fabrication photograph of the pseudo-elliptic waveguide filter.

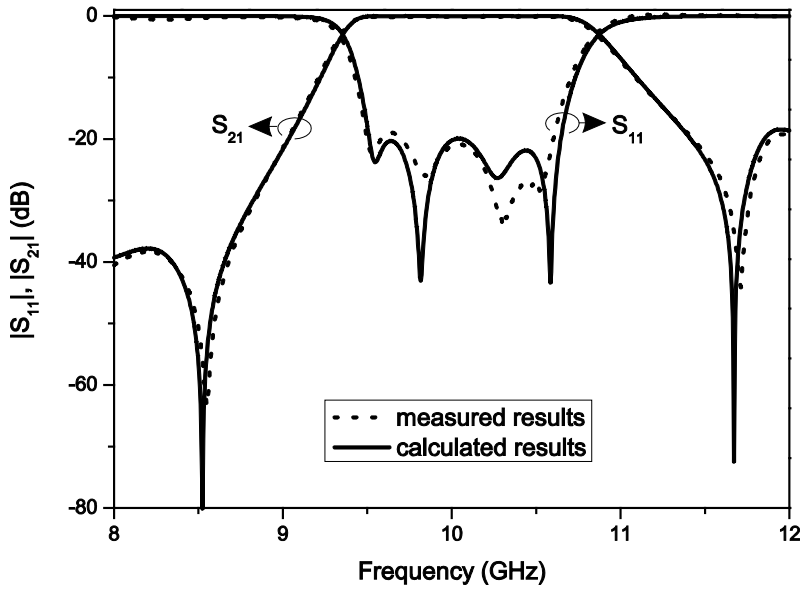

Fig. 5.14 The calculated and measured scattering parameters of the filter.

5.5 Discussion

5.5.1 Advantage

The dimensional synthesis method introduced in this chapter is an extension of the technique in the last chapter. However, it presents a great improvement since it is applicable to the design of pseudo-elliptic filters, which have better selectivity than Chebyshev filters. The TZs in the filter response are realized by the cavity-backed inverter, which can produce TZs beyond the passband and simultaneously acts like a normal iris inverter in the passband. Due to the special characteristics of the cavity-backed inverters, the out-of-band TZs can be individually controlled and meanwhile the equal-ripple Chebyshev response can be synthesized in the passband.

Compared with the traditional synthesis method based on the coupling matrix, the proposed method in this chapter has its advantage in that it can be applied for wide-band waveguide filters without resorting to circuit or full-wave optimization. Due to the frequency dispersion of coupling coefficients, so far no synthesis method based on the coupling matrix has been reported for the design of wide-band pseudo-elliptic waveguide filters without global optimization.

Another advantage of the proposed synthesis method lies in that we employ the element values of Chebyshev lowpass prototype filters g_i in the synthesis, which is very convenient to calculate. Since Chebyshev response is synthesized in the passband, we use the same element values for the design of filters with different TZs, which is different from the synthesis method based on the coupling matrix, in which the design of filters with different TZs needs different coupling matrix, which is very difficult to calculate.

5.5.2 Limitations

Although the proposed synthesis method in this chapter has many advantages, it has its own limitations. So far it is only applicable to the design of in-line waveguide filters due to the structure limitations of the cavity-backed inverter. Besides, the requirements for the design of cavity-backed inverters are very strict. First of all, the position of the TZ should be individually controlled by some parameters of the

cavity-backed inverter and the K-parameter in the passband can be adjusted by other independent parameters. That is why we employ an E-plane iris in addition to the aperture-coupled cavity in the realizations of cavity-backed inverters as shown in Fig. 5.2 and Fig. 5.3. Secondly, it is required that the cavity-backed inverter is less frequency-dispersive in the passband, which results in the employment of the E-plane iris, not H-plane irises or other structures. Finally, the change of K-parameter in the passband should have little effect on the positions of TZs. For the two novel realizations proposed in this chapter, the E-plane cavity-backed inverter completely satisfies the requirement as shown in Fig. 5.4, but it is not that good for the H-plane cavity-backed inverter as shown in Fig. 5.5. However, the small effect on the positions of TZs is still allowed since the positions of TZs can be still approximated.

5.6 Summary

In this chapter, we have presented a dimensional synthesis method for the design of wide-band pseudo-elliptic waveguide filters without resorting to global full-wave optimization. In this approach, we introduced and employed two novel cavity-backed inverters, which produce TZs in the out-of-band response, meanwhile, whose frequency response in the passband is similar to that of normal iris inverters. So the design procedures for the passband and out-of-band filter responses are carried out separately. As design examples, pseudo-elliptic waveguide filters with TZs in the lower and upper frequency bands are designed. A prototype filter has also been fabricated and measured. The results show good equal-ripple performance in the passband and improved rejection in the out-of-band response.

CHAPTER 6
WIDE-BAND IN-LINE PSEUDO-ELLIPTIC WAVEGUIDE FILTERS WITH CUSTOMIZED RESONATORS

6.1 Introduction

In the last chapter we have introduced an extended dimensional synthesis method for the design of wide-band in-line pseudo-elliptic waveguide filters. In the method, two novel cavity-backed inverters were proposed, which can produce transmissions zeros in the out-of-band response while behaving similar to the normal iris inverters in the passband. In this chapter, we will propose another extended dimensional synthesis method for the design of wide-band in-line pseudo-elliptic waveguide filters. Different from the cavity-backed inverters in the last chapter, the customized resonators are employed to produce the transmission zero (TZ) in the out-of-band response.

In the second section of this chapter, we will introduce the theory of the extended dimensional synthesis method. In the third section, three design examples will be presented. In the last section, the advantage and limitation of the proposed dimensional synthesis method will be discussed.

6.2 Theory

6.2.1 Half-Wavelength-Transmission-Line Resonators

In the design of bandpass filters with Chebyshev response, the half-wavelength transmission lines are always employed as resonators to connect the inverters. So we would like to study the traditional half-wavelength-transmission-line resonator before introducing the customized resonators. The exact equivalent Pi-network for the half-wavelength transmission line [6] is given in Fig. 6.1, where the $1:-1$ ideal transformer represents the phase reversal of the half-wavelength transmission line

and it plays no part in the filter performance. The series reactance and shunt susceptance can be presented as

$$\begin{cases} Z_\theta = -jZ_0 \sin\theta \\ Y_\theta = -jY_0 \cot\dfrac{\theta}{2} \end{cases}, \tag{6-1}$$

where Z_0 and Y_0 are the characteristics impedance and conductance of the transmission line, respectively. When θ is close to π, the shunt susceptance is near zero, which is very small compared with the series reactance and can be neglected. So the half-wavelength transmission line can be equivalent to a series reactance Z_θ which is expressed in (6-1). Since the series reactance Z_θ cannot reach infinity, the half-wavelength-transmission-line resonator cannot produce transmission zeros. If we can customize a resonator whose series reactance in the equivalent Pi-network can reach infinity beyond the passband and its shunt susceptance can be still neglected in the passband, then the customized resonator can be employed to design a wide-band pseudo-elliptic filter without global full-wave optimization.

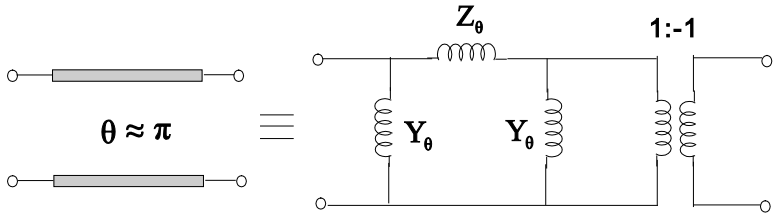

Fig. 6.1 The equivalent network for the half-wavelength-transmission-line resonator.

6.2.2 Customized Resonators

As introduced above, the customized resonator should satisfy the following requirements: 1) the series reactance in the equivalent Pi-network can reach infinity in preset frequency f_z, 2) the series reactance and shunt susceptance are both zero in the center frequency f_0 and the shunt susceptance is very small in the passband compared with the series reactance. The equivalent Pi-network of an arbitrary resonator can be calculated using its scattering parameters. As shown in Fig. 6.2, the series reactance and shunt susceptance can be expressed as

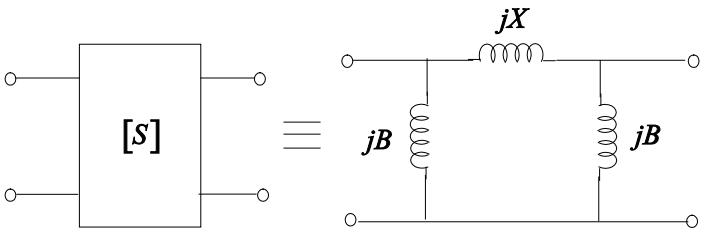

Fig. 6.2 The equivalent Pi-network calculated using the scattering parameters.

$$\begin{cases} jX = \dfrac{Z_0}{2} \cdot \left[\dfrac{(1+S_{11})^2}{S_{21}} - S_{21} \right] \\ jB = Y_0 \cdot \dfrac{1-S_{11}-S_{21}}{1+S_{11}+S_{21}} \end{cases}, \tag{6-2}$$

where Z_0 and Y_0 are the characteristics impedance and conductance of the port, respectively. The detailed derivation of (6-2) is given in APPENDIX A. Then the requirements for the customized resonator can be presented as

$$\begin{cases} S_{21}(f_z) = 0 \\ S_{11}(f_0) = 0 \\ X(f_0) = 0 \end{cases}. \tag{6-3}$$

As we know, the waveguide slit-coupled cavity can produce transmission zero and thereby it can be customized to satisfy (6-3). The position of the transmission zero is mainly controlled by the cavity dimension and the slit width can be adjusted to control the resonance frequency f_0. So the first two requirements in (6-3) have been satisfied. For the last requirement in (6-3), we can satisfy it by moving the reference plane of the port. In the practical implementation, we find that the shunt susceptance is very small and the equivalent network can be represented using a series reactance as shown in Fig. 6.3. However, it is also noted that the reference planes of the input port and output port are very close to the slit-coupled cavity. So the mutual coupling may be produced between the slit-coupled cavity and the adjacent inverters. To eliminate the mutual coupling, we add two half-wavelength transmission lines on both ends as shown in Fig. 6.4. The new customized resonator can be still equivalent to a Pi-network and the new series reactance and shunt susceptance in Fig. 6.4 can be calculated as

$$\begin{cases} X^* = Z_0 \sin(\theta_1 + \theta_2) + X \cos\theta_1 \cos\theta_2 \\ B^* \approx Y_0 \cdot \tan\dfrac{\theta_1 + \theta_2}{2} \end{cases} . \tag{6-4}$$

The detailed derivation of (6-4) is given in APPENDIX B. It is noted from (6-4) that, when θ_1 and θ_2 are both close to π, the shunt susceptance B^* is very small compared with the series reactance X^* and thereby it can be neglected in the passband. So only the series reactance is employed in the synthesis of wide-band pseudo-elliptic waveguide filters.

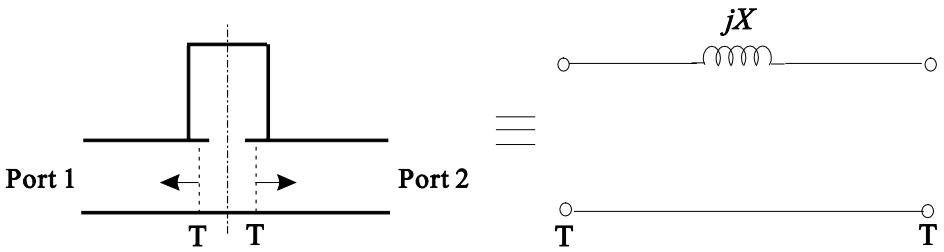

Fig. 6.3 The equivalent network of the waveguide slit-coupled cavity.

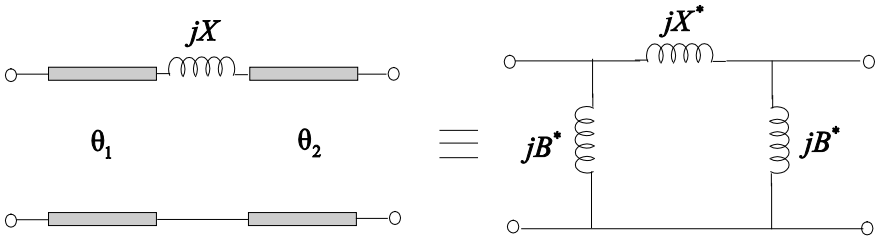

Fig. 6.4 The equivalent Pi-network of the waveguide slit-coupled cavity with two transmission line added on both ends.

6.2.3 Filter Synthesis

Since the customized resonator has been introduced, we apply it to the synthesis of wide-band pseudo-elliptic waveguide filters. If we employ the customized resonator as the *m*-th resonator in the *n*-pole filter, the iteration formula in (4-17) and (4-18) will be modified as

$$\begin{cases} L_{ai}^{(j)} = \dfrac{Z_0}{\omega_1}\cdot\left[\dfrac{K_{i-1,i}^{(j-1)}(f_1)}{K_{i-1,i}^{(j-1)}(f_0)}\right]^{\frac{i-1}{n}-1}\cdot\left[\dfrac{K_{i,i+1}^{(j-1)}(f_1)}{K_{i,i+1}^{(j-1)}(f_0)}\right]^{\frac{-i}{n}}\cdot\sin\left(\theta_{i-1}+\theta_i\right)\Big|_{i=1,2,...m-1,m+1,...n} \\ L_{am}^{(j)} = \dfrac{Z_0}{\omega_1}\cdot\left[\dfrac{K_{m-1,m}^{(j-1)}(f_1)}{K_{m-1,m}^{(j-1)}(f_0)}\right]^{\frac{i-1}{n}-1}\cdot\left[\dfrac{K_{m,m+1}^{(j-1)}(f_1)}{K_{m,m+1}^{(j-1)}(f_0)}\right]^{\frac{-i}{n}}\cdot\left[\sin\left(\theta_{m-1}+\theta_m\right)+\dfrac{X(f_1)}{Z_0}\cos\theta_{m-1}\cos\theta_m\right] \end{cases} \tag{6-5}$$

and

$$\begin{cases} K_{0,1}^{(j)}(f_0) = \sqrt{\dfrac{Z_0 L_{a1}^{(j)}}{g_0 g_1}} \\ K_{i,i+1}^{(j)}(f_0) = \sqrt{\dfrac{L_{ai}^{(j)} L_{a(i+1)}^{(j)}}{g_i g_{i+1}}}\Bigg|_{i=1,2,...,n-1} \\ K_{n,n+1}^{(j)}(f_0) = \sqrt{\dfrac{L_{an}^{(j)} Z_{n+1}}{g_n g_{n+1}}} \end{cases}, \tag{6-6}$$

where

$$\theta_i = \begin{cases} \sqrt{\dfrac{f_1^2 - f_c^2}{f_0^2 - f_c^2}}\cdot\left(\dfrac{\pi}{2}+\varphi_i^{(j-1)}(f_0)\right)-\varphi_i^{(j-1)}(f_1) & i = 0,1,...m-2,m+1,...n \\ \sqrt{\dfrac{f_1^2 - f_c^2}{f_0^2 - f_c^2}}\cdot\left(\pi+\varphi_i^{(j-1)}(f_0)\right)-\varphi_i^{(j-1)}(f_1) & i = m-1,m \end{cases} \tag{6-7}$$

and $X(f_1)$ is the series reactance of the customized resonator in the lower edge frequency.

6.2.4 Design Procedure

The synthesis procedure comprises the following steps:

Step 1) Determine the center frequency, lower edge frequency and position of the transmission zero for the waveguide filter.

Step 2) Design the customized resonator using the waveguide slit-coupled cavity according to the requirements in (6-3). Calculate the series reactance in Fig.

6.3 using (6-2). The series reactance in the lower edge frequency will be employed in the synthesis.

Step 3) Decide which resonator to be substituted with the customized resonator. All the other resonators are still half-wavelength-transmission-line resonators.

Step 4) Calculate the converged parameters using an iteration procedure according to the modified formula (6-5), (6-6) and (6-7) together with the procedure in Chapter 4.

Step 5) Calculate the insertion loss and return loss of the in-line pseudo-elliptic waveguide filter.

6.3 Design Examples

6.3.1 Realization of the Customized Resonators

The realization of the customized resonators will be introduced first before the design examples are given. As examples, we design X-band waveguide filters centered at 10 GHz with WR-90 (22.86mm×10.16mm) as the house waveguide. We will introduce three different customized resonators, which can produce transmission zeros in the upper frequency band, lower frequency band and both frequency bands.

The configuration of the customized resonator Ⅰ is shown in Fig. 6.5 and the dimensions are listed in Table III. It is actually a waveguide cavity coupled through a 1.5mm-thick slit on the broad wall of the main waveguide. The cavity length h_1 has a main effect on the position of the transmission zero and the slit width w_1 can be used to tune the resonant frequency to 10GHz. The reference plane T is used to adjust the series reactance of its equivalent Pi-network to make it equal to zero at 10GHz. Fig. 6.6 shows the series reactance and shunt susceptance of the equivalent Pi-network for the customized resonator Ⅰ, which is calculated using a mode-matching program. It is noted that the shunt susceptance is nearly zero in the frequency band and can be neglected. The series reactance can reach infinity at 11.92GHz, where the transmission zero locates. Therefore, the customized resonator Ⅰ can be applied to

the design of pseudo-elliptic waveguide filters with a transmission zero in the upper frequency band.

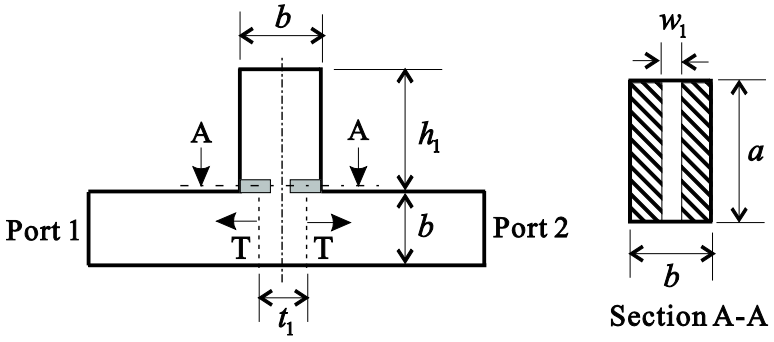

Fig. 6.5 Configuration of the customized resonator Ⅰ (side view).

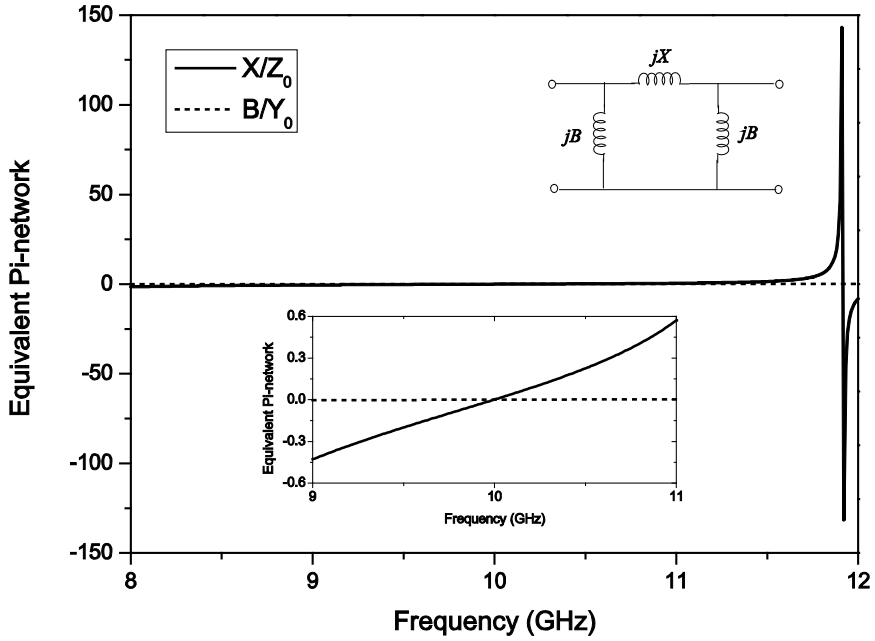

Fig. 6.6 Calculated series reactance and shunt susceptance for the customized resonator Ⅰ.

The configuration of the customized resonator Ⅱ is shown in Fig. 6.7 and the dimensions are listed in Table IV. Its configuration is similar to that of the customized resonator Ⅰ except the slit structure. The slit thickness is also 1.5mm but the slit is placed in the H plane of the waveguide cavity. Fig. 6.8 shows the series reactance and shunt susceptance of the equivalent Pi-network for the customized

resonator Ⅱ. It is noted that the series reactance can reach infinity at 8.12GHz, where the transmission zero locates. Therefore, the customized resonator Ⅱ can be applied to the design of pseudo-elliptic waveguide filters with a transmission zero in the lower frequency band.

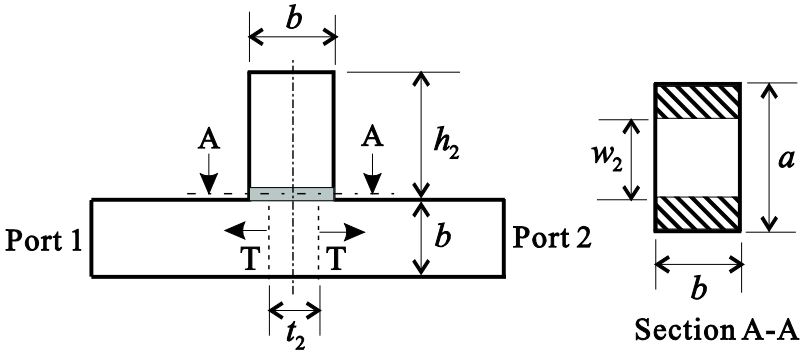

Fig. 6.7 Configuration of the customized resonator Ⅱ (side view).

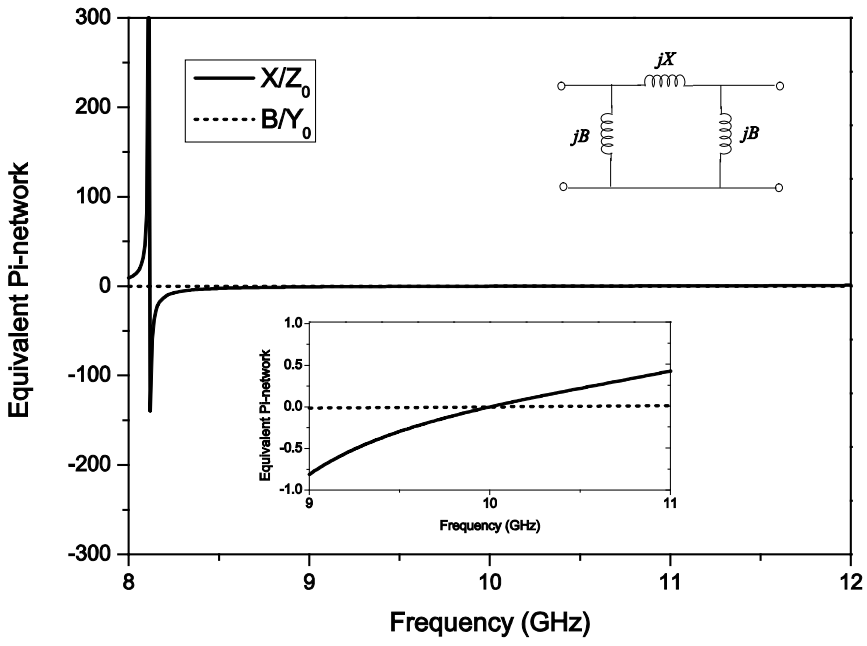

Fig. 6.8 Calculated series reactance and shunt susceptance for the customized resonator Ⅱ.

The configuration of the customized resonator Ⅲ is shown in Fig. 6.9 and the dimensions are listed in Table V. It is actually a combination of the customized resonator Ⅰ and customized resonator Ⅱ. The two waveguide cavities are coupled

through two 1.5mm-thick slit on top and bottom broad walls of the main waveguide. Fig. 6.10 shows the series reactance and shunt susceptance of the equivalent Pi-network for the customized resonator Ⅲ. It is noted that the series reactance can reach infinity at 8.19GHz and 11.92GHz, where the transmission zeros locate. Therefore, the customized resonator Ⅲ can be applied to the design of pseudo-elliptic waveguide filters with two transmission zeros both in the lower and upper frequency bands.

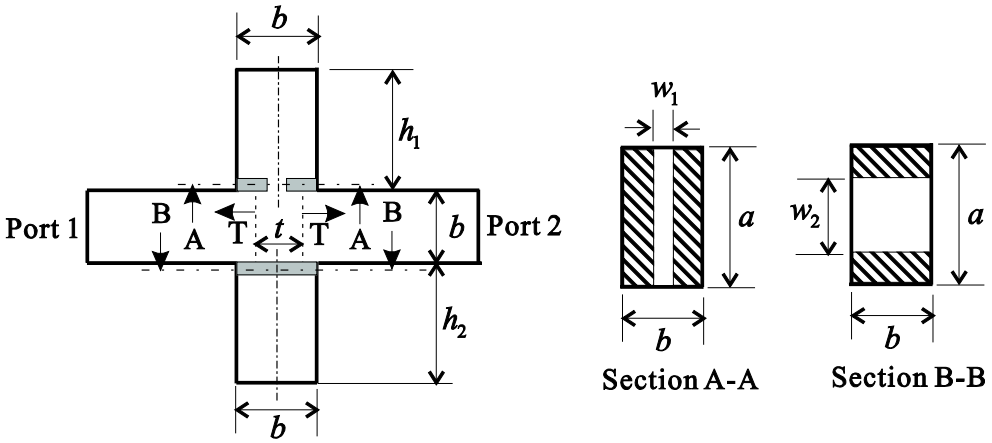

Fig. 6.9 Configuration of the customized resonator Ⅲ (side view).

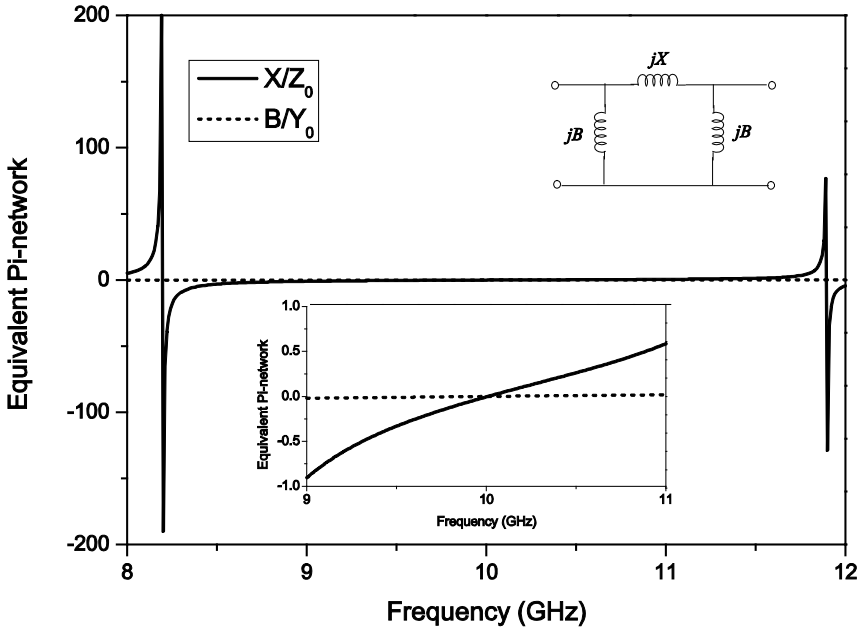

Fig. 6.10 Calculated series reactance and shunt susceptance for the customized resonator Ⅲ.

6.3.2 Filter Examples

Since the customized resonators have been designed, it can be substituted for the half-wavelength-transmission-line resonator in the waveguide iris filter to produce transmission zeros. As examples, we design X-band four-pole waveguide pseudo-elliptic filters and the customized resonator is placed at the second resonator as shown in Fig. 6.11. Three pseudo-elliptic waveguide filters are designed using three different customized resonators and their dimensions are listed in TABLE Ⅰ, TABLE Ⅱ and TABLE Ⅲ. WR-90 (22.86 mm×10.16 mm) is chosen as the house waveguide and the thickness of the irises are all 1.5 mm.

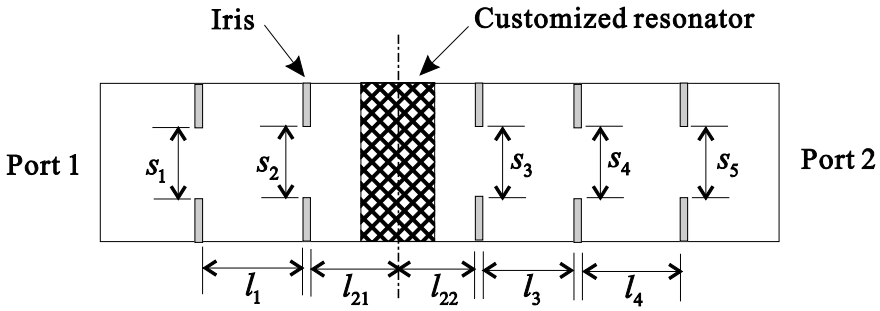

Fig. 6.11 Configuration of the pseudo-elliptic waveguide filters using the customized resonator (top view).

Table III: DIMENSIONS FOR THE FILTER USING RESONATOR Ⅰ (UNITS: MILLIMETERS)

w_1	h_1	t_1	s_1	s_2	s_3	s_4
7.21	19.40	0.68	14.64	13.98	12.90	11.66
s_5	l_1	l_{21}	l_{22}	l_3	l_4	
14.90	11.83	16.33	16.85	13.75	12.87	

Table IV: DIMENSIONS FOR THE FILTER USING RESONATOR Ⅱ (UNITS: MILLIMETERS)

w_2	h_2	t_2	s_1	s_2	s_3	s_4
18.75	18.37	1.39	14.74	14.31	13.15	11.73
s_5	l_1	l_{21}	l_{22}	l_3	l_4	
15.02	11.66	16.55	17.08	13.60	12.78	

Table V: DIMENSIONS FOR THE FILTER USING RESONATOR III (UNITS: MILLIMETERS)

w_1	h_1	w_2	h_2	t
4.06	8.67	9.97	14.03	1.22
s_1	s_2	s_3	s_4	s_5
14.61	14.26	13.14	11.64	14.90
l_1	l_{21}	l_{22}	l_3	l_4
11.73	16.49	17.00	13.64	12.88

An efficient mode-matching program is employed in the dimensional synthesis and the results are verified by the finite element method (FEM) using the commercial software Ansoft HFSS [98]. Fig. 6.12 shows the scattering parameters of the pseudo-elliptic waveguide filter using the customized resonator Ⅰ. It is noted from the figure that a transmission zero is produced at 11.92 GHz, which agrees well with the transmission zero position in Fig. 6.6. A good equal-ripple response is also achieved in the passband for the reflection magnitude below −20 dB and the fractional bandwidth of the filter is about 14% (9.35-10.72 GHz). Fig. 6.13 shows the scattering parameters of the pseudo-elliptic waveguide filter using the customized resonator Ⅱ. It is noted from the figure that a transmission zero is produced at 8.12 GHz, which agrees well with the transmission zero position in Fig. 6.8. A good equal-ripple response is achieved in the passband for the reflection magnitude below −20 dB and the fractional bandwidth of the filter is about 14% (9.37-10.78 GHz). Fig. 6.14 shows the scattering parameters of the pseudo-elliptic waveguide filter using the customized resonator Ⅲ. It is noted from the figure that two transmission zeros are produced at 8.19 GHz and 11.92 GHz, which agrees well with the transmission zero positions in Fig. 6.10. A good equal-ripple response is also achieved in the passband for the reflection magnitude below −20 dB and the fractional bandwidth of the filter is about 14% (9.37-10.75 GHz). It should be also noted from the three figures that the calculated results using mode-matching are in a good agreement with the simulated results using HFSS, thereby providing the final validation of the synthesis method proposed in this paper.

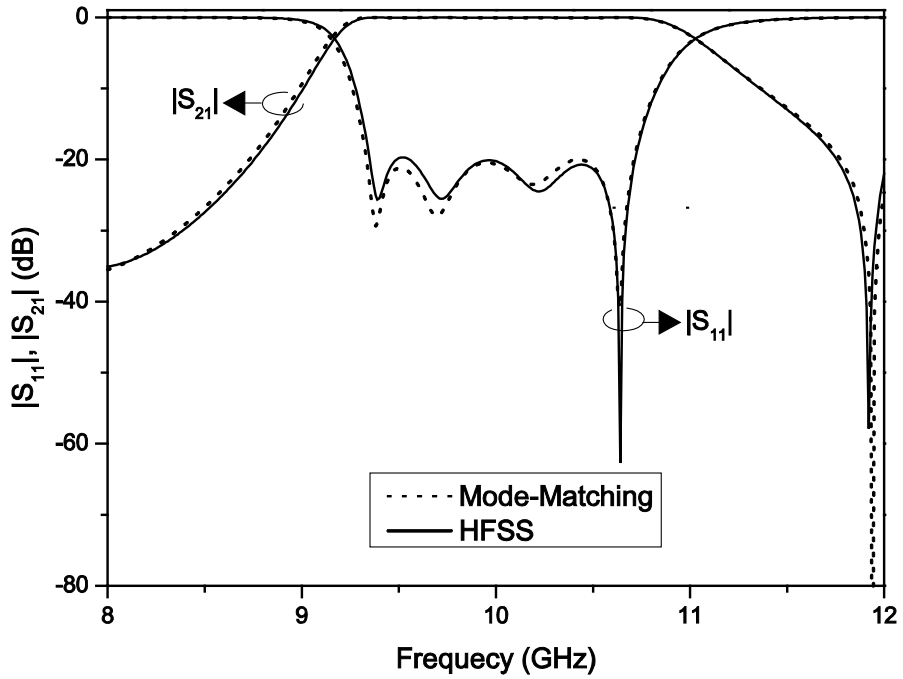

Fig. 6.12 Scattering parameters of the pseudo-elliptic waveguide filters the customized resonator Ⅰ.

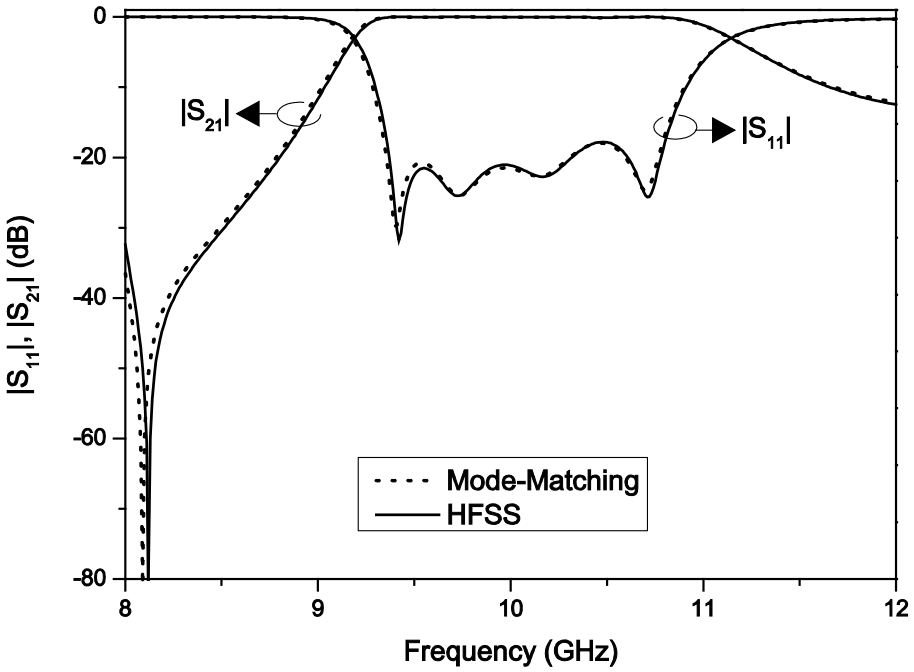

Fig. 6.13 Scattering parameters of the pseudo-elliptic waveguide filters the customized resonator Ⅱ.

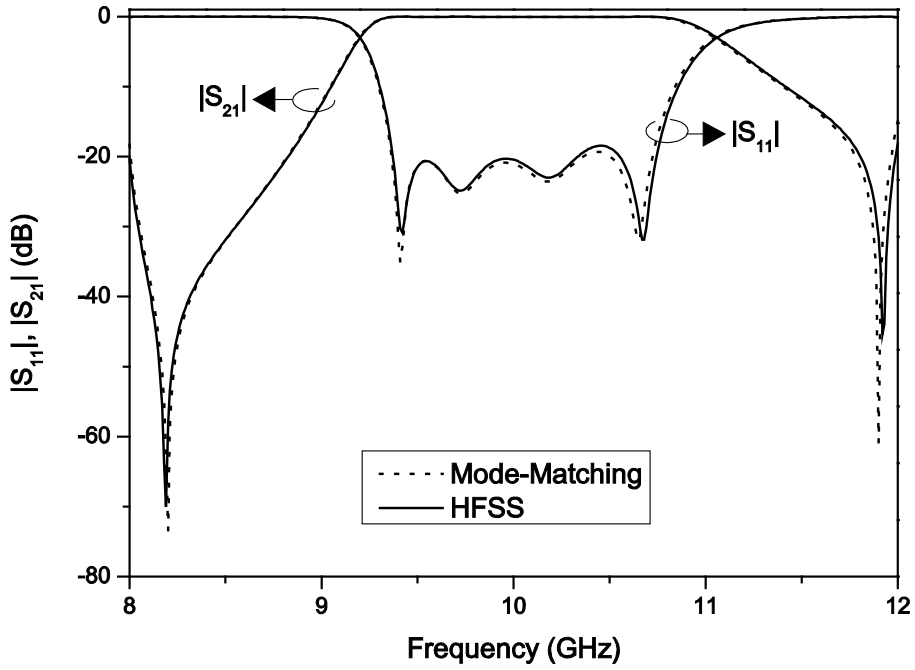

Fig. 6.14 Scattering parameters of the pseudo-elliptic waveguide filters the customized resonator Ⅲ.

6.4 Discussion

The synthesis of pseudo-elliptic waveguide filters using the customized resonator in this chapter or using the cavity-backed inverter in Chapter 5 are all extensions of the synthesis technique in Chapter 4. They present a great improvement since they are applicable to the design of pseudo-elliptic filters, which have better selectivity than Chebyshev filters. The difference between the two method lies in the realization of the transmission zeros. In Chapter 5, the transmission zeros are realized by the cavity-backed inverters, which can produce transmission zeros beyond the passband and simultaneously act like a normal iris inverter in the passband. In this chapter, the transmission zeros are realized by the customized resonators, which can produce transmission zeros beyond the passband and simultaneously acts like a normal half-wavelength-transmission-line resonator in the passband.

Compared with the cavity-backed inverter technique in Chapter 5, the proposed method in this chapter presents an advantage in that the positions of the transmission zero can be individually controlled with more precision. As introduced in Chapter 5,

the change of the E-plane iris in the cavity-backed inverters will have an effect on the positions of the transmission zero, especially for the H-plane cavity-backed inverters. This will result in a slight difference between the final position of the transmission zero and the preset one. However, the customized resonators in this chapter are designed with fixed transmission zeros and the waveguide pseudo-elliptic filters have the same transmission zeros as the customized resonators that they employ. It has been shown that the transmission zeros in Fig. 6.6, Fig. 6.8 and Fig. 6.10 are the same as those in Fig. 6.12, Fig. 6.13 and Fig. 6.14. Despite of the advantage, the proposed method in this chapter also has its limitation in that the position of the transmission zero cannot be placed too close to the passband because it will degrade the equal-ripple performance in the passband.

6.5 Summary

In this chapter, we have presented a dimensional synthesis method for the design of wide-band pseudo-elliptic waveguide filters without resorting to global full-wave optimization. In this approach, we introduced and employed three customized resonators, which can produce transmission zeros in the lower frequency band, upper frequency band and both frequency bands, respectively. The synthesis procedure has been presented and three pseudo-elliptic waveguide filters with about 14% fractional bandwidth were designed using different customized resonators. The results show good equal-ripple performance in the passband and improved rejection performance with preset transmission zeros beyond the passband. The proposed method is expected to find more applications in the design of wide-band pseudo-elliptic filters.

CHAPTER 7
WIDE-BAND CROSS-COUPLED WAVEGUIDE FILTERS

7.1 Introduction

Pseudo-elliptic microwave filters, which find ever-increasing applications in a wide range of modern communication systems, are often designed as a set of cross-coupled resonators [17], [87]-[88]. Cross coupling between non-adjacent resonators in the pseudo-elliptic filters is used to bring the transmission zeros from infinity to finite positions in the complex plane. These filters can provide a skirt selectivity, or a flat group delay, or even both simultaneously.

Both positive and negative couplings are needed to generate transmission zeros at finite frequencies for achieving a high selectivity in a cross-coupled filter [89]. The actual implementation of cross coupling is either physical or modal. In the case of physical cross coupling, a physical element is employed, such as a metal rod in waveguide combline resonator filter [90], electrical probe in the combline filter [91], a square aperture at the center of the broad walls in the canonical folded waveguide filter [92]-[93]. An alternative approach is the use of other modes, propagating or evanescent, as separate paths for energy flow. Some designs based on this technique used higher order modes in waveguide cavities to generate the transmission zeros for a pseudo-elliptic response [94]. Although these techniques mentioned above are widely employed to design cross-coupled waveguide filters, they are only applicable to narrowband cases. Due to the limitation of the circuit model and frequency dispersion problem, excessive global full-wave optimizations have to be employed in the design of wide-band cross-coupled waveguide filters. So far no synthesis method has been reported for the design of wide-band cross-coupled waveguide filters without global optimization.

In the last two chapters we have introduced two extended dimensional synthesis method for the design of wide-band in-line pseudo-elliptic waveguide

filters. In the two methods, the transmission zero is produced either by the inverters or the resonators. However, these two methods are only applicable to in-line waveguide filters, which is not the type dealt with in this chapter. In this chapter, we will propose an extended dimensional synthesis method for the design of wide-band cross-coupled waveguide filters without global full-wave optimization.

In the second section of this chapter, we will introduce two circuit models suitable for the synthesis of wide-band cross-coupled filters. In the third section, the synthesis method for the cross-coupled waveguide filters will be presented. In the fourth section, an X-band four-pole cross-coupled waveguide filter will be introduced as the design example. In the last section, the advantage and limitation of the proposed dimensional synthesis method will be discussed.

7.2 Circuit Model

An ideal symmetrical circuit model suitable for the synthesis of wide-band cross-coupled filters has been shown in Fig. 7.1. As shown in the figure, a series cross-coupled K-inverter is inserted before the $(m-1)$-th resonator. Basically, the extra cross-coupled K-inverter is its major difference from the conventional direct-coupled Chebyshev filter. Based on this, we examine the central portion of the network, as shown in Fig. 7.2(a), which can be analyzed using the even mode and odd mode. The even- and odd-mode impedance of the network as shown in Fig. 7.2(a) can be calculated as

$$\begin{cases} \dfrac{Z_{even}}{Z_0} = -j\dfrac{K_c}{Z_0} + j\dfrac{-K_m/Z_0 + \tan\left(\theta_{m-1}\cdot\lambda_g(f_0)/\lambda_g(f)\right)}{1+(K_m/Z_0)\cdot\tan\left(\theta_{m-1}\cdot\lambda_g(f_0)/\lambda_g(f)\right)} \\ \dfrac{Z_{odd}}{Z_0} = j\dfrac{K_c}{Z_0} + j\dfrac{K_m/Z_0 + \tan\left(\theta_{m-1}\cdot\lambda_g(f_0)/\lambda_g(f)\right)}{1-(K_m/Z_0)\cdot\tan\left(\theta_{m-1}\cdot\lambda_g(f_0)/\lambda_g(f)\right)} \end{cases}, \qquad (7\text{-}1)$$

where Z_0 , λ_g denote the characteristics impedance and guided wavelength of the transmission-line resonator, and f_0 is the center frequency of the filter. The transmission zero occurs when $Z_{even}=Z_{odd}$ [78]. By substituting it in (7-1), the condition can be expressed as

$$K_c = -K_m \cdot \frac{1+\tan^2\left(\theta_{m-1}\cdot\lambda_g(f_0)/\lambda_g(f_z)\right)}{1-(K_m/Z_0)^2\cdot\tan^2\left(\theta_{m-1}\cdot\lambda_g(f_0)/\lambda_g(f_z)\right)} \quad , \tag{7-2}$$

where f_z is frequency of the transmission zero. It is noted from (7-2) that a pair of transmission zeros can be achieved by bring in one cross-coupled K-inverter and the sign of K_c is usually opposite to that of K_m if the transmission zeros occur at real frequencies. It is more interesting to note from (7-2) that even if K_c and K_m exchange signs, the locations of transmission zeros are not changed. Therefore, it does not matter which one is positive or negative as long as their signs are opposite.

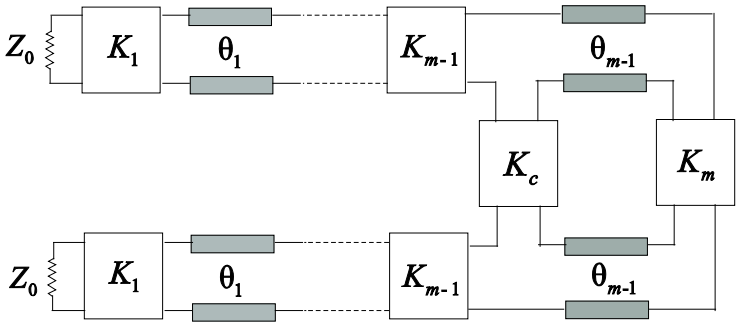

Fig. 7.1 The proposed circuit model suitable for the synthesis of wide-band cross-coupled filters.

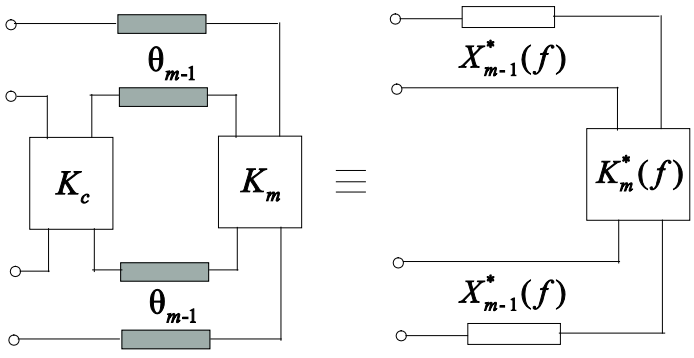

(a) (b)

Fig. 7.2 (a) The central portion of the network in Fig. 7.1. (b) Its equivalent network.

Since the cross-coupled network in Fig. 7.2 (a) is difficult to be synthesized, we propose an equivalent network without cross-coupled K-inverter, as shown in Fig. 7.2 (b). By calculating its even- and odd-mode impedance and substituting it in (7-1), we can obtain the equivalent K-inverter and series resonator as

$$\begin{cases} \dfrac{X_{m-1}^{*}(f)}{Z_0} = \dfrac{\left(1+(K_m/Z_0)^2\right)\cdot\tan\left(\theta_{m-1}\cdot\lambda_g(f_0)/\lambda_g(f)\right)}{1-(K_m/Z_0)^2\cdot\tan^2\left(\theta_{m-1}\cdot\lambda_g(f_0)/\lambda_g(f)\right)} \\ K_m^{*}(f) = K_c + \dfrac{K_m\cdot\left(1+\tan^2\left(\theta_{m-1}\cdot\lambda_g(f_0)/\lambda_g(f)\right)\right)}{1-(K_m/Z_0)^2\cdot\tan^2\left(\theta_{m-1}\cdot\lambda_g(f_0)/\lambda_g(f)\right)} \end{cases} . \tag{7-3}$$

Based on this, the whole circuit model in Fig. 7.1 can be equivalent to the network in Fig. 7.3. Since all the transmission lines are half-wavelength transmission line resonators, the series resonators in Fig. 7.3 can be expressed as

$$\begin{cases} \dfrac{X_i(f)}{Z_0} = -\sin\left(\pi\cdot\dfrac{\lambda_g(f_0)}{\lambda_g(f)}\right)\Bigg| i = 1,2....m-2 \\ \dfrac{X_{m-1}^{*}(f)}{Z_0} \approx \left(1+(\dfrac{K_m}{Z_0})^2\right)\cdot\tan\left(\pi\cdot\dfrac{\lambda_g(f_0)}{\lambda_g(f)}\right) \end{cases} . \tag{7-4}$$

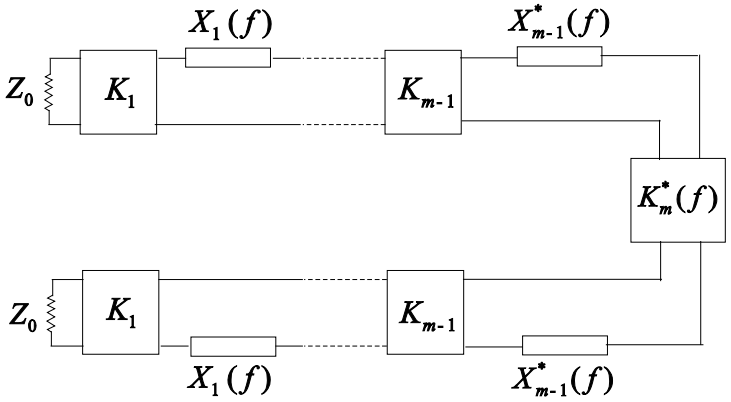

Fig. 7.3 The equivalent network without cross-coupled K-inverter.

The detailed derivation of (7-4) is given in APPENDIX C. We can see that the network in Fig. 7.3 is the same as the conventional bandpass filter network except the K-inverter and series resonator in the central portion. It is noted from (7-4) that the equivalent series resonator is similar to the conventional half-wavelength-

transmission-line resonator. They all resonate at the frequency f_0, but the equivalent series reactance has a different slope. It can be also noted from (7-3) that the equivalent K-inverter is frequency-dependent, even though K_c and K_m are all ideal inverters. However, it is not a problem because the practical inverters are all frequency-dependent and the frequency dispersion problem of inverters has already been addressed in CHAPTER 4. Also the frequency-dependent information of K_c and K_m is included in the equivalent K-inverter and hereby the equivalent network in Fig. 7.3 can be synthesized using the technique in CHAPTER 4.

Although the circuit model in Fig. 7.1 is suitable for the synthesis of wide-band cross-coupled filters, it is difficult to realize physically. As shown in Fig. 7.1, the inverter K_{m-1} and the cross-coupled K-inverter K_c are connected directly, which is difficult to realize practically because the physical structures of the two inverters may have mutual couplings. So we propose a revised circuit model as shown in Fig. 7.4. It can be seen that an extra half-wavelength transmission line is inserted between the two inverters. The revised circuit can be still equivalent to the network in Fig. 7.3. Since the extra half-wavelength transmission line can be approximated using a series reactance, the $(m-1)$-th series resonator is modified as

$$\frac{X_{m-1}^{*}(f)}{Z_0} \approx \left(1+(\frac{K_m}{Z_0})^2\right)\cdot\tan\left(\pi\cdot\frac{\lambda_g(f_0)}{\lambda_g(f)}\right)-\sin\left(\pi\cdot\frac{\lambda_g(f_0)}{\lambda_g(f)}\right) \quad , \tag{7-5}$$

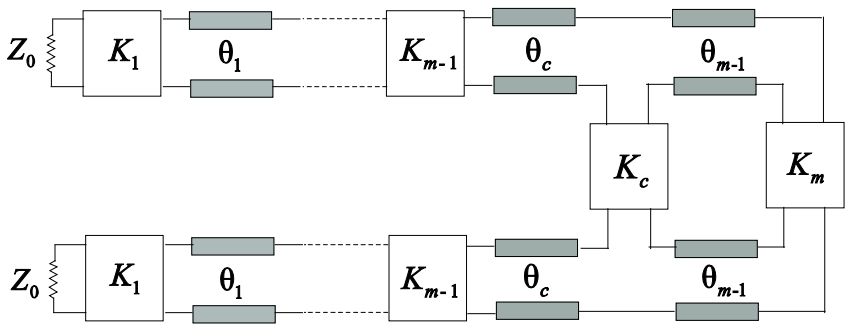

Fig. 7.4 The revised circuit model suitable for the synthesis of practical wide-band cross-coupled filters.

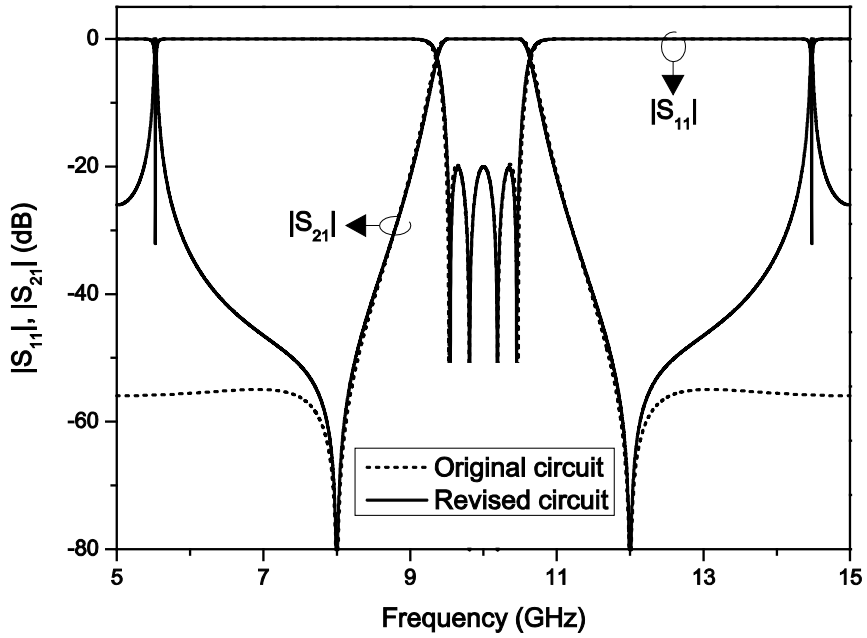

Fig. 7.5 Scattering parameters of an ideal four-pole filter designed using the original circuit model and the revised circuit model.

and the equivalent K-inverter is presented as

$$K_m^*(f) = K_c + \frac{K_m \cdot \left(1 + \tan^2\left(\pi \cdot \lambda_g(f_0)/\lambda_g(f)\right)\right)}{1 - (K_m/Z_0)^2 \cdot \tan^2\left(\pi \cdot \lambda_g(f_0)/\lambda_g(f)\right)} \quad . \tag{7-6}$$

Equation (7-5) is the addition of the two formula in (7-4) because the extra half-wavelength transmission line can be approximated using a series reactance which has the same formula as the first one in (7-4). And (7-6) is the same as the second equation in (7-3) when $\theta_{m-1} = \pi$ is substituted. Fig. 7.5 shows the calculated scattering parameters of an ideal four-pole filter designed using the original circuit model in Fig. 7.1 and the revised circuit model in Fig. 7.4. All the inverters in the two circuits are regarded as ideal and the designed filter is centered at 10 GHz with 10% fractional bandwidth (9.5-10.5 GHz), and two transmission zeros at 8 GHz and 12 GHz, respectively. It is noted from Fig. 7.5 that the filter designed using the revised circuit can achieve the same performance as the original circuit in the frequency band from 8 GHz to 12 GHz. Although the far out-of-band performance of the filter designed using the revised circuit model is a little worse due to the

harmonics generated by the extra transmission line, the revised circuit model is easier to realize physically.

7.3 Synthesis of Waveguide Cross-Coupled Filters

7.3.1 Physical Realization of the Cross-Coupled Inverter

In the synthesis of wide-band filters, it is proposed to study all the structures in a wide frequency band, not only in a narrow frequency band close to the center frequency. For the realization of the cross-coupled K-inverter in Fig. 7.2(a), it is required that its even- and odd-mode impedances are pure series reactance and they have the same magnitude but different signs. We propose a novel realization of the cross-coupled K-inverter in waveguide filters as shown in Fig. 7.6. Two waveguide transmission lines are coupled through an E-plane aperture-coupled cavity.

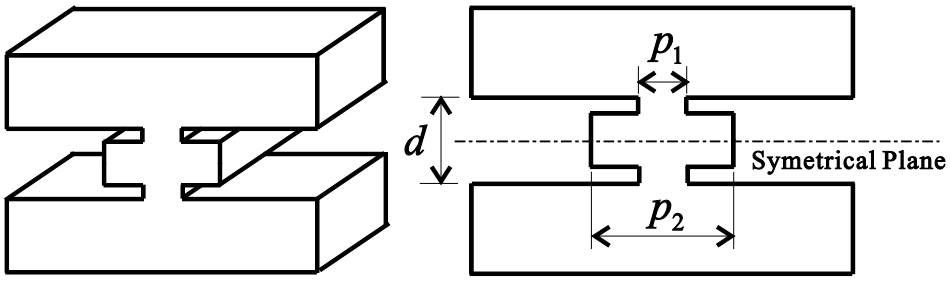

(a) (b)

Fig. 7.6 Configuration of the cross-coupled inverter. (a) Perspective view. (b) Side view.

By assuming the electric and magnetic walls on the symmetrical plane, we can analyze the even mode and odd mode using a two-port network as shown in Fig. 7.7(a). It is an E-plane junction and can be always equivalent to a Pi-network. If we select the reference plane T suitably, it can be equivalent to a pure series reactance [99] as shown in Fig. 7.7(b). In the practical implementation we find that, if aperture width p_1 is not too large and the reference plane T is very close to the symmetrical plane, the parallel reactance in the Pi-network can be neglected in a very wide frequency band and the Pi-network can be simplified to be a series reactance. The

even- and odd-mode series reactance can be calculated from the admittance matrix of the two-port network as [99]

$$\begin{cases} jX_{even} = \left(1/Y_{12}\right)_{even} \\ jX_{odd} = \left(1/Y_{12}\right)_{odd} \end{cases}, \tag{7-7}$$

where Y_{12} is the element of the admittance matrix.

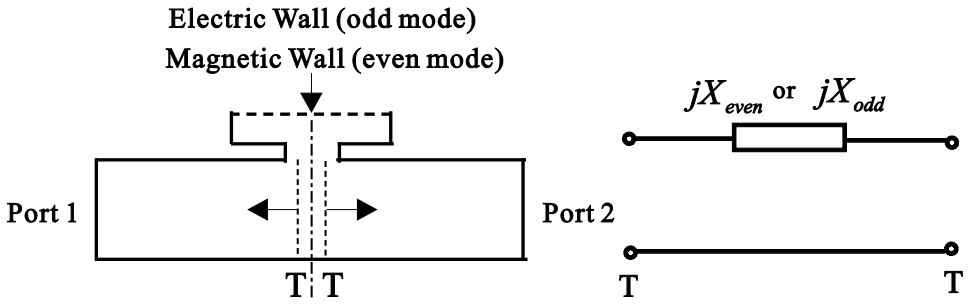

(a) (b)

Fig. 7.7 Analysis of the even mode and odd mode. (a) Analysis model. (b) Equivalent circuit.

The aperture width p_1 has a main effect on the even-mode reactance and the cavity width p_2 has a main effect on the odd-mode reactance. The two parameters can be employed to adjust the even-mode and odd-mode reactance and make them have the same magnitude but different signs. Fig. 7.8 shows a calculated example centered at 10 GHz in the case that d=5 mm, p_1=3.05 mm, p_2=8.75 mm, the thickness of the iris is 1 mm and the reference plane T is 0.05 mm away from the symmetrical plane. It is noted from the figure that the two series reactance have the same magnitude only at the center frequency 10 GHz and we should consider their frequency dispersion in a wide frequency band. We define two parameters as

$$\begin{cases} \Delta X_c(f) = \left(X_{odd} + X_{even}\right)/2 \\ K_c(f) = \left(X_{odd} - X_{even}\right)/2 \end{cases}. \tag{7-8}$$

It is noted from (7-8) that the frequency dispersion of the even- and odd-mode reactance are included in the two parameters. The synthesis formula (7-5) and (7-6) are modified as

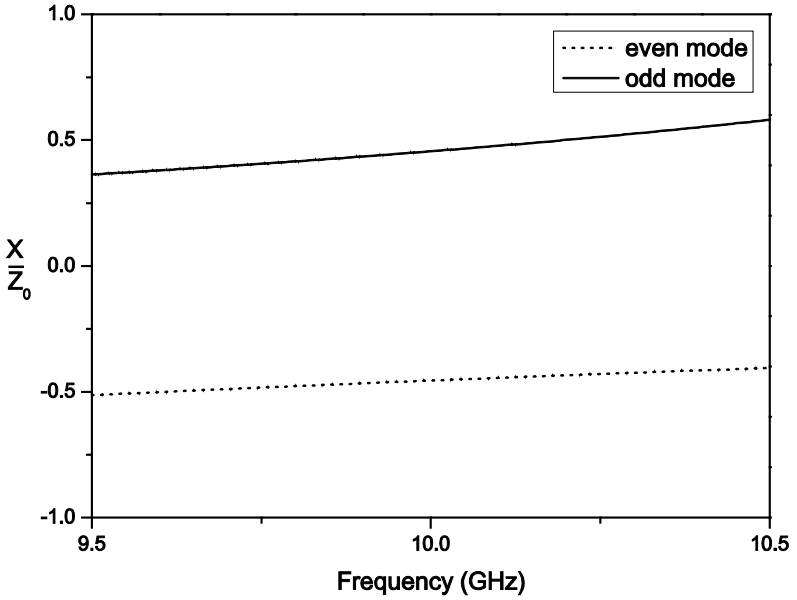

Fig. 7.8 Frequency dependence of relative reactance for even and odd mode.

$$\frac{X_{m-1}^{*}(f)}{Z_0} = \frac{\Delta X_c(f)}{Z_0} - \sin\left(\pi \cdot \frac{\lambda_g(f_0)}{\lambda_g(f)}\right) + \left(1 + (\frac{K_m}{Z_0})^2\right) \cdot \tan\left(\pi \cdot \frac{\lambda_g(f_0)}{\lambda_g(f)}\right) \qquad (7\text{-}9)$$

and

$$K_m^{*}(f) = K_c(f) + \frac{K_m \cdot \left(1 + \tan^2\left(\pi \cdot \lambda_g(f_0)/\lambda_g(f)\right)\right)}{1 - (\frac{K_m}{Z_0})^2 \cdot \tan^2\left(\pi \cdot \lambda_g(f_0)/\lambda_g(f)\right)} \quad . \qquad (7\text{-}10)$$

It is noted from (7-9) and (7-10) that the frequency dispersion of the cross-coupled inverter is included in the synthesis formula. At the center frequency f_0, (7-10) can be simplified as

$$K_m^{*}(f_0) = K_m(f_0) + K_c(f_0) \quad . \qquad (7\text{-}11)$$

7.3.2 Filter Synthesis

As introduced in Section 7.2, the cross-coupled filter circuit can be equivalent to a direct-coupled filter without cross-coupled inverters, which is the same as the conventional Chebyshev filter circuit except the resonator $X_{m-1}^{*}(f)$ and inverter

$K_m^*(f)$ in the central portion of the circuit. In the practical implementation, as we know, all the inverters are frequency-dependent. The frequency-dispersion of the cross-coupled inverter can be included in the equivalent resonator $X_{m-1}^*(f)$ and inverter $K_m^*(f)$. So we can employ the technique in CHAPTER 4 to synthesize the equivalent network in Fig. 7.3 when all the inverters are considered to be frequency-dependent. However, due to the difference in the central portion of the circuit, the iteration formula (4-17) and (4-18) are modified as

$$\begin{cases} L_{ai}^{(j)}\Big|_{i=1,2...m-2} = \left[\dfrac{K_i^{(j-1)}(f_1)}{K_i^{(j-1)}(f_0)}\right]^{\frac{i-1}{2m-2}-1} \cdot \left[\dfrac{K_{i+1}^{(j-1)}(f_1)}{K_{i+1}^{(j-1)}(f_0)}\right]^{\frac{-i}{2m-2}} \cdot X_i^{(j-1)}(f_1) \\ L_{a(m-1)}^{(j)} = \left[\dfrac{K_{m-1}^{(j-1)}(f_1)}{K_{m-1}^{(j-1)}(f_0)}\right]^{\frac{m-2}{2m-2}-1} \cdot \left[\dfrac{K_m^{*(j-1)}(f_1)}{K_m^{(j-1)}(f_0)+K_c(f_0)}\right]^{-\frac{1}{2}} \cdot X_{m-1}^{*(j-1)}(f_1) \end{cases} \tag{7-12}$$

and

$$\begin{cases} K_1^{(j)}(f_0) = \sqrt{\dfrac{Z_0 L_{a1}^{(j)}}{g_0 g_1}}\ , K_m^{*(j)}(f_0) = \dfrac{L_{a(m-1)}^{(j)}}{\sqrt{g_m g_{m-1}}} \\ K_i^{(j)}(f_0) = \sqrt{\dfrac{L_{ai}^{(j)} L_{a(i-1)}^{(j)}}{g_i g_{i-1}}}\Bigg|_{i=2,3,...,m-1} \\ K_m^{(j)}(f_0) = K_m^{*(j)}(f_0) - K_c(f_0) \end{cases}, \tag{7-13}$$

where

$$\frac{X_i^{(j-1)}(f_1)}{Z_0} = \sin\Big[\big(\lambda_g(f_0)/\lambda_g(f_1)\big)\cdot\big(\pi+\varphi_i^{(j-1)}(f_0)+\varphi_{i+1}^{(j-1)}(f_0)\big) - \varphi_i^{(j-1)}(f_1) - \varphi_{i+1}^{(j-1)}(f_1)\Big], \tag{7-14}$$

$$\frac{X_{m-1}^{*(j-1)}(f_1)}{Z_0} = \frac{\Delta X_c(f_1)}{Z_0} - \sin\left[\frac{\lambda_g(f_0)}{\lambda_g(f_1)}\cdot\big(\pi+\varphi_{m-1}^{(j-1)}(f_0)\big) - \varphi_{m-1}^{(j-1)}(f_1)\right] + \left(1+\left(\frac{K_m^{(j-1)}(f_1)}{Z_0}\right)^2\right)\cdot\tan\left[\frac{\lambda_g(f_0)}{\lambda_g(f_1)}\cdot\big(\pi+\varphi_m^{(j-1)}(f_0)\big) - \varphi_m^{(j-1)}(f_1)\right], \tag{7-15}$$

$$K_m^{*(j-1)}(f_1) = K_c(f_1) + \frac{K_m^{(j-1)}(f_1)\cdot\left(1+\tan^2\left(\pi\cdot\lambda_g(f_0)/\lambda_g(f_1)\right)\right)}{1-\left(\frac{K_m^{(j-1)}(f_1)}{Z_0}\right)^2\cdot\tan^2\left(\pi\cdot\lambda_g(f_0)/\lambda_g(f_1)\right)} \quad , \qquad (7\text{-}16)$$

where the superscript j denotes all the parameters after j iterations and f_1 is the lower edge frequency of the filter. It is noted from (7-12) and (7-16) that the calculation of $L_{a(m-1)}^{(j)}$ involves the frequency dispersion of the equivalent K-inverter $K_m^{*(j-1)}(f_1)$, which includes the frequency dispersion of the cross-coupled K-inverter $K_c(f_1)$ and the m-th K-inverter $K_m^{(j-1)}(f_1)$. It is also noted from (7-13) that we should calculate the required $K_m^{(j)}(f_0)$, not only the equivalent K-inverter $K_m^{*(j)}(f_0)$, because $K_m^{(j)}(f_0)$ is required for the practical inverter and $K_m^{*(j)}(f_0)$ is only a virtual inverter. In addition to the modified iteration formula (7-12)-(7-16), the calculation of initial parameters and the K-parameter extraction is the same as that in CHAPTER 4.

7.3.3 Design Procedure

The design procedure comprises the following steps:

Step 1) Determine the center frequency, lower edge frequency and the positions of transmission zeros for the waveguide cross-coupled filter.

Step 2) Calculate the approximated value for the cross-coupled K-inverter using (7-2) according to the position of transmission zeros. K_{m} can be approximated using the value of the ideal direct-coupled-cavity waveguide filters.

Step 3) Design the cross-coupled K-inverter according to the approximated value in Step 2). Calculate the required parameters using (7-7) and (7-8).

Step 4) Determine the layout of the whole filter. Calculate the converged parameters using an iteration procedure according to (7-12)-(7-16) together with the synthesis procedure in CHAPTER 4.

Step 5) Calculate the scattering parameters of the filter. If the position of transmission zeros is not precise enough, we can go back to Step 2) and use the

converged value for K_m instead of the approximated value. Repeat the steps from 3) to 5) until the position of transmission zeros satisfies our requirement.

Step 6) Calculate the insertion loss and return loss of the designed filter before it is fabricated and measured.

7.4 Design Example

To provide a better verification on the dimensional synthesis method, we design and fabricate a four-pole waveguide cross-coupled filter centered at 10 GHz. Fig. 7.9 shows 3D view of the filter and its fabricated photo. Since the filter is symmetrical around the middle plane of the waveguide, we display half of the symmetrical parts to give a better view of the inner structure. It is noted from Fig. 7.9 that the two transmission lines in the middle have smooth round corners to enable the filter to be folded. The effect of the round corner can be included in the design of the adjacent waveguide iris. The waveguide filter is fabricated without tuning screws and WR-90 (22.86 mm×10.16 mm) is chosen as the house waveguide. The dimension annotations for the waveguide cross-coupled filter are shown in Fig. 7.10 and its calculated dimensions are listed in Table VI. The filter is analyzed by commercial software Ansoft HFSS [98]. The calculated and measured scattering parameters and group delay of the waveguide cross-coupled filter are shown in Fig. 7.11 and Fig. 7.12, respectively. It can be seen from Fig. 7.11 that two transmission zeros are produced at 8.03 GHz and 11.94 GHz, respectively. A good equal-ripple response is achieved for the reflection magnitude below −20 dB and the fractional bandwidth of the filter is about 11% (9.48-10.58 GHz). It should be noted that the measured results are in a good agreement with the calculated results, thereby providing the final experimental validation of the method proposed in this chapter.

Table VI: DIMENSIONS FOR THE CROSS-COUPLED FILTER (UNITS: MILLIMETERS)

w_1	h_1	t_1	s_1	s_2	s_3	s_4
7.21	19.40	0.68	14.64	13.98	12.90	11.66
s_5	l_1	l_{21}	l_{22}	l_3	l_4	
14.90	11.83	16.33	16.85	13.75	12.87	

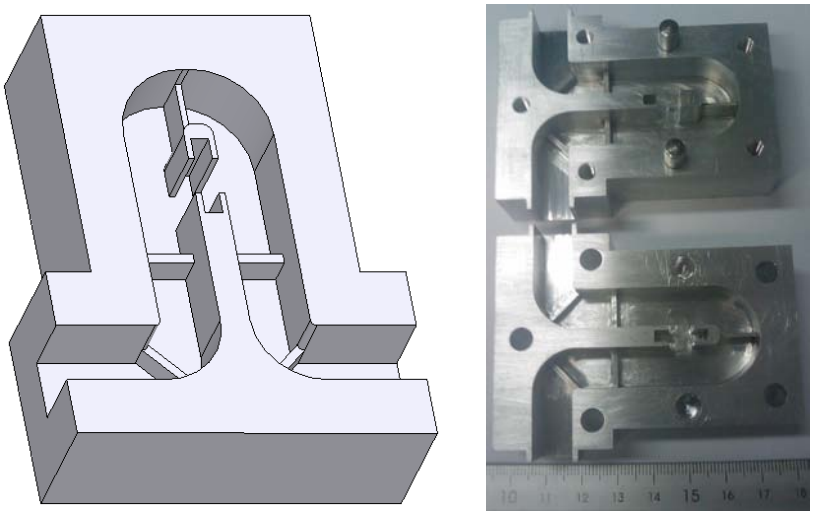

(a) (b)

Fig. 7.9 Configuration of the four-pole waveguide cross-coupled filter: (a) Half of the symmetrical structure. (b) Fabricated photo.

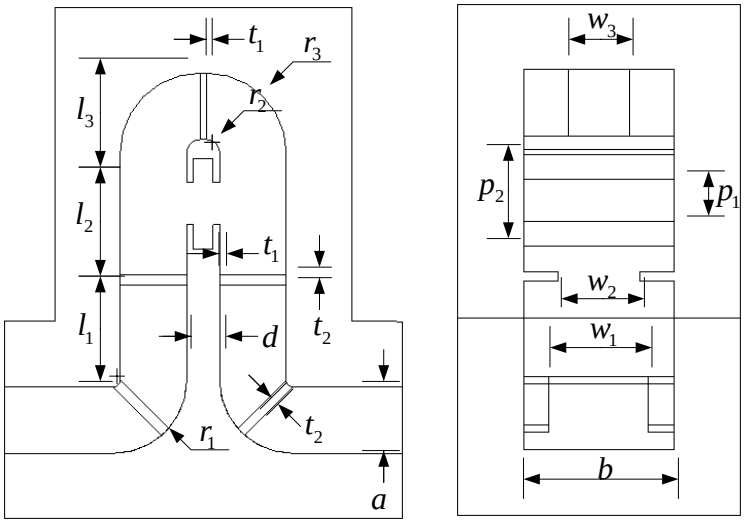

(a) (b)

Fig. 7.10 Dimension annotation for the four-pole waveguide cross-coupled filter: (a) top view. (b) side view.

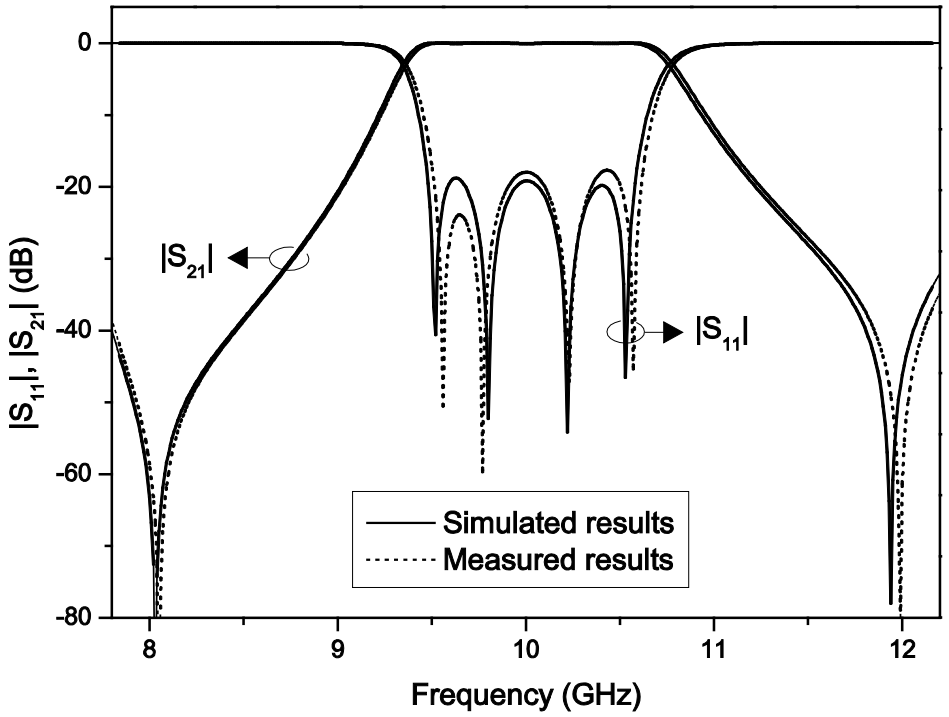

Fig. 7.11 The calculated and measured scattering parameters.

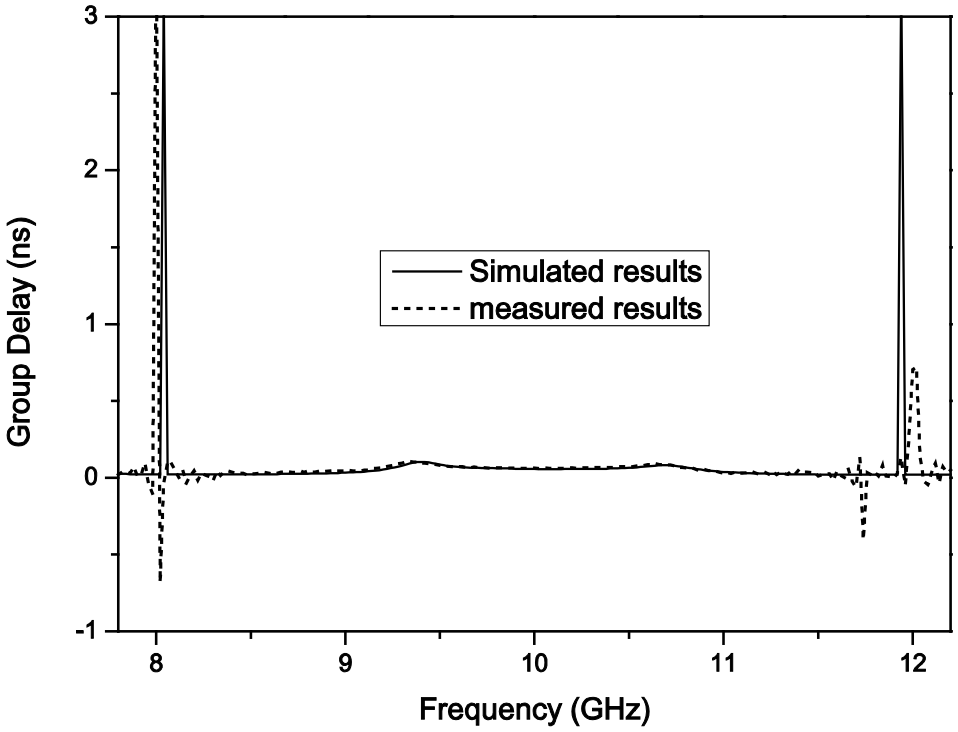

Fig. 7.12 The calculated and measured group delay.

7.5 Discussion

The key point of the proposed synthesis method in this chapter is that the cross-coupled filter circuit, based on the even-mode and odd-mode analysis, is made equivalent to a direct-coupled filter circuit, in which an equivalent resonator and K-inverter is employed. An advantage of this equivalence is that the frequency dispersion of the cross-coupled K-inverter and the *m*-th K-inverter can be included in the equivalent K-inverter as expressed in (7-10). Besides, the equivalent direct-coupled filter circuit is easy to be synthesized using the technique in CHAPTER 4.

There are also limitations for the transformation of the cross-coupled circuit model into a direct-coupled equivalent circuit. It cannot be applied in a very wide frequency band because some approximations are used in the transformation. Therefore, the cross-coupled waveguide filter using the proposed synthesis technique may not achieve a bandwidth as large as that of the direct-coupled waveguide filter in CHAPTER 4. However, the filter example of 11% bandwidth is already very wide for waveguide cross-coupled filters because the waveguide cross-coupled filter designed using the traditional coupling matrix method without optimization can only achieve a bandwidth of about 1%.

Besides, there is still much that can be done to improve the work. As shown in Fig. 7.5, the revised circuit model has the limitation that it cannot provide good out-of-band response. The original filter circuit in Fig. 7.1, though difficult to realize due to the mutual coupling between the cross-coupled K-inverter and its adjacent K-inverter, has better performance than the revised filter circuit in Fig. 7.4. If any techniques can be employed to solve the mutual coupling in a wide frequency band, that will be a great improvement to this work. Besides, only even-degree cross-coupled filter was discussed in this chapter and the odd-degree cross-coupled filter may be analyzed in the future work.

7.6 Summary

In this chapter, we have presented a dimensional synthesis method for the design of symmetric wide-band waveguide cross-coupled filters without resorting to global

full-wave optimization. In this method, we proposed two filter circuit models suitable for the synthesis of wide-band cross-coupled filters. Besides, we proposed a novel physical realization of the cross-coupled K-inverter in the waveguide filter. As a design example, an X-band four-pole waveguide cross-coupled filter has been designed and fabricated. The results show good equal-ripple performance in the passband and improved rejection performance beyond the passband. The proposed synthesis method is expected to find more applications in the synthesis of wide-band pseudo-elliptic filters.

CHAPTER 8
SYNTHESIS OF WIDE-BAND FILTERS WITH QUARTER-WAVELENGTH RESOANTORS

8.1 Introduction

In previous chapters, we have introduced some dimensional synthesis methods for the design of direct-coupled, in-line pseudo-elliptic and cross-coupled waveguide filters without global full-wave optimization. These filters are all designed with half-wavelength-transmission-line resonators. In this chapter, we will introduce a different type of bandpass filters, called quarter-wavelength-resonator bandpass filters, as shown in Fig. 8.1, which are composed of quarter-wavelength transmission lines with alternative K-inverters and J-inverters, as well as alternative high and low impedance levels. Advantages over half-wavelength-resonator filters include [95]: shorter length, second passband is centered at $3f_0$ instead of $2f_0$ (f_0 is center frequency), mid-stop-band attenuation is higher, precision design for a prescribed insertion loss characteristic is tractable to greater bandwidths, can be made in "bar transmission line" form without dielectric supports.

So far, however, the quarter-wavelength-resonator bandpass filters are still designed according to the classic method in [95] and no improved synthesis method was reported. In this chapter, we will extend the dimensional synthesis method for half-wavelength-resonator bandpass filters and enable it applicable to the design of wide-band quarter-wavelength-resonator bandpass filters without global full-wave optimization.

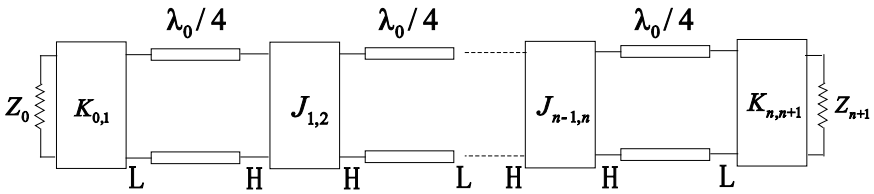

Fig. 8.1 Bandpass filters with quarter-wavelength resoantors (*n* is even).

In the second section of this chapter, we will introduce the application of the edge frequency mapping method to the quarter-wavelength-resonator bandpass filters. In the third section, the synthesis theory will be applied to rectangular coaxial filters and a design example will be presented. A summary will be given in the final section.

8.2 Theory

8.2.1 Equivalent Network for the Quarter-Wavelength-Resonator Filter

The classic quarter-wavelength-resonator bandpass filter is shown in Fig. 8.1, which has alternating high and low impedance levels on two ends of the quarter-wavelength transmission lines [95]. Here we only discuss the case that the first inverter is impedance inverter and the resonator number is even. Other cases can be derived in a similar way.

In order to derive the equivalent network for the quarter-wavelength-resonator bandpass filter, we should first derive the equivalent network for the quarter-wavelength transmission line, which has been discussed in [95]. As shown on the left side of Fig. 8.2, the input impedance can be expressed as

$$Z_{in} = Z_0 \cdot \frac{Z_L + jZ_0 \tan\frac{\pi\omega}{2\omega_0}}{Z_0 + jZ_L \tan\frac{\pi\omega}{2\omega_0}} \quad , \tag{8-1}$$

where Z_0 is the characteristic impedance of the transmission line and ω_0 is the center frequency when the transmission line is quarter wavelength. If $|Z_L| >> Z_0$, (8-1) can be approximated by

$$Z_{in} \approx Z_0 \cdot \frac{Z_L + jZ_0 \tan\frac{\pi\omega}{2\omega_0}}{jZ_L \tan\frac{\pi\omega}{2\omega_0}} = jX(\omega) + \frac{Z_0^2}{Z_L} \quad , \tag{8-2}$$

where

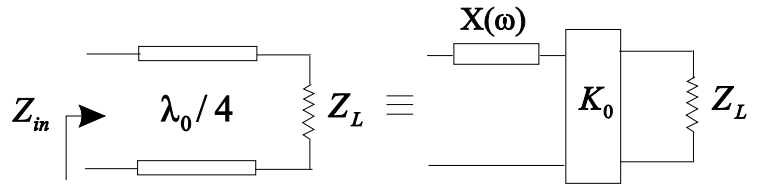

(a)

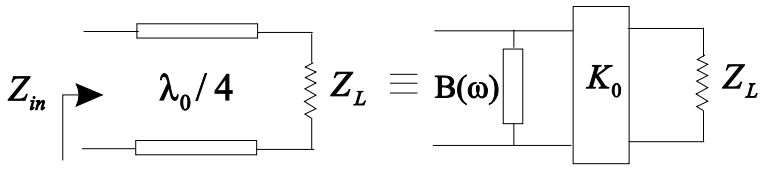

(b)

Fig. 8.2 Equivalent network for the quarter-wavelength transmission line: (a) $Z_L >> Z_0$, (b) $Z_L << Z_0$.

$$X(\omega) = -Z_0 \cot\frac{\pi\omega}{2\omega_0} \quad . \tag{8-3}$$

If $|Z_L| << Z_0$, (8-1) can be approximated by

$$Z_{in} \approx Z_0 \cdot \frac{jZ_0 \tan\dfrac{\pi\omega}{2\omega_0}}{Z_0 + jZ_L \tan\dfrac{\pi\omega}{2\omega_0}} = \frac{1}{jB(\omega) + \dfrac{Z_L}{Z_0^2}} \quad , \tag{8-4}$$

where

$$B(\omega) = -Y_0 \cot\frac{\pi\omega}{2\omega_0} \quad . \tag{8-5}$$

The equivalent network for the quarter-wavelength transmission line is shown in Fig. 8.2, where K_0 is an ideal unit K-inverter with the value Z_0. It is noted from the figure that the quarter-wavelength transmission line with a high impedance load can be equivalent to an ideal K-inverter with a series reactance and the quarter-wavelength transmission line with a low impedance load can be equivalent to an ideal K-inverter with a shunt susceptance. Since the quarter-wavelength-resonator bandpass filter has

an alternative high and low impedance level, we can easily derive the equivalent network for the quarter-wavelength-resonator bandpass filter as shown in Fig. 8.3.

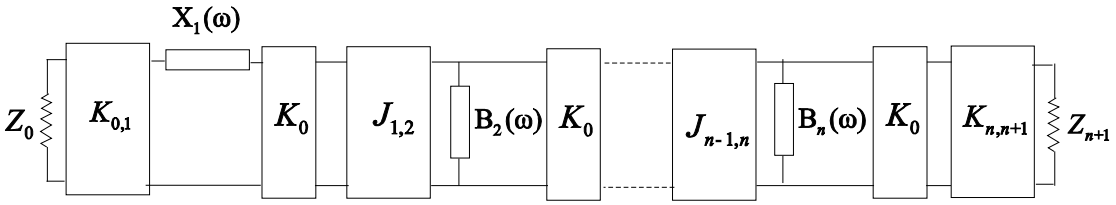

Fig. 8.3 Equivalent network for the quarter-wavelength-resonator bandpass filter.

8.2.2 Alternative Lowpass Prototype Filter

It is noted from Fig. 8.3 that the equivalent network for the quarter-wavelength-resonator bandpass filter has alternative K-inverters and J-inverters, and alternative series reactance and shunt susceptance. In order to employ the edge frequency mapping method, we have to transform the classic lowpass prototype filter in Fig. 8.4 into a new lowpass prototype filter which also has alternating K-inverters and J-inverters.

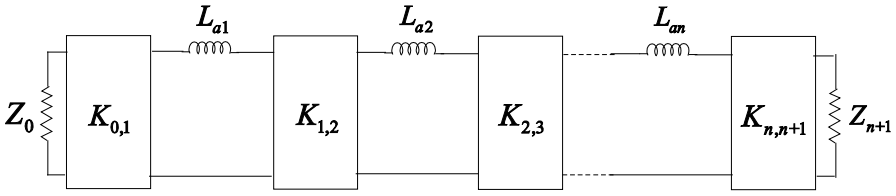

Fig. 8.4 The classic lowpass prototype filter.

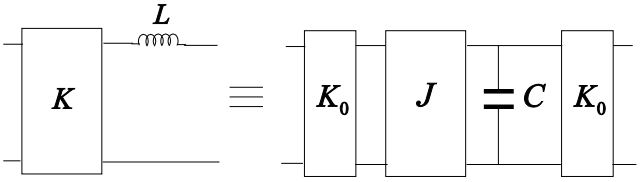

Fig. 8.5 The equivalence of two inverter networks.

In order to add J-inverter to the classic lowpass prototype filter in Fig. 8.4, we can employ the equivalence in Fig. 8.5. The K-inverter with series inductance can be

equivalent to a J-inverter and shunt capacitance with two ideal unit K-inverters on both sides. The transfer matrix of the ideal unit K-inverter is given by

$$\begin{bmatrix} 0 & jZ_0 \\ \dfrac{j}{Z_0} & 0 \end{bmatrix}, \tag{8-6}$$

where Z_0 is the input terminating impedance in Fig. 8.4. The following condition should be satisfied:

$$\begin{cases} \dfrac{K}{Z_0} = -\dfrac{J}{Y_0} \\ \dfrac{L}{Z_0} = \dfrac{C}{Y_0} \end{cases}, \tag{8-7}$$

where $Y_0 = 1/Z_0$.

So the classic lowpass prototype filter in in Fig. 8.4 can be transformed into the alternative lowpass prototype filter in Fig. 8.6. By substituting (8-7) into (2-4), we can calculate the K-inverters and J-inverters in the alternative lowpass prototype filter as

$$\begin{cases} \dfrac{K_{0,1}}{Z_0} = \sqrt{\dfrac{L_{a1}}{Z_0 g_0 g_1}} \\ \dfrac{K_{i,i+1}}{Z_0} = \sqrt{\dfrac{C_{ai} L_{a(i+1)}}{g_i g_{i+1}}}\Bigg|_{i=2,4,6.....}, \quad \dfrac{J_{i,i+1}}{Y_0} = \sqrt{\dfrac{L_{ai} C_{a(i+1)}}{g_i g_{i+1}}}\Bigg|_{i=1,3,5.....} \\ \dfrac{K_{n,n+1}}{Z_0} = \sqrt{\dfrac{C_{an} Z_{n+1}}{g_n g_{n+1}}} \end{cases}. \tag{8-10}$$

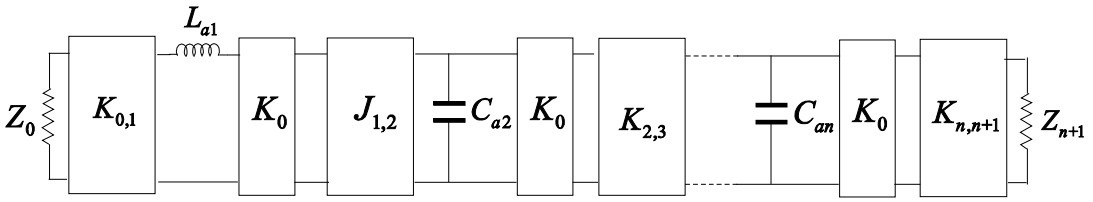

Fig. 8.6 The alternative lowpass prototype filter.

8.2.3 Edge Frequency Mapping Method

Since the alternative lowpass prototype filter in Fig. 8.6 and the equivalent network for the quarter-wavelength-resonator bandpass filter in Fig. 8.3 have been derived, the edge frequency mapping method can applied. The mapping function can be expressed as

$$f:\ \begin{cases} \Omega L_{ai} \rightarrow X_i(\omega), & i = 1,3,...n-1 \\ \Omega C_{ai} \rightarrow B_i(\omega), & i = 2,4,...n \end{cases} . \tag{8-9}$$

The following condition should be imposed:

$$\begin{cases} X_i(\omega_0) = 0,\ B_i(\omega_0) = 0 \\ X_i(\omega_1) = -\Omega_1 L_{ai},\ B_i(\omega_1) = -\Omega_1 C_{ai} \\ X_i(\omega_2) = \Omega_1 L_{ai},\ B_i(\omega_2) = \Omega_1 C_{ai} \end{cases} , \tag{8-10}$$

where Ω_1 is the cutoff angular frequency of the lowpass filter, and ω_0, ω_1, ω_2 denote the center angular frequency, lower and upper edge angular frequency of the bandpass filter, respectively. By solving (8-9) and (8-10), we can get

$$\begin{cases} L_{ai} = -X_i(\omega_1)/\Omega_1 & i = odd \\ C_{ai} = -B_i(\omega_1)/\Omega_1 & i = even \end{cases} \tag{8-11}$$

and

$$\begin{cases} X_i(\omega_1) + X_i(\omega_2) = 0 & i = odd \\ B_i(\omega_1) + B_i(\omega_2) = 0 & i = even \end{cases} . \tag{8-12}$$

Equation (8-12) denotes the condition imposed on the center frequency, lower and upper frequency of the bandpass filter. By substituting (8-8) with (8-11), the K-parameters and J-parameters can be calculated.

If the K-inverters and J-inverters in Fig. 8.3 are considered as ideal inverters, we can get a simple case. By substituting (8-11) and (8-12) with (8-3) and (8-5), we can get

$$\begin{cases} \dfrac{L_{ai}}{Z_0} = \dfrac{C_{ai}}{Y_0} = \dfrac{1}{\Omega_1} \cdot \cot\dfrac{\pi\omega_1}{2\omega_0} \\ \cot\dfrac{\pi\omega_1}{2\omega_0} + \cot\dfrac{\pi\omega_2}{2\omega_0} = 0 \end{cases} . \tag{8-13}$$

8.2.4 Frequency-Dependent Inverter

The result in (8-13) is calculated on the condition that all the inverters are ideal. However, the practical inverters are all frequency-dependent. Similarly, we define a general turn ratio as

$$m_{i,i+1}(\omega) = \begin{cases} K_{i,i+1}(\omega)/K_{i,i+1}(\omega_0) \ , & i = 0,2,...n \\ J_{i,i+1}(\omega)/J_{i,i+1}(\omega_0) \ , & i = 1,3,...n-1 \end{cases} . \tag{8-14}$$

It is noted from Fig. 8.3 that there is an ideal unit K-inverter on the left side of every frequency-dependent inverter. So we combine the ideal unit K-inverter and the frequency-dependent inverter in the decomposition. The transfer matrix of the frequency-dependent K-inverter together with the ideal unit K-inverter can be presented as

$$\begin{aligned} &\begin{bmatrix} 0 & jZ_0 \\ \dfrac{j}{Z_0} & 0 \end{bmatrix} \begin{bmatrix} 0 & jK_{i,i+1}(\omega) \\ \dfrac{j}{K_{i,i+1}(\omega)} & 0 \end{bmatrix} \\ &= \begin{bmatrix} -\dfrac{Z_0}{K_{i,i+1}(\omega)} & 0 \\ 0 & -\dfrac{K_{i,i+1}(\omega)}{Z_0} \end{bmatrix} \\ &= \begin{bmatrix} m_{i,i+1}^{-i/n}(\omega) & 0 \\ 0 & m_{i,i+1}^{i/n}(\omega) \end{bmatrix} \begin{bmatrix} -\dfrac{Z_0}{K_{i,i+1}(\omega_0)} & 0 \\ 0 & -\dfrac{K_{i,i+1}(\omega_0)}{Z_0} \end{bmatrix} \begin{bmatrix} m_{i,i+1}^{i/n-1}(\omega) & 0 \\ 0 & m_{i,i+1}^{1-i/n}(\omega) \end{bmatrix} \\ &= \begin{bmatrix} m_{i,i+1}^{-i/n}(\omega) & 0 \\ 0 & m_{i,i+1}^{i/n}(\omega) \end{bmatrix} \begin{bmatrix} 0 & jZ_0 \\ \dfrac{j}{Z_0} & 0 \end{bmatrix} \begin{bmatrix} 0 & jK_{i,i+1}(\omega_0) \\ \dfrac{j}{K_{i,i+1}(\omega_0)} & 0 \end{bmatrix} \begin{bmatrix} m_{i,i+1}^{i/n-1}(\omega) & 0 \\ 0 & m_{i,i+1}^{1-i/n}(\omega) \end{bmatrix} . \end{aligned} \tag{8-15}$$

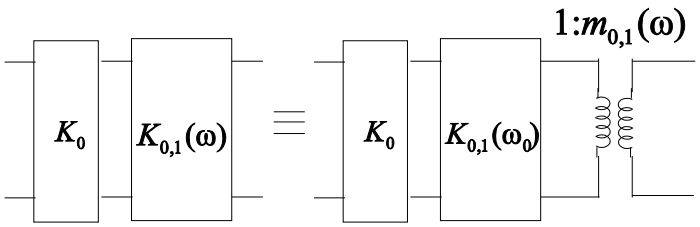

(a)

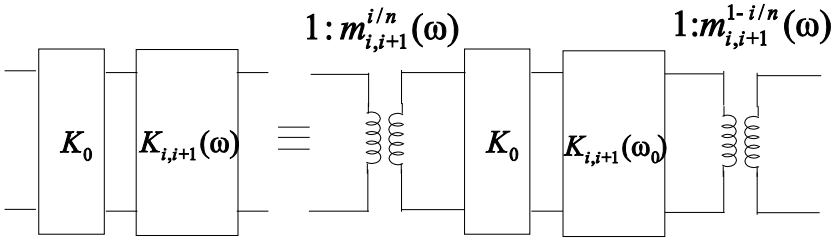

(b)

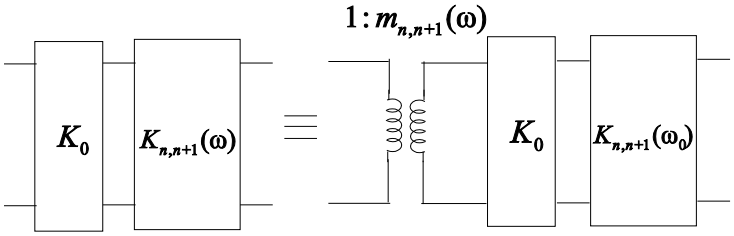

(c)

Fig. 8.7 Decomposition of the frequency-dependent K inverters: (a) The first inverter (b) The (i+1)-th inverter (c) The last inverter.

According to (8-15), the decomposition for the K-inverter is shown in Fig. 8.7. It can be seen that the transformer is added only on one side for the first and last inverter by using the weight exponent. So the frequency dependence of the two end inverters can be distributed equally to all the others. Similarly, the transfer matrix of the frequency-dependent J-inverter together with the ideal unit K-inverter can be presented as

$$\begin{bmatrix} 0 & jZ_0 \\ \dfrac{j}{Z_0} & 0 \end{bmatrix} \begin{bmatrix} 0 & \dfrac{j}{J_{i,i+1}(\omega)} \\ jJ_{i,i+1}(\omega) & 0 \end{bmatrix}$$

$$= \begin{bmatrix} m_{i,i+1}^{i/n}(\omega) & 0 \\ 0 & m_{i,i+1}^{-i/n}(\omega) \end{bmatrix} \begin{bmatrix} 0 & jZ_0 \\ \dfrac{j}{Z_0} & 0 \end{bmatrix} \begin{bmatrix} 0 & \dfrac{j}{J_{i,i+1}(\omega_0)} \\ jJ_{i,i+1}(\omega_0) & 0 \end{bmatrix} \begin{bmatrix} m_{i,i+1}^{1-i/n}(\omega) & 0 \\ 0 & m_{i,i+1}^{i/n-1}(\omega) \end{bmatrix} .$$

(8-16)

The decomposition of the frequency-dependent J-inverter is shown in Fig. 8.8.

Similar to CHAPTER 4, the turns ratio can be absorbed by the adjacent distributed resonators. Fig. 8.9 and Fig. 8.10 show the turns ratio absorbed by the series reactance and shunt susceptance. By applying (8-3) and (8-5), the new reactance and susceptance can be expressed as

$$\begin{aligned} X_i^*(\omega) &= m_{i-1,i}^{(i-1)/n-1}(\omega) \cdot m_{i,i+1}^{-i/n}(\omega) \cdot X_i(\omega) \\ &= -Z_0 m_{i-1,i}^{(i-1)/n-1}(\omega) m_{i,i+1}^{-i/n}(\omega) \cot\left(\frac{\pi\omega}{2\omega_0}\right) \end{aligned} , \quad (8\text{-}17)$$

$$\begin{aligned} B_i^*(\omega) &= m_{i-1,i}^{(i-1)/n-1}(\omega) \cdot m_{i,i+1}^{-i/n}(\omega) \cdot B_i(\omega) \\ &= -Y_0 m_{i-1,i}^{(i-1)/n-1}(\omega) m_{i,i+1}^{-i/n}(\omega) \cot\left(\frac{\pi\omega}{2\omega_0}\right) \end{aligned} . \quad (8\text{-}18)$$

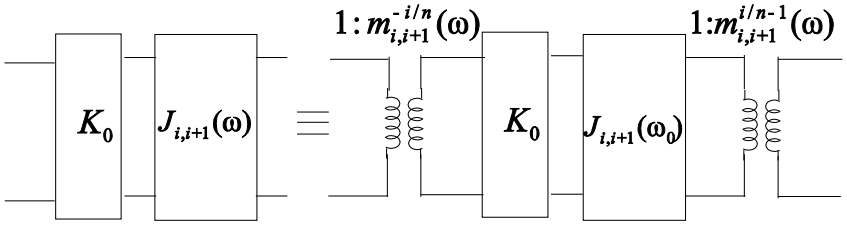

Fig. 8.8 Decomposition of the frequency-dependent J inverters.

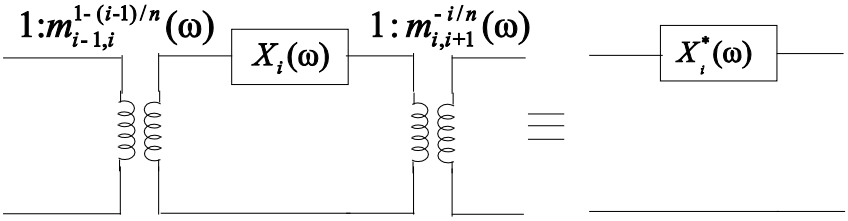

Fig. 8.9 Turns ratio absorbed by the series reactance.

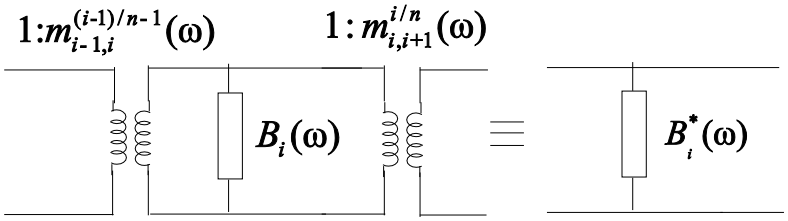

Fig. 8.10 Turns ratio absorbed by the shunt susceptance.

By applying the edge frequency mapping method, the mapping function can be expressed as

$$f:\begin{cases}\Omega L_{ai}\rightarrow -Z_0 m_{i-1,i}^{(i-1)/n-1}(\omega)m_{i,i+1}^{-i/n}(\omega)\cot\left(\dfrac{\pi\omega}{2\omega_0}\right) & i=odd\\ \Omega C_{ai}\rightarrow -Y_0 m_{i-1,i}^{(i-1)/n-1}(\omega)m_{i,i+1}^{-i/n}(\omega)\cot\left(\dfrac{\pi\omega}{2\omega_0}\right) & i=even\end{cases}. \tag{8-19}$$

By applying (8-11), we can get

$$\begin{cases}\dfrac{L_{ai}}{Z_0}=\dfrac{1}{\Omega_1}m_{i-1,i}^{(i-1)/n-1}(\omega_1)\cdot m_{i,i+1}^{-i/n}(\omega_1)\cdot\cot\left(\dfrac{\pi\omega_1}{2\omega_0}\right) & i=odd\\ \dfrac{C_{ai}}{Y_0}=\dfrac{1}{\Omega_1}m_{i-1,i}^{(i-1)/n-1}(\omega_1)\cdot m_{i,i+1}^{-i/n}(\omega_1)\cdot\cot\left(\dfrac{\pi\omega_1}{2\omega_0}\right) & i=even\end{cases}. \tag{8-20}$$

The K-parameters and J-parameters can be calculated by substituting (8-10) with (8-20).

8.3 Synthesis of Rectangular Coaxial Filters

Since the synthesis theory for the quarter-wavelength-resonator bandpass filters has been introduced, we will apply it to the design of rectangular coaxial filters. Rectangular coaxial cable has the advantage of low dielectric loss, low radiation loss and weak cross coupling with other circuits in a system [100]. They can be fabricated using the micromachining techniques and many applications are reported in [100]-[102]. Fig. 8.11 shows the cross section of the rectangular coaxial line. The dimensions are chosen according to [103] and [104] to make the characteristics

impedance is close to 50 ohms and the cutoff frequency of the higher modes is above the frequency band of the designed filter.

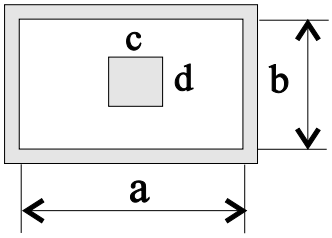

Fig. 8.11 Cross section of the rectangular coaxial cable.

8.3.1 Realization of the K-Inverter and J-Inverter

In order to apply the theories in the last section to the rectangular coaxial filters, it is necessary to find two rectangular coaxial structures to realize the K-inverter and J-inverter. As shown in Fig. 8.12, we employed an inductive iris structure with two compensated transmission lines added on both sides as the K-inverter. Its equivalent model consists of a frequency-dependent K-inverter and two extra transmission lines on both sides. Similarly, Fig. 8.13 shows the capacitive gap structure as the J-inverter and its equivalent model. The extra transmission line phase can be expressed as

$$\Delta\varphi_i(\omega) = \left(\omega/\omega_0\right)\cdot\varphi_i(\omega_0) - \varphi_i(\omega) \quad . \tag{8-21}$$

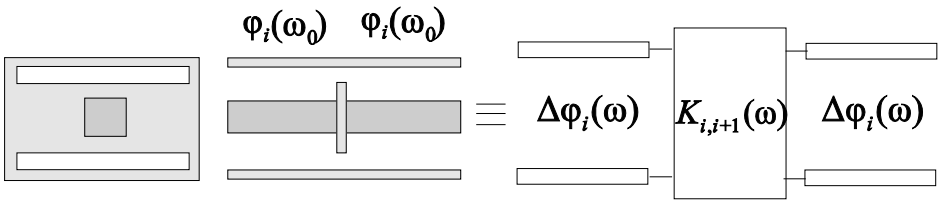

Fig. 8.12 Realization of the K-inverter and its frequency-dependent model.

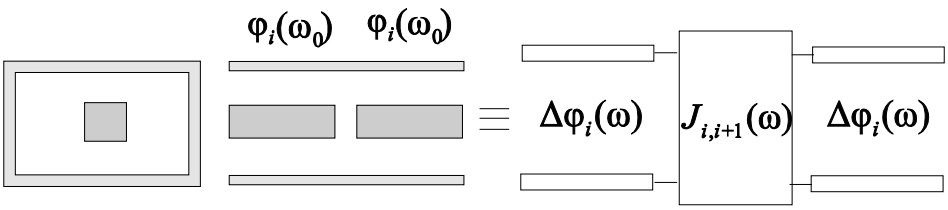

Fig. 8.13 Realization of the J-inverter and its frequency-dependent model.

The derivation of (8-21) is similar to that of (4-16). The frequency-dependent inverter in Fig. 8.12 and Fig. 8.13 can be decomposed further into frequency-independent inverter with exponent-weighted turns ratio on both sides as introduced in the last section.

8.3.2 Filter Synthesis

By applying the equivalent model for the inductive iris and capacitive gap structure introduced above together with the decomposition of frequency-dependent inverter in the last section, we can derive the expression for the series reactance and shunt susceptance, which absorb the turns ratio and the extra transmission lines from the adjacent inverters. They can be expressed as

$$X_i(\omega)/Z_0 = -m_{i-1,i}^{(i-1)/n-1}(\omega)\cdot m_{i,i+1}^{-i/n}(\omega) \cdot\cot\left[\frac{\omega}{\omega_0}\cdot\left(\frac{\pi}{2}+\varphi_i(\omega_0)+\varphi_{i-1}(\omega_0)\right)-\left(\varphi_i(\omega)+\varphi_{i-1}(\omega)\right)\right] \quad i=odd \quad , \tag{8-22}$$

$$B_i(\omega)/Y_0 = -m_{i-1,i}^{(i-1)/n-1}(\omega)\cdot m_{i,i+1}^{-i/n}(\omega) \cdot\cot\left[\frac{\omega}{\omega_0}\cdot\left(\frac{\pi}{2}+\varphi_i(\omega_0)+\varphi_{i-1}(\omega_0)\right)-\left(\varphi_i(\omega)+\varphi_{i-1}(\omega)\right)\right] \quad i=even \quad . \tag{8-23}$$

For derivation convenience, we take the following notations:

$$E_i(\omega)=\begin{cases} X_i(\omega)/Z_0 & i=odd \\ B_i(\omega)/Y_0 & i=even \end{cases} \quad , \tag{8-24}$$

$$D_i=\begin{cases} L_{ai}/Z_0 & i=odd \\ C_{ai}/Y_0 & i=even \end{cases} \quad , \tag{8-25}$$

$$A_{i,i+1}(\omega)=\begin{cases} K_{i,i+1}(\omega)/Z_0 & i=0,2,...n \\ J_{i,i+1}(\omega)/Y_0 & i=1,3,...n-1 \end{cases} \quad . \tag{8-26}$$

By substituting (8-14) with (8-26), we can get

$$m_{i,i+1}(\omega)=A_{i,i+1}(\omega)/A_{i,i+1}(\omega_0) \quad . \tag{8-27}$$

The mapping function can be written as

$$f:\ \Omega D_i \to E_i(\omega) \quad . \tag{8-28}$$

By applying (8-11) and (8-10), we can get

$$\begin{aligned} D_i = \frac{1}{\Omega_1}\cdot\left[\frac{A_{i-1,i}(\omega_1)}{A_{i-1,i}(\omega_0)}\right]^{(i-1)/n-1} \cdot\left[\frac{A_{i,i+1}(\omega_1)}{A_{i,i+1}(\omega_0)}\right]^{-i/n} \\ \cdot\cot\left[\frac{\omega}{\omega_0}\cdot\left(\frac{\pi}{2}+\varphi_i(\omega_0)+\varphi_{i-1}(\omega_0)\right)-\left(\varphi_i(\omega_1)+\varphi_{i-1}(\omega_1)\right)\right] \end{aligned} \tag{8-29}$$

$$\begin{cases} A_{0,1}(\omega_0)=\sqrt{\dfrac{D_1}{g_0 g_1}} \\ A_{i,i+1}(\omega_0)=\sqrt{\dfrac{D_i D_{i+1}}{g_i g_{i+1}}}\Bigg|_{i=1,2,\ldots,n-1} \\ A_{n,n+1}(\omega_0)=\sqrt{\dfrac{D_n}{g_n g_{n+1}}} \end{cases} . \tag{8-30}$$

Similarly to CHAPTER 4, we should employ an iteration procedure to calculate the parameters. $A_{i,i+1}^{(j)}(\omega_0)$, $A_{i,i+1}^{(j)}(\omega_1)$, $\varphi_i^{(j)}(\omega_0)$ and $D_i^{(j)}$ are used to represent all the parameters after *j* iterations. The parameters after *j* iterations can be calculated using the parameters after (*j*-1) iterations as

$$\begin{aligned} D_i^{(j)} = \frac{1}{\Omega_1}\cdot\left[\frac{A_{i-1,i}^{(j-1)}(\omega_1)}{A_{i-1,i}^{(j-1)}(\omega_0)}\right]^{(i-1)/n-1} \cdot\left[\frac{A_{i,i+1}^{(j-1)}(\omega_1)}{A_{i,i+1}^{(j-1)}(\omega_0)}\right]^{-i/n} \\ \cdot\cot\left[\frac{\omega}{\omega_0}\cdot\left(\frac{\pi}{2}+\varphi_i^{(j-1)}(\omega_0)+\varphi_{i-1}^{(j-1)}(\omega_0)\right)-\left(\varphi_i^{(j-1)}(\omega_1)+\varphi_{i-1}^{(j-1)}(\omega_1)\right)\right] \end{aligned} , \tag{8-31}$$

$$\begin{cases} A_{0,1}^{(j)}(\omega_0)=\sqrt{\dfrac{D_1^{(j)}}{g_0 g_1}} \\ A_{i,i+1}^{(j)}(\omega_0)=\sqrt{\dfrac{D_i^{(j)} D_{i+1}^{(j)}}{g_i g_{i+1}}}\Bigg|_{i=1,2,\ldots,n-1} \\ A_{n,n+1}^{(j)}(\omega_0)=\sqrt{\dfrac{D_n^{(j)}}{g_n g_{n+1}}} \end{cases} . \tag{8-32}$$

Since the synthesis is an iteration procedure, we should set initial parameters for the iteration. The initial parameters $A_{i,i+1}^{(0)}(\omega_0)$, $A_{i,i+1}^{(0)}(\omega_1)$, $\varphi_i^{(0)}(\omega_0)$ and $D_i^{(0)}$ can be calculated from the ideal inverter model. For the ideal inverter case, the exponent-weighted turns ratio and the extra transmission lines are not considered. So the calculation of $D_i^{(0)}$ is a compact form of (8-31) and it is written as

$$D_i^{(0)} = \frac{1}{\Omega_1} \cdot \cot\left(\frac{\pi\omega_1}{2\omega_0}\right) = D \quad . \tag{8-33}$$

By substituting (8-32) with (8-33), we can get

$$\begin{cases} A_{0,1}^{(0)}(\omega_0) = \sqrt{\dfrac{D}{g_0 g_1}} \\ A_{i,i+1}^{(0)}(\omega_0) = \left.\dfrac{D}{\sqrt{g_i g_{i+1}}}\right|_{i=1,2,\ldots,n-1} \\ A_{n,n+1}^{(0)}(\omega_0) = \sqrt{\dfrac{D}{g_n g_{n+1}}} \end{cases} . \tag{8-34}$$

8.3.3 Element Prameters Extraction

Fig. 8.14 depicts the quarter-wavelength resonator bandpass filter realized in rectangular coaxial structures. In order to achieve the required Chebyshev response, the iris widths, gap widths and the resonator lengths must be derived.

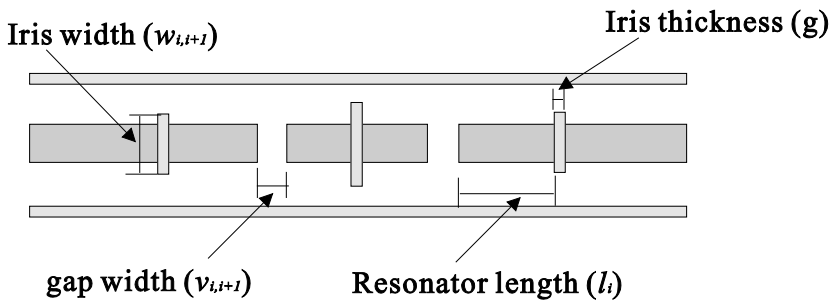

Fig. 8.14 Configuration of the quarter-wavelength-resonator bandpass filter realized in rectangular coaxial structures.

For a given inductive iris or capacitive gap dimension, we can calculate the scattering parameters using the full-wave simulation or mode-matching program. The K-parameters and the compensated transmission line phase can be calculated by

$$\begin{cases} \dfrac{K_{i,i+1}(\omega)}{Z_0} = \sqrt{\dfrac{1-\left|S_{11}(\omega)_i\right|}{1+\left|S_{11}(\omega)_i\right|}} \\ \varphi_i(\omega) = \dfrac{1}{2}(\angle S_{11}(\omega)_i - \pi) \end{cases}, \tag{8-35}$$

where $S_{11}(\omega)_i$ is the reflection coefficient of the inductive iris element. The J-parameters and the compensated transmission line phase can be also calculated by

$$\begin{cases} \dfrac{J_{i,i+1}(\omega)}{Y_0} = \sqrt{\dfrac{1-\left|S_{11}(\omega)_i\right|}{1+\left|S_{11}(\omega)_i\right|}} \\ \varphi_i(\omega) = \dfrac{1}{2}\angle S_{11}(\omega)_i \end{cases}, \tag{8-36}$$

where $S_{11}(\omega)_i$ is the reflection coefficient of the capacitive gap element.

Here we still use the cubic spline data interpolation to calculate the element dimension and other parameters. First we employ a full-wave simulation to calculate the scattering parameters of the inductive iris with a series of widths $[w]$ and the capacitive gap with a series of widths $[v]$. Then the sampling data of $[K(\omega_0)]$, $[K(\omega_1)]$ and $[\varphi_K(\omega_0)]$ can be calculated using (8-35). The sampling data of $[J(\omega_0)]$, $[J(\omega_1)]$ and $[\varphi_J(\omega_0)]$ can be also calculated using (8-36). With these sampling data, we can build the cubic spline functions. The widths of the inductive iris and the capacitive gap can be calculated as

$$\begin{cases} w_{i,i+1} = S\left([K(\omega_0)],[w],A_{i,i+1}(\omega_0)\right) & i = 0,2,...n \\ v_{i,i+1} = S\left([J(\omega_0)],[v],A_{i,i+1}(\omega_0)\right) & i = 1,3,...n-1 \end{cases}, \tag{8-37}$$

where the function $S([a],[b],x)$ denotes the cubic spline interpolation function based on the sampling data $[a]$ and $[b]$ and x is the interpolation variable. The calculations of $A_{i,i+1}(\omega_1)$ and $\varphi_i(\omega_0)$ can be also expressed as

$$A_{i,i+1}(\omega_1) = \begin{cases} S\left([K(\omega_0)],[K(\omega_1)],A_{i,i+1}(\omega_0)\right) & i = 0,2,...n \\ S\left([J(\omega_0)],[J(\omega_1)],A_{i,i+1}(\omega_0)\right) & i = 1,3,...n-1 \end{cases} , \quad (8\text{-}38)$$

$$\varphi_i(\omega_0) = \begin{cases} S\left([K(\omega_0)],[\varphi_K(\omega_0)],A_{i,i+1}(\omega_0)\right) & i = 0,2,...n \\ S\left([J(\omega_0)],[\varphi_J(\omega_0)],A_{i,i+1}(\omega_0)\right) & i = 1,3,...n-1 \end{cases} . \quad (8\text{-}39)$$

After the compensated transmission line phase $\varphi_i(\Omega_0)$ is calculated, the lengths of the transmission line resonator are given by

$$l_i = \frac{\lambda_g(\omega_0)}{2\pi}\left[\frac{\pi}{2} + \varphi_{i-1}(\omega_0) + \varphi_i(\omega_0)\right] . \quad (8\text{-}40)$$

With this approach, the element parameters extraction using the full-wave simulation is performed only one time and the sampling data can be calculated.

8.3.4 Design Procedure

The design procedure comprises the following steps:

Step 1) First we should determine the center frequency and lower edge frequency according to the filter design requirement. Then different inductive iris and capacitive gap elements with a series of widths are chosen and the full-wave simulation is employed to calculate the scattering parameters at the center frequency and lower edge frequency. By applying (8-35) and (8-36), the sampling data of the K- and J-parameters at the center frequency and the lower edge frequency, as well as the phase of the compensated transmission line can be calculated.

Step 2) The ideal inverter model is employed to calculate the initial parameters $A_{i,i+1}^{(0)}(\omega_0)$ by applying (8-33) and (8-34). The other two initial parameters $A_{i,i+1}^{(0)}(\omega_1)$ and $\varphi_i^{(0)}(\omega_0)$ are obtained using the cubic spline data interpolation in (8-38) and (8-39) together with the sampling data in Step 1).

Step 3) Based on the initial parameters in Step 2), the improved frequency-dependent inverter model is then established. The corrected K- and J-

parameters at the center frequency $A_{i,i+1}^{(1)}(\omega_0)$ are calculated according to (37) and (38). Using the cubic spline data interpolation in (8-38) and (8-39) together with the sampling data in Step 1), the other two corrected parameters $A_{i,i+1}^{(1)}(\omega_1)$ and $\varphi_i^{(1)}(\omega_0)$ are obtained.

Step 4) A further improved inverter model is then established based on the corrected parameters. By repeating Step 3), all the parameters $A_{i,i+1}^{(j)}(\omega_0)$, $A_{i,i+1}^{(j)}(\omega_1)$ and $\varphi_i^{(j)}(\omega_0)$ will be further corrected.

Step 5) The Step 3) and Step 4) are repeated until the K and J parameters after *N* iterations $A_{i,i+1}^{(N)}(\omega_0)$ converge. With the converged K and J parameters, the inductive iris and the capacitive gap widths and the resonator lengths are calculated using (8-37) and (8-40). Finally, a full-wave analysis of the computed filter is carried out.

8.3.5 Design Example and Results

The filters here are designed without global optimizations and are expected to have good in-band equal-ripple performance in a wide bandwidth. Since no excessive global optimizations are needed, the time and complexity of the design procedure can be improved significantly. One example of rectangular coaxial quarter-wavelength-resonator bandpass filter with a center frequency of 5 GHz is designed and presented here. The dimensions for the filter are listed in Table VII. The dimension of the rectangular coaxial cable is chosen as *a*=16 mm, *b*=6.5 mm, *c*=3 mm and *d*=3 mm.

The filters are designed for Chebyshev response with equal ripple performance in the passband. The scattering parameters of the designed filter is calculated by full-wave simulations using the commercial software Ansoft HFSS [98]. Fig. 8.15 shows the scattering parameters of the rectangular coaxial filters designed using the proposed synthesis method and the traditional method in [95]. It is noted from the figure that the filter designed using the proposed synthesis method has a good equal-ripple performance in the passband and the fractional bandwidth is about 70% (3.7-7.2 GHz). It is also noted that the performance of the filter using the traditional

method are seriously degraded in such a large bandwidth, which finally verify the efficiency of the proposed synthesis method.

Table VII: DIMENSIONS OF THE RECTANGULAR COAXIAL FILTER (UNITS: MILLIMETERS)

g	$w_{0,1}$, $w_{4,5}$	$v_{1,2}$, $v_{3,4}$	$w_{2,3}$	l_1, l_4	l_2, l_3
0.5	0.265	0.373	3.674	5.600	7.878

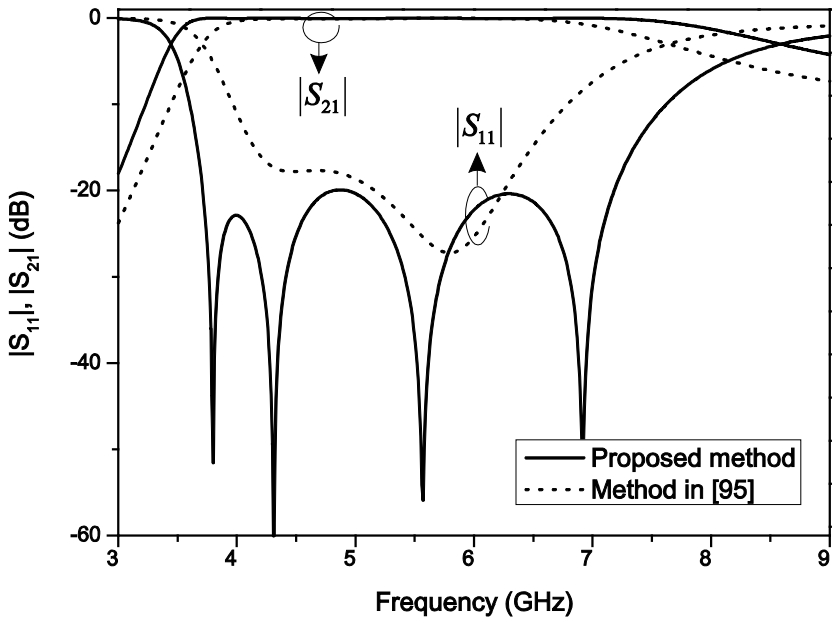

Fig. 8.15 Scattering parameters comparison between the proposed method and the traditional method in [95].

8.4 Summary

In this chapter we have presented a dimensional synthesis method for the design of wide-band quarter-wavelength-resonator bandpass filters. In this synthesis method, an alternative lowpass prototype filter was proposed to enable the edge frequency mapping method to be applied. The frequency-dependent K- and J-inverter model was also employed in order to incorporate the frequency dependence of inverters. Based on the edge frequency mapping method, an iterative dimensional synthesis procedure has been presented. As design examples, a four-pole rectangular coaxial

bandpass filter with about 70% fractional bandwidth was designed. The results show better equal ripple performance in the passband, compared with that of the filter designed using the traditional method. The proposed synthesis method is expected to find more applications in designing wide-band bandpass filters.

CHAPTER 9
CONCLUSIONS AND RECOMMENDATIONS

9.1 Conclusions

In this dissertation, a new mapping method, edge frequency mapping method, has been proposed for the synthesis of wide-band bandpass filters. In the method, the distributed-element bandpass filter was directly transformed from the lowpass prototype filter, and the reactance values at the center frequency and band edge frequency were employed in the transformation. In order to apply the new mapping method to the design of bandpass filters with frequency-dispersive inverters, we presented a general approach to deal with the frequency dispersion of inverters, in which the frequency-dispersive inverter is decomposed into a frequency-invariant inverter with two exponent-weighted frequency-dispersive transformers on both sides.

To provide the validation of the edge frequency mapping method, we apply it to the design of direct-coupled waveguide filters and propose a dimensional synthesis method without global full-wave optimization. As design examples, two four-pole filters with fractional bandwidth of 16.7% and 20.2% were designed and presented, respectively. The results show good equal ripple performance in the passband for the return loss below －20 dB. Besides, a comparison of the proposed method with the traditional method has also been conducted to provide the final validation of the proposed method.

To extend the dimensional synthesis method for direct-coupled waveguide filters to include pseudo-elliptic waveguide filters, three approaches has been proposed. The first approach was to employ the cavity-backed K-inverters, which can produce transmission zeros in the out-of-band response, however, whose frequency response in the passband is similar to that of normal iris inverters. This approach could be applied to the synthesis of in-line pseudo-elliptic waveguide filters. The second approach was to employ the customized resonators, which can produce

transmission zeros in the out-of-band response, however, whose frequency response in the passband is similar to that of normal half-wavelength-transmission-line resonators. This approach could be also applied to the synthesis of in-line pseudo-elliptic waveguide filters. The third approach is applied to the synthesis of cross-coupled waveguide filters. To synthesize an equal-ripple response in the passband, a direct-coupled filter network equivalent to the cross-coupled filter network is proposed based on the even-mode and odd-mode analysis.

In addition to the pseudo-elliptic waveguide filters, we also extended the dimensional synthesis method to include quarter-wavelength-resonator bandpass filters. To apply the edge frequency mapping method to the quarter-wavelength-resonator bandpass filters, a new lowpass prototype filter with alternative K-inverters and J-inverters was proposed. The decomposition approach for frequency-dispersive inverters and the synthesis procedure were also modified to be suitable for the dimensional synthesis of quarter-wavelength-resonator bandpass filters. As examples, a rectangular coaxial bandpass filter was designed for about 70% fractional bandwidth without resort to global full-wave optimization. The results show a good equal-ripple performance for the return loss below －20 dB, which provided the final validation of extended dimensional synthesis method.

The proposed dimensional synthesis method in this dissertation is expected to find more applications in the design of wide-band bandpass filters without resort to global full-wave optimization.

9.2 Recommendations for Future Work

This dissertation has presented a dimensional synthesis method for the design of wide-band filters without resorting to global full-wave optimization. There are still much work that can be done in the future. The recommendations for future work are listed as follows:

- In the synthesis of in-line pseudo-elliptic waveguide filters using customized resonators, some common techniques to suppress the spurious harmonics can be tried in the future.

- As discussed in CHAPTER 7, the realization of the original cross-coupled filter network can be explored in the future.

- In CHAPTER 8, only quarter-wavelength-resonator bandpass filters with Chebyshev response was discussed. The quarter-wavelength-resonator pseudo-elliptic filters may be tried in the future. Besides, the dimensional synthesis method could also be applied to the design of ultra wide-band (UWB) filters without global full-wave optimization.

- More extended dimensional synthesis method for pseudo-elliptic waveguide filters can be explored in future, such as dual-mode filters, extracted pole techniques, and so on.

- More flexible lowpass prototype filter with frequency-dispersive inverters can be explored in the future.

BIBLIOGRAPHY

[1] A. A. Oliner, "Historical perspectives on microwave field theory," *IEEE Trans. Microwave Theory Tech*, vol. 32, no. 9, pp. 1022-1045, Sept. 1984.

[2] H. Sobol and K. Tomiyasu, "Milestones of microwaves," *IEEE Trans. Microwave Theory Tech*, vol. 50, no. 3, pp. 594-611, Mar. 2002.

[3] R. Levy and S. B. Cohn, "A history of microwave filter research, design, and development," *IEEE Trans. Microwave Theory Tech*, vol. 32, no. 9, pp. 1055-1067, Sept. 1984.

[4] R. Levy, R. V. Snyder, and G. Matthaei, "Design of microwave filters," *IEEE Trans. Microwave Theory Tech*, vol. 50, no. 3, pp. 783-793, Mar. 2002.

[5] R. M. Fano and A. W. Lawson, *Microwave Transmission Circuits*, M.I.T. Rad. Lab., New York: McGraw-Hill, 1948, vol. 9, ch. 9, 10.

[6] S. B. Cohn, "Direct-coupled resonator filters," *Proc. IRE*, vol. 45, pp. 187-196, Feb. 1957.

[7] L. Young, "Direct-coupled cavity filters for wide and narrow bandwidths," *IEEE Trans. Microwave Theory Tech*, vol. 11, pp. 162-178, May 1963.

[8] R. Levy, "Theory of direct coupled-cavity filters," *IEEE Trans. Microwave Theory Tech*, vol. 15, pp. 340-348, June 1967.

[9] G. L. Matthaei, L. Young, and E. M. T. Jones, *Microwave Filters, Impedance Matching Networks and Coupling Structures*. Norwood, MA: Artech House, 1964, pp. 165-173, 243-252, 889-920.

[10] S. B. Cohn, "Parallel-coupled transmission-line resonator filters," *IRE Trans. Microwave Theory Tech.*, vol. 10, pp. 223-231, Apr. 1958.

[11] G. L. Matthaei, "Interdigital band-pass filter," *IRE Trans. Microwave Theory Tech.*, vol. 10, pp. 479-491, Nov. 1962.

[12] G. L. Matthaei, "Comb-line filters of narrow or moderate bandwidth," *Microwave J.*, vol. 6, pp. 82-91, Aug. 1963.

[13] R. J. Wenzel, "Synthesis of combline and capacitively-coupled interdigital filters of arbitrary bandwidth," *IEEE Trans. Microwave Theory Tech*, vol. 19, no. 9, pp. 678-686, Aug. 1971.

[14] G. L. Matthaei, L. Young, and E. M. T. Jones, *Microwave Filters, Impedance Matching Networks and Coupling Structures*. Norwood, MA: Artech House, 1964, pp. 1027-1086.

[15] C. Kudsia, R. Cameron, and W. Tang, "Innovations in microwave filters and multiplexing networks for communication satellite systems," *IEEE Trans. Microwave Theory Tech*, vol. 40, pp. 1133-1149, June 1992.

[16] W. G. Lin, "Microwave filters employing a single cavity excited in more than one mode," *J. Appl. Phys*., vol. 22, pp. 989-1001, Aug. 1951.

[17] A. E. Atia and A. E. Williams, "New types of waveguide bandpass filters for satellite transponders," *Comsat Tech. Rev*., vol. 1, no. 1, pp. 21-43, Fall 1971.

[18] A. E. Atia and A. E. Williams, "Narrow bandpass waveguide filters," *IEEE Trans. Microwave Theory Tech*, vol. 20, pp. 258-265, Apr. 1972.

[19] A. E. Atia, A. E. Williams, and R. W. Newcom, "Synthesis of dual-mode filters," *IEEE Trans. Circuits Syst.*, vol. CAS-21, pp. 649-655, Sept. 1974.

[20] M. Guglielmi, O. Roquebrun, P. Jarry, E. Kerherve, M. Capurso, and M. Piloni, "Low-cost dual-mode asymmetric filters in rectangular waveguide," *IEEE MTT-S Int. Microwave Symp. Dig*., Phoenix, AZ, June 2001, pp. 1787-1790.

[21] W. C. Tang and S. K. Chaudhuri, "A true elliptic-function filter using triple-mode degenerate cavities," *IEEE MTT-S Int. Microwave Symp. Dig*., Boston, MA, May 1983, pp. 83-85.

[22] R. R. Bonetti and A. E. Williams, "Application of dual TM-modes to triple and quadrupole mode filters," *IEEE Trans. Microwave Theory Tech*, vol. 35, pp. 1143-1149, Dec. 1987.

[23] S. J. Fiedziuszko, I. C. Hunter, T. Itoh, Y. Kobayashi, T. Nishikawa, S. N. Stitzer, and K.Wakino, "Dielectric materials, devices, and circuits," *IEEE Trans. Microwave Theory Tech.*, vol. 50, pp. 706–720, Mar. 2002.

[24] S. J. Fiedziuszko, "Dual-mode dielectric resonator loaded cavity filters," *IEEE Trans. Microwave Theory Tech.*, vol. 30, pp. 1311–1316, Sept. 1982.

[25] M. J. Lancaster, *Passive Microwave Device Applications of High-Temperature Superconductors*. Cambridge, U.K.: Cambridge Univ. Press, 1997.

[26] R. R. Mansour, S. Ye, S. Peik, B. Jolley, V. Dokas, T. Romano, and G. Thomson, "HTS filter technology for space applications," *IEEE MTT-S Filter Technol. Commun. Syst. Workshop*, Baltimore, MD, June 1998.

[27] C. Lascaux, F. Rouchaud, V. Madrangeas, M. Aubourg, P. Guillon, B. Theron, and M. Maignan, "Planar Ka-band high temperature superconducting filters for space applications," *IEEE MTT-S Int. Microwave Symp. Dig.*, Phoenix, AZ, June 2001, pp. 487–490.

[28] R. C. Peach, "SAW filters for space applications," *IEEE MTT-S Filter Technol. Commun. Syst. Workshop*, Baltimore, MD, June 1998.

[29] C. M. Kudsia and M. N. S. Swamy, "Computer-aided optimization of microwave filter networks for space applications," *IEEE MTT-S Int. Microwave Symp. Dig.*, Washington, DC, May 1980, pp. 410–412.

[30] J. D. Rhodes and I. H. Zabalawi, "Synthesis of symmetric dual-mode in-line prototype networks," *Int. J. Circuit Theory Applicat.*, vol. 8, no. 2, pp. 145–160, 1980.

[31] R. J. Cameron, "Fast generation of Chebyshev filter prototypes with asymmetrically prescribed transmission zeros," *ESA J.*, vol. 6, pp. 83–95, 1982.

[32] R. J. Cameron and J. D. Rhodes, "Asymmetric realizations for dual-mode bandpass filters," *IEEE Trans. Microwave Theory Tech.*, vol. 29, pp. 51–58, Jan. 1981.

[33] K.Wakino, T. Nishikawa, and Y. Ishikawa, "Miniaturization techniques for dielectric resonator filters for mobile communications," *IEEE Trans. Microwave Theory Tech.*, vol. 42, pp. 1295–1300, July 1994.

[34] I. C. Hunter, J. D. Rhodes, and V. Dassonville, "Dual-mode filters with conductor loaded dielectric resonators," *IEEE Trans. Microwave Theory Tech.*, vol. 47, pp. 2304–2311, Dec. 1999.

[35] V. Walker and I. C. Hunter, "Dielectric loaded waveguide filters," *Proc. Inst. Elect. Eng.*, vol. 148, no. 2, pp. 91–96, Apr. 2001.

[36] H. Tanaka, H. Nishida, and Y. Ishikawa, "Spherical dielectric resonator filter coupled with NRD guide," *Proc. IEICE Jpn. Spring Conf.*, 1991, C-103.

[37] T. Nishikawa, K.Wakino, H.Wada, and Y. Ishikawa, “800 MHz channel dropping filter using TM triple mode resonance,” *IEEE MTT-S Int. Microwave Symp. Dig.*, 1985, K-5, pp. 289–292.

[38] I. C. Hunter, J. D. Rhodes, and V. Dassonville, “Triple mode dielectric resonator hybrid reflection filters,” *Proc. Inst. Elect. Eng.*, pt. H, vol. 145, pp. 337–343, 1998.

[39] D. Zhang, G.-C. Liang, C. F. Shih, M. E. Johansson, and R. S. Withers, “Narrow-band lumped-element microstrip filters using capacitively loaded inductors,” *IEEE Trans. Microwave Theory Tech.*, vol. 42, pp. 3030–3036, Dec. 1995.

[40] E. Soares, K. F. Raihn, and J. D. Fuller, “Dual 5 MHz PCS receiver front-end,” *IEEE MTT-S Int. Microwave Symp. Dig.*, Phoenix, AZ, June 2001, pp. 1981–1984.

[41] M. Kahrizi, S. Safavi-Naeini, and S. K. Chaudhuri, “Computer diagnosis and tuning of microwave filters using model-based parameter estimation and multi-level optimization,” *IEEE MTT-S Int. Microwave Symp. Dig.*, Boston, MA, June 2000, pp. 1641–1644.

[42] D. Ibbetsen, “A synthesis based approach to automated filter tuning,” *IEE Microwave Filters Multiplexers Colloq.*, London, U.K., Nov. 2000, Paper 00/117, pp. 11/1–11/3.

[43] J. Dunsmore, “Simplify filter tuning in the time domain,” *Microwaves RF*, vol. 38, no. 4, pp. 68–84, Mar. 1999.

[44] K. Wakino, “Miniaturization trend of filters for mobile communication handsets,” *IEEE MTT-S Int. Microwave Symp. Miniaturization Filters Commun. Handsets Workshop*, Anaheim, CA, June 1999.

[45] T. Tagami, H. Ehera, K. Noguchi, and T.Komaski, “Resonator type SAW filter,” *Oki Tech. Rev.*, vol. 63, p. 59, 1997.

[46] J. D. Larson, R. C. Ruby, P. Bradley, J. Wen, S. Kok, and A. Chien, “Power handling and temperature coefficient studies in FBAR duplexers for 1900 MHz PCS band,” *IEEE Ultrason. Symp. Dig.*, 2000, pp. 869–874.

[47] R. Weigel, D. P. Morgan, J. M. Owens, A. Ballato, K. M. Lakin, K. Hashimoto, and C. C. W. Ruppel, “Microwave acoustic materials, devices,

and applications," *IEEE Trans. Microwave Theory Tech.*, vol. 50, pp. 738–749, Mar. 2002.

[48] C. T.-C. Nguyen, "Transceiver front-end architectures using high-Q micromechanical resonators," *IEEE Eur. MIDAS MEMS for High-Q Filters Workshop*, Surrey, U.K., July 2000.

[49] D. Peroulis, S. Pacheco, K. Sarabandi, and L. P. B. Katehi, "Tunable lumped components with applications to reconfigurable MEMS filters," *IEEE MTT-S Int. Microwave Symp. Dig.*, Phoenix, AZ, 2001, pp. 341–344.

[50] M. J. Lancaster, J. Powell, and A. Porch, "Thin-film ferroelectric microwave devices," *Superconduct. Sci. Technol.*, no. 11, pp. 1323–1334, 1998.

[51] I. Vendik, O. Vendik, V. Sherman, A. Svishchev, V. Pleskachev, and A. Kurbanov, "Performance limitation of a tunable resonator with a ferroelectric capacitor," *IEEE MTT-S Int. Microwave Symp. Dig.*, Boston, MA, June 2000, pp. 1371–1374.

[52] A. Brucher, C. Cenac, M. Delmond, P. Meunier, L. Billonet, B. Jarry, P. Guillon, and S. E. Sussman-Fort, "Improvement of microwave planar active filters with MMIC technology," *Proc. Eur. GaAs Related III–IV Compounds Applicat. Symp.*, Apr. 1994, pp. 315–318.

[53] S. E. Sussman-Fort, "An NIC-based negative resistance circuit for microwave active filters," *Int. J. Microwave Millimeter-Wave Computer-Aided Eng.*, vol. 4, no. 2, pp. 130–139, Apr. 1994.

[54] W. Mouzannar, L. Billonet, B. Jarry, and P. Guillon, "A new design concept for wide-band frequency tuneable and high order MMIC active recursive filters," *Microwave Opt. Technol. Lett.*, vol. 24, no. 6, pp. 380–385, Mar. 2000.

[55] K. B. Niclas, "Active matching with common-gate MESFET," *IEEE Trans. Microwave Theory Tech.*, vol. 43, pp. 492–499, 1996.

[56] C. Rauscher, "Microwave active filter based on transversal and recursive principles," *IEEE Trans. Microwave Theory Tech.*, vol. 33, Dec. 1985.

[57] L. Billonet et al., "Design concepts for microwave recursive and transversal filters using Lange couplers," *IEEE MTT-S Int. Microwave Symp. Dig.*, vol. 2, June 1992, pp. 925–928.

[58] M. Delmond, L. Billonet, B. Jarry, and P. Guillon, “Microwave tuneable active filter design in MMIC technology using recursive concepts,” *IEEE MTT-S Int. Microwave Symp. Dig.*, vol. 3, May 1995, pp. 105–108.

[59] J. Uher, J. Bornemann, and U. Rosenberg, *Waveguide Components for Antenna Feed Systems: Theory and CAD*. Norwood: Artech House, 1993.

[60] F. Arndt, R. Beyer, J.M. Reiter, T. Sieverding, and T. Wolf, “Automated design of waveguide components using hybrid mode-matchning/numerical EM building-blocks in optimization-oriented CAD frameworks-State-of-the-art and recent advances,” *IEEE Trans. Microwave Theory Tech.*, vol. 45, no. 5, pp. 747–760, May 1997.

[61] U. Papziner and F. Arndt, “Field theoretical computer-aided design of rectangular and circular iris coupled rectangular or circular waveguide cavity filters,” *IEEE Trans. Microwave Theory Tech.*, vol. 41, no. 3, pp. 462–471, Mar. 1993.

[62] A. Alvarez, G. Connor, and M. Guglielmi, “New simple procedure for the computation of the multimode admittance or impedance matrix of planar waveguide junctions,” *IEEE Trans. Microwave Theory Tech.*, vol. 44, no. 3, pp. 413–418, Mar. 1996.

[63] G. Gerini, M. Guglielmi, and G. Lastoria, “Efficient integral equation formulations for admittance or impedance representation of planar waveguide junctions,” *IEEE MTT-S Int. Microwave Symp. Dig.*, Baltimore, MD, Jun. 1998, pp. 1747–1750.

[64] M. Israel and R. Miniowitz, “An efficient finite element method for nonconvex waveguide based on hermitian polynomials,” *IEEE Trans. Microwave Theory Tech.*, vol. 35, no. 11, pp. 1019–1026, Nov. 1987.

[65] A.S. Rong, H. Yang, X.H. Chen, and A. Cangellaris, “Efficient FDTD modeling of irises/slots in microwave structures and its application to the design of combline filters,” *IEEE Trans. Microwave Theory Tech.*, vol. 49, no. 12, pp. 2266–2275, Dec. 2001.

[66] J.R. Montejo and J. Zapata, “Full-wave design and realization of multicoupled dual-mode circular waveguide filters,” *IEEE Trans. Microwave Theory Tech.*, vol. 43, no. 6, pp. 1290–1297, Jun. 1995.

[67] R.H. MacPhie and K.-L. Wu, “A full-wave modal analysis of arbitrarily shaped waveguide discontinuities using the finite plane-wave series expansion,” *IEEE Trans. Microwave Theory Tech.*, vol. 47, no. 2, pp. 232–237, Feb. 1999.

[68] F. Arndt, J. Brandt, V. Catina, J. Ritter, I. Rullhusen, J. Dauelsberg, U. Hilgefort, and W. Wessel, “Fast CAD and optimization of waveguide components and aperture antennas by hybrid MM/FE/MoM/FD methods—State-of-the-art and recent advances,” *IEEE Trans. Microwave Theory Tech.*, vol. 52, no. 1, pp. 292–305, Jan. 2004.

[69] G. Conciauro, M. Bressan, and C. Zuffada, “Waveguide modes via an integral equation leading to a linear matrix eigenvalue problem,” *IEEE Trans. Microwave Theory Tech.*, vol. 32, no. 11, pp. 1495–1504, Nov. 1984.

[70] G. Conciauro, M. Guglielmi, and R. Sorrentino, *Advanced Modal Analysis—CAD Techniques for Waveguide Components and Filters*. Chichester: Wiley, 2000.

[71] S. Cogollos, S. Marini, V.E. Boria, P. Soto, A. Vidal, H. Esteban, J. V. Morro, and B. Gimeno, “Efficient modal analysis of arbitrarily shaped waveguides composed of linear, circular and elliptical arcs using the BI-RME method,” *IEEE Trans. Microwave Theory Tech.*, vol. 51, no. 12, pp. 2378–2390, Dec. 2003.

[72] J.W. Bandler, Ed., “Special Issue on Automated circuit design using electromagnetic simulators,” *IEEE Trans. Microwave Theory Tech.*, vol. 45, no. 5, pp. 709–866, May 1997.

[73] J.W. Bandler and M. Mongiardo, Eds., “Special Issue on Electromagnetics-based optimization of microwave components and circuits,” *IEEE Trans. Microwave Theory Tech.*, vol. 52, no. 1, pp. 245–456, Jan. 2004.

[74] R.J. Cameron, “Advanced coupling matrix synthesis techniques for microwave filters,” *IEEE Trans. Microwave Theory Tech.*, vol. 51, no. 1, pp. 1–10, Jan. 2003.

[75] S. Bila, D. Baillargeat, M. Aubourg, S. Verdeyme, P. Guillon, F. Seyfert, J. Grimm, L. Baratchart, C. Zanchi, and J. Sombrin, “Direct electromagnetic optimization of microwave filters,” *IEEE Microwave Mag.*, vol. 2, no. 1, pp. 46–51, Mar. 2001.

[76] J.V. Morro, P. Soto, H. Esteban, V.E. Boria, C. Bachiller, M. Taroncher, S. Cogollos, and B. Gimeno, "Fast automated design of waveguide filters using aggressive space mapping with a new segmentation strategy and a hybrid optimization algorithm," *IEEE Trans. Microwave Theory Tech.*, vol. 53, no. 4, pp. 1130–1142, Apr. 2005.

[77] G. L. Matthaei, L. Young, and E. M. T. Jones, *Microwave Filters, Impedance Matching Networks and Coupling Structures*. Norwood, MA: Artech House, 1964.

[78] J.-S. Hong and M. J. Laucaster, *Microstrip filter for RF/Microwave Applications*, John Wiely & Sons, 2001.

[79] F. M. Vanin, D. Schmitt, and R. Levy, "Dimensional Synthesis for Wide-Band Waveguide Filters and Diplexers," *IEEE Trans. Microwave Theory Tech.*, vol. 52, NO. 11, Nov. 2004.

[80] J. D. Rhodes and R. J. Cameron, "General extracted pole synthesis technique with application to low-loss TE_{011}-mode filters", *IEEE Trans. Microwave Theory Tech.*, vol. 28, pp. 1018-1028, Sept. 1980.

[81] S. Amari and U. Rosenberg, "Synthesis and design novel in-line filters with one or two real transmission zeros", *IEEE Trans. Microwave Theory Tech.*, vol. 52, no. 5, pp. 1464-1478, May 2004.

[82] S. Amari and U. Rosenberg, "A third order in-line pseudoelliptic filter with a transmission zero extracted at its center," *IEEE MTT-S Int. Microwave Symp. Dig.*, Fort Worth, TX, Jun. 2004, pp. 459-462.

[83] S. Amari, U. Rosenberg and J. Bornemann, "Singlets, cascaded singlets, and the nonresonating node model for advanced modular design of elliptic filters", *IEEE Microwave Wireless Compon. Lett.*, vol. 14, no. 5, pp. 237-239, May 2004.

[84] S. Amari and U. Rosenberg, "New building blocks for modular design of elliptic and self-equalized filters", *IEEE Trans. Microwave Theory Tech.*, vol. 52, no. 2, pp. 721-735, Feb. 2004.

[85] S. Cogollos, R.J. Cameron, R.R. Mansour, M. Yu and V.E. Boria, "Synthesis and design procedure for high performance waveguide filters based on nonresonating nodes," *IEEE MTT-S Int. Microwave Symp. Dig.*, Jun. 2007, pp. 1297-1300.

[86] S. Cogollos, R V.E. Boria., J. Cameron and R.R. Mansour, “Design procedure of low cost substrate microstrip filters based on nonresonating nodes,” *IEEE MTT-S Int. Microwave Symp. Dig.*, Jun. 2008, pp. 543-546.

[87] R. Levy, “Filters with single transmission zeros at real and imaginary frequencies,” *IEEE Trans. Microwave Theory Tech.*, vol. 24, no. 4, pp. 172-181, Apr. 1976.

[88] R. J. Cameron, “General prototype network synthesis methods for microwave filters,” *ESA J.*, vol. 6, pp. 193-206, 1982.

[89] J.-S. Hong and M. J. Lancaster, “Couplings of microstrip square open-loop resonators for cross-coupled planar microwave filters,” *IEEE Trans. Microwave Theory Tech.*, vol. 24, no. 12, pp. 2099-2109, Dec. 1976.

[90] H. W. Yao, K. A. Atia, and R. Hershtig, “Full wave modeling of conducting posts in rectangular waveguides and its applications to slot coupled combline filters,” *IEEE Trans. Microwave Theory Tech.*, vol. 43, no. 12, pp. 2824-2829, Dec. 1995.

[91] C. Wang and K. A. Zaki, “Full wave modeling of electric coupling probes comb-line resonators and filters,” *IEEE Trans. Microwave Theory Tech.*, vol. 48, no. 12, pp. 2459-2464, Dec. 1995.

[92] T. Shen, H.-T. Hsu, K. A. Zaki, A. E. Atia, and T. G. Dolan, “Full-wave design of canonical waveguide filters by optimization,” *IEEE Trans. Microwave Theory Tech.*, vol. 51, no. 2, pp. 504-510, Feb. 2003.

[93] J.A. Ruiz-Cruz, M.A.E. Sabbagh, K.A. Zaki, J.M. Rebollar, and Y. Zhang, “Canonical ridge waveguide filters in LTCC or metallic resonators,” *IEEE Trans. Microwave Theory Tech.*, vol. 53, no. 1, pp. 174-182, Jan. 2005.

[94] M. Guglielmi, F. Montauti, L. Pellegrini, and P. Arcioni, “Implementing transmission zeros in the inductive-window bandpass filters,” *IEEE Trans. Microwave Theory Tech.*, vol. 43, no. 8, pp. 1911-1915, Aug. 1995.

[95] G. Matthaei, “Direct-coupled, Band-Pass with $\lambda_0/4$ Resonators”, *IRE National Convention Record*, Part 1, pp. 98-111, 1958.

[96] J.-F. Liang, X.-P. Liang, K. A. Zaki, and A. E. Atia, “Dual-mode dielectric or air-filled rectangular waveguide filters,” *IEEE Trans. Microwave Theory Tech.*, vol. 42, no. 7, pp. 1330-1335, Jul. 1994.

[97] CST MICROWAVE STUDIO, http://www.cst.com, accessed by Oct. 2010.

[98] ANSOFT HFSS, http://www.ansoft.com, accessed by Oct. 2010.

[99] N. Marcuvitz, *Waveguide Handbook*, IEE, London, 1986.

[100] M. J. Lancaster, J. Zhou, M. Ke, Y. Wang and K. Jiang, "Design and high performance of a micromachined K-band rectangular coaxial cable", *IEEE Trans. Microwave Theory Tech.*, vol. 55, no. 7, July 2007.

[101] Llamas-Garro, I., Lancaster, M.J., and Hall, P.S., "A low loss wideband suspended coaxial transmission line", *Microw. Opt. Technol. Lett.*, vol. 43, no. 1, pp. 93-95, Jan. 2004.

[102] R. T. Chen, E. R. Brown, and C. A. Bang, "A compact low-loss Ka-band filter using 3-dimensional micromachined integrated coax," in *17th IEEE Int. MEMS Conf.*, Maastricht, The Netherlands, Jan. 25-29, 2004, pp. 801-804.

[103] T. –S. Chen, "Determination of the capacitance, inductance, and Characteristics impedance of rectangular lines," *IEEE Trans. Microw. Theory Tech.*, vol. 8, no. 5, pp. 510-519, Sep. 1960.

[104] Gruner L., "Higher order modes in rectangular coaxial waveguides," *IEEE Trans. Microw. Theory Tech.*, vol. 15, no. 8, pp. 483-485, Aug. 1967.

[105] Mician μWave Wizard, http://www.mician.com, accessed by Oct. 2010.

AUTHOR'S PUBLICATIONS

PUBLISHED/ACCEPTED JOURNAL PAPERS

[1] Q.F. Zhang and S.J. Xu, "Design of a novel 2-D uniplanar CRLH-TL structure," *International Journal of Infrared and Millimeter Waves*, vol. 27, no. 11, pp.1539–1552, Nov. 2006.

[2] Q.F. Zhang and Y.L. Lu, "Design of 45-degree linearly polarized substrate integrated waveguide-fed slot array antennas," *International Journal of Infrared and Millimeter Waves*, vol. 29, no. 11, pp.1019-1027, Nov. 2008.

[3] Q.F Zhang and Y.L. Lu "Dimensional synthesis for wide-band bandpass filters with quarter-wavelength resonators," *Progress In Electromagnetics Research B*, Vol. 17, pp.213-231, Sep. 2009.

[4] Q.F. Zhang and Y.L. Lu, "Design of a Waveguide Bandpass Filter Based on Nonresonating 'T' Junctions", *Electronics Letters*, vol. 46, no. 16, pp. 1107-1108, Aug. 2010.

[5] Q.F. Zhang and Y.L. Lu, "Dimensional Synthesis Method for Wide-Band Waveguide Iris Filters", *IET Microwaves, Antennas & Propagation*, vol. 4, no. 9, pp. 1256-1263, Sep. 2010.

[6] Q.F. Zhang and Y.L. Lu, "Design of Wide-Band Pseudo-Elliptic Waveguide Filters with Cavity-Backed Inverters", *IEEE Microwave and Wireless Components Letters*, vol. 20, no. 11, pp. 604 - 606, Nov. 2010.

[7] Q.F. Zhang and Y.L. Lu, "Dimensional Synthesis of Symmetric Wide-Band Waveguide Cross-Coupled Filters without Global Full-Wave Optimization", *IEEE Trans. Microw. Theory Tech.*, vol 58, no. 12, pp. 3742-3748, Dec. 2010.

[8] Q.F. Zhang and Y.L. Lu, "Dimensional Synthesis for Wide-Band Pseudo-Elliptic Waveguide Filters Using Cavity-Backed Inverters", in press, accepted by *IET Microwaves, Antennas & Propagation*, vol. 4, no. 12, pp. 2212-2218, Dec. 2010.

CONFERENCE PAPERS

[1] Q.F. Zhang and Y.L. Lu, "45° linearly polarized substrate integrated waveguide-fed slot array antennas," *Proc 2008 International Conference on Microwave and Millimeter Wave Technology*, Nanjing, China, 21-24 April 2008.

[2] Q.F. Zhang and Y.L. Lu, "A novel reflection-canceling design for substrate integrated waveguide based 45-degree linearly polarized slot antenna array," *Proc. 2008 IEEE International Symposium on Antennas and Propagation*, San Diego, CA, USA, 5-11 July 2008.

[3] Q.F. Zhang and Y.L. Lu, "E-band T Shape Transitions between Substrate Integrated Waveguide and Standard Waveguide," *Proc. 2008 Asia-Pacific Microwave Conference*, Hong Kong and Macau, China, 16-20 Dec 2008.

[4] Q.F. Zhang and Y.L. Lu, "Wideband Waveguide Iris Filter Design with A Novel Synthesis Procedure," *Progress in Electromagnetics Research Symposium*, Moscow, Russia, 18-21 Aug 2009. (Chapter 4)

[5] Q.F. Zhang and Y.L. Lu, "Design of Rectangular Coaxial Wide-band Bandpass Filters with Quarter-wavelength Resonators," *Proc. 2009 Asia-Pacific Microwave Conference (APMC 2009)*, Singapore, 7-10 Dec 2009. (Chapter 8)

APPENDIX A DERIVATION (6-2)

To derive the equation (6-2), we can use even mode and odd mode to analyze the Pi-network in Fig. 6.2. The even- and odd-mode conductance of the Pi-network in Fig. 6.2 can be calculated as

$$\begin{cases} Y_e = jB \\ Y_0 = jB + \dfrac{2}{jX} \end{cases}, \tag{A-1}$$

where Y_e and Y_0 are the conductance of the even-mode and odd-mode, respectively. If we calculate the even- and odd-mode conductance using its scattering parameters, we can get

$$\begin{cases} Y_e = \dfrac{1 - S_{11} - S_{21}}{1 + S_{11} + S_{21}} \\ Y_0 = \dfrac{1 - S_{11} + S_{21}}{1 + S_{11} - S_{21}} \end{cases}. \tag{A-2}$$

By substituting (A-1) with (A-2), we can get the equation (6-2).

APPENDIX B DERIVATION (6-4)

Since the two transmission line in Fig. 6.4 is nearly the same, the network in the left side can be regarded as symmetrical. Therefore, in the calculation of the ABCD matrix, we only need to calculate two elements in the final ABCD matrix. The ABCD matrix of the network in the left side of Fig. 6.4 can be written as

$$\begin{bmatrix} \cos\theta_1 & jZ_0\sin\theta_1 \\ jY_0\sin\theta_1 & \cos\theta_1 \end{bmatrix}\begin{bmatrix} 1 & jX \\ 0 & 1 \end{bmatrix}\begin{bmatrix} \cos\theta_2 & jZ_0\sin\theta_2 \\ jY_0\sin\theta_2 & \cos\theta_2 \end{bmatrix} = \begin{bmatrix} \cos(\theta_1+\theta_2) - XY_0\cos\theta_1\sin\theta_2 & jZ_0\sin(\theta_1+\theta_2) + jX\cos\theta_1\cos\theta_2 \\ \cdots & \cdots \end{bmatrix} \quad . \tag{B-1}$$

And the ABCD matrix of the network in the right side of Fig. 6.4 can be written as

$$\begin{bmatrix} 1 & 0 \\ jB^* & 1 \end{bmatrix}\begin{bmatrix} 1 & jX^* \\ 0 & 1 \end{bmatrix}\begin{bmatrix} 1 & 0 \\ jB^* & 1 \end{bmatrix} = \begin{bmatrix} 1 - X^*B^* & jX^* \\ \cdots & \cdots \end{bmatrix} \quad . \tag{B-2}$$

Since (B-1) and (B-2) should be equal, we can get

$$\begin{cases} X^* = Z_0\sin(\theta_1+\theta_2) + X\cos\theta_1\cos\theta_2 \\ B^* = \dfrac{\cos(\theta_1+\theta_2) - 1 - XY_0\cos\theta_1\sin\theta_2}{-Z_0\sin(\theta_1+\theta_2) - X\cos\theta_1\cos\theta_2} \end{cases} \quad . \tag{B-3}$$

In the frequency band close to the center frequency, we have $X << Z_0$. So (B-3) can be written as

$$\begin{aligned} B^* &= \frac{\cos(\theta_1+\theta_2) - 1 - XY_0\cos\theta_1\sin\theta_2}{-Z_0\sin(\theta_1+\theta_2) - X\cos\theta_1\cos\theta_2} \\ &\approx Y_0 \cdot \frac{1-\cos(\theta_1+\theta_2)}{\sin(\theta_1+\theta_2)} \\ &= Y_0\tan\frac{\theta_1+\theta_2}{2} \end{aligned} \quad . \tag{B-4}$$

APPENDIX C DERIVATION (7-4)

The first equation in (7-4) is the equivalent series reactance of a half-wavelength transmission line. As we know, the transmission line can be equivalent to a Pi-network [17]. When the length is close to half wavelength, the shunt susceptance in the Pi-network can be neglected and the transmission line can be equivalent to a series reactance [17]

$$X = -Z_0 \sin\theta \quad , \tag{C-1}$$

where Z_0 and θ are the characteristics impedance and phase of the transmission line, respectively. By considering the frequency dependence of the phase in (C-1), then we can deduce the first equation in (7-4).

As for the second equation in (7-4), it can be derived from (7-3). By substituting $\theta_{m-1} = \pi$ to the first equation in (7-3), we can get

$$\frac{X^*_{m-1}(f)}{Z_0} = \frac{\left(1+(K_m/Z_0)^2\right)\cdot\tan\left(\pi\cdot\lambda_g(f_0)/\lambda_g(f)\right)}{1-(K_m/Z_0)^2\cdot\tan^2\left(\pi\cdot\lambda_g(f_0)/\lambda_g(f)\right)} \quad . \tag{C-2}$$

When f is close f_0, we have

$$\pi\cdot\lambda_g(f_0)/\lambda_g(f) \approx \pi \quad . \tag{C-3}$$

Also we have another condition

$$K_m/Z_0 < 1 \quad . \tag{C-4}$$

Therefore we can get

$$(K_m/Z_0)^2\cdot\tan^2\left(\pi\cdot\lambda_g(f_0)/\lambda_g(f)\right) << 1 \quad . \tag{C-5}$$

By applying the condition (C-5) to (C-2), we can derive the second equation in (7-4).